

AD-A047 994

ARMY ENGINEER WATERWAYS EXPERIMENT STATION VICKSBURG MISS F/G 4/2
NEARSHORE NUMERICAL STORM SURGE AND TIDAL SIMULATION.(U)
SEP 77 J J WANSTRATH

UNCLASSIFIED

WES-TR-H-77-17

NL

1 OF 2
ADA047994



AD A047994



12



TECHNICAL REPORT H-77-17

NEARSHORE NUMERICAL STORM SURGE AND TIDAL SIMULATION

by

John J. Wanstrath

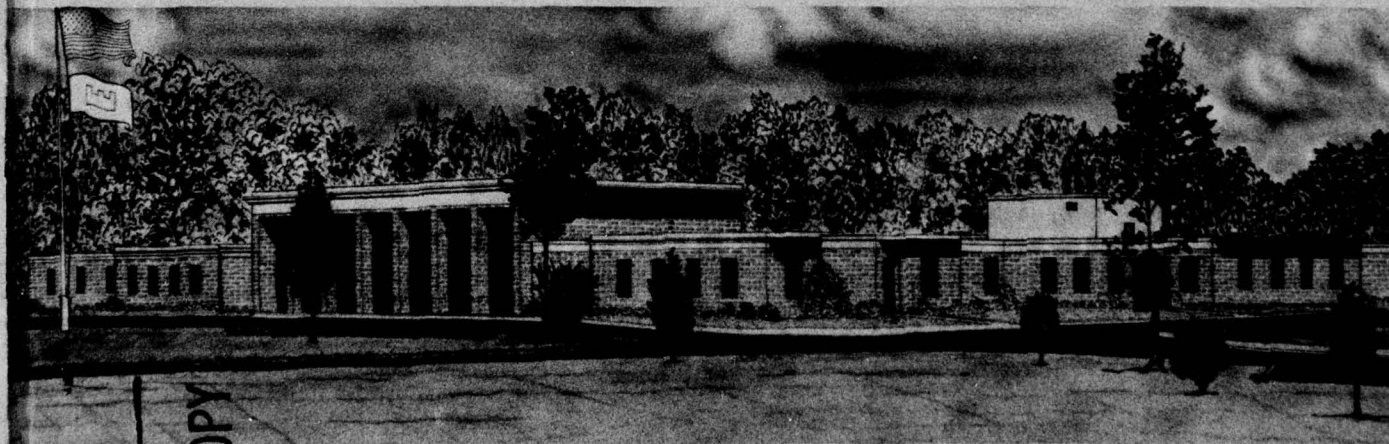
Hydraulics Laboratory
U. S. Army Engineer Waterways Experiment Station
P. O. Box 631, Vicksburg, Miss. 39180

September 1977

Final Report

Approved For Public Release; Distribution Unlimited

DDC
RECEIVED
DEC 30 1977
REGULATED



AD No. _____
DDC FILE COPY

Prepared for Assistant Secretary of the Army (R&D)
Washington, D. C. 20314

Under Project 4A161101A91D

Destroy this report when no longer needed. Do not return
it to the originator.



DEPARTMENT OF THE ARMY
WATERWAYS EXPERIMENT STATION, CORPS OF ENGINEERS
P. O. BOX 631
VICKSBURG, MISSISSIPPI 39180

IN REPLY REFER TO: WESHH

5 December 1977

Errata Sheet

NEARSHORE NUMERICAL STORM SURGE AND TIDAL SIMULATION

Technical Report H-77-17

September 1977

1. Page 6, Equation 2 should read

$$y(\xi, \eta) = B_0 + \eta + \sum_{n=1}^N (B_n \cosh nk\eta + C_n \sinh nk\eta) \cos nk\xi$$

2. Page 19, lines 2 and 3 should read "and F_H are the point values of F from Equation 11 at Q_S , Q_T , and H points, respectively, w_H is the point value of μ from"
3. Page 28, the second line following Equation 49 should read " α is a rotation angle used, primarily, to fine tune the alignment of"
4. Page 45, line 22 should read "mately 0900Z, 8 September (between the time of Plates 70 and 71). The"

Unclassified
SECURITY CLASSIFICATION OF THIS PAGE (When Data Entered)

REPORT DOCUMENTATION PAGE		READ INSTRUCTIONS BEFORE COMPLETING FORM
1. REPORT NUMBER Technical Report H-77-17	2. GOVT ACCESSION NO.	3. RECIPIENT'S CATALOG NUMBER
4. TITLE (and Subtitle) NEARSHORE NUMERICAL STORM SURGE AND TIDAL SIMULATION	5. TYPE OF REPORT & PERIOD COVERED Final report	6. PERFORMING ORG. REPORT NUMBER
7. AUTHOR(s) John J. Wanstrath	8. CONTRACT OR GRANT NUMBER(s)	
9. PERFORMING ORGANIZATION NAME AND ADDRESS U. S. Army Engineer Waterways Experiment Station Hydraulics Laboratory P. O. Box 631, Vicksburg, Miss. 39180	10. PROGRAM ELEMENT, PROJECT, TASK AREA & WORK UNIT NUMBERS Project No. 4A161101A91D	
11. CONTROLLING OFFICE NAME AND ADDRESS Assistant Secretary of the Army (R&D) Washington, D. C. 20314	12. REPORT DATE September 1977	13. NUMBER OF PAGES 151
14. MONITORING AGENCY NAME & ADDRESS (if different from Controlling Office)	15. SECURITY CLASS. (of this report) Unclassified	15a. DECLASSIFICATION/DOWNGRADING SCHEDULE
16. DISTRIBUTION STATEMENT (of this Report) Approved for public release; distribution unlimited.		
17. DISTRIBUTION STATEMENT (of the abstract entered in Block 20, if different from Report)		
18. SUPPLEMENTARY NOTES		
19. KEY WORDS (Continue on reverse side if necessary and identify by block number) Hydrodynamics Long wave Mathematical models Water waves Conformal mapping		
20. ABSTRACT (Continue on reverse side if necessary and identify by block number) ➤ A two-dimensional, time-dependent, open-coast, long-wave, shallow-water model is presented. The model employs an orthogonal curvilinear coordinate system with telescoping computing cells. This permits greater resolution of the v in the nearshore coastal region where principal interest is focused than at the continental shelf break or at far lateral distances from the coast. The model treats the coastline as a finite height barrier (Continued)		

DD FORM 1 JAN 73 1473 EDITION OF 1 NOV 65 IS OBSOLETE

Unclassified
SECURITY CLASSIFICATION OF THIS PAGE (When Data Entered)

038100

JP

Unclassified

SECURITY CLASSIFICATION OF THIS PAGE(When Data Entered)

20. ABSTRACT (Continued)

which is broken with bay entrances. Coastal overtopping and bay communication with the open sea provide the means for the transport of water across the nominal coastline. Mass is conserved with all water lost from the ocean during the flood stage being stored in discrete bay ponding areas. Each ponding area is described by its particular storage area curve and its particular series of coastline computing grid segments. A prediction/correction method is employed for the computation of the coastal water level.

The model has been employed in 11 verification studies. Included in the studies are simulations of storm surges from five hurricanes of record and astronomical tide and pseudosurge (transient large amplitude free wave) from two hydraulic physical models. Results from the simulations are presented. In all studies, the same barrier coefficients and procedure for determining the channel discharge coefficient were used. ↙

Unclassified

SECURITY CLASSIFICATION OF THIS PAGE(When Data Entered)

PREFACE

The investigation reported herein was conducted under Department of the Army Project No. 4A161101A91D, In-House Laboratory Independent Research (ILIR) Program. The program is sponsored by the Assistant Secretary of the Army (R&D). The research was performed at the U. S. Army Engineer Waterways Experiment Station (WES), Vicksburg, Mississippi.

The study was conducted by Dr. John J. Wanstrath of the Coastal Branch, under the general supervision of Mr. H. B. Simmons, Chief of the Hydraulics Laboratory, Dr. R. W. Whalin, Chief of the Wave Dynamics Division, and Dr. C. L. Vincent, Chief of the Coastal Branch. Dr. D. L. Durham, CAPT F. C. Perry, and Mr. J. W. McCoy assisted in the operation and data collection of the Murrells Inlet physical model surge experiments. Special assistance in providing data and other services was given by the U. S. Army Engineer District, New Orleans, the U. S. Army Engineer Division, Lower Mississippi Valley, and the U. S. Army Engineer District, Jacksonville. Prof. R. O. Reid of the Department of Oceanography, Texas A&M University, College Station, Texas, contributed to the initial formation of the flooding coast concept in open-coast surge computations.

Directors of WES during the conduct of this investigation and the preparation and publication of this report were COL. G. H. Hilt, CE, and COL John L. Cannon, CE. Technical Director was Mr. F. R. Brown.

ACCESSION for	
NTIS	Write Section <input checked="" type="checkbox"/>
DDC	Buff Section <input type="checkbox"/>
UNANNOUNCED	<input type="checkbox"/>
JUSTIFICATION	
BY	
DISTRIBUTION/AVAILABILITY CODES	
DI	SPECIAL
A	

CONTENTS

	<u>Page</u>
PREFACE	1
CONVERSION FACTORS, METRIC (SI) TO U. S. CUSTOMARY AND U. S. CUSTOMARY TO METRIC (SI) UNITS OF MEASUREMENT	3
PART I: INTRODUCTION	4
PART II: CONFORMAL MAPPING	6
PART III: MATHEMATICAL MODEL	9
Stretched Shelf Coordinate System	9
Governing Equations	12
Recursion Equations	17
Boundary Condition	19
Hurricane Wind and Atmospheric Pressure Models	27
PART IV: MATHEMATICAL MODEL APPLICATIONS	31
Galveston Bay Physical Model Study	31
Murrells Inlet Physical Model Study	33
Variable Grid Spacing Study	36
West Coast of Florida, Hurricane Donna Surge Study	38
Louisiana Coast, Hurricanes Flossy, Hilda, Betsy and Carmen Surge Study	41
PART V: CONCLUSIONS AND RECOMMENDATIONS	47
REFERENCES	49
TABLES 1-19	
PLATES 1-78	
APPENDIX A: NOTATION	A1

CONVERSION FACTORS, METRIC (SI) TO U. S. CUSTOMARY AND
U. S. CUSTOMARY TO METRIC (SI) UNITS OF MEASUREMENT

Units of measurement used in this report can be converted as follows:

<u>Multiply</u>	<u>By</u>	<u>To Obtain</u>
<u>Metric (SI) to U. S. Customary</u>		
metres	3.280839	feet
kilometres	0.5399568	miles (U. S. nautical)
metres per second	3.280839	feet per second
square centimetres per second	0.1550	square inches per second
millibars	0.01450377	pounds per square inch
<u>U. S. Customary to Metric (SI)</u>		
inches	25.4	millimetres
feet	0.3048	metres
miles (U. S. nautical)	1.852	kilometres
miles (U. S. statute)	1.609344	kilometres
square feet	0.09290304	square metres
pounds (force) per square inch	6894.757	pascals
feet per second	0.3048	metres per second
miles per hour (U. S. statute)	1.609344	kilometres per hour
degrees (angle)	0.01745329	radians

NEARSHORE NUMERICAL STORM SURGE AND TIDAL SIMULATION

PART I: INTRODUCTION

1. Three-dimensional partial differential equations govern the motion of an infinitesimal fluid element. These equations result from basic considerations of mass conservation and Newton's second law of motion. The assumptions involving the incompressibility and homogeneity of the water, negligible vertical accelerations of the fluid parcel, reasonably uniform horizontal flow over the fluid depth, and others result in the classical, vertically integrated long-wave equations of motion and mass conservation. Energy is supplied at the free surface, in general, through the action of the wind and dissipated at the seabed through friction. The system of equations is time-dependent, two-dimensional in terms of the horizontal coordinates, and readily integrable through numerical techniques. These equations are applicable to the study of storm surge generation¹ on the continental shelf and to the degree that the assumptions are valid, nearshore astronomical tide simulation.

2. In the past, numerical integration of the two-dimensional as well as the three-dimensional equations of motion have been performed using rectilinear grids. Recently, curvilinear coordinates^{2,3,4} have been employed in two-dimensional models, with particular applications to free and forced long wave simulations for large (hundreds of miles*) open-coast stretches of the continental shelf.

3. Open-coast curvilinear models are considered superior to rectilinear models because rectilinear models must represent the coast boundary as a series of straight-line segments connected at right angles. Spurious oscillations are injected into the calculation by the boundary. Furthermore, the stair-step boundary must retain more water over that

* A table of factors for converting metric (SI) units of measurement to U. S. customary units and U. S. customary units to metric (SI) units is presented on page 3.

natural coastal configuration where water is free to move artificially unobstructed and in accord with the forces.

4. The use of any of the previously mentioned open-coast models in simulating circulation and water level conditions is made difficult because of the requirement of specifying appropriate boundary conditions. This is especially the case in the nearshore region where these models simulate the coast boundary as an infinitely high, continuous wall. This boundary condition neglects overtopping of low-lying land and bay communication with the open sea. These coastal processes have a considerable effect on the nearshore water levels and fluid velocities. Furthermore, it is precisely this zone where much environmental interest is focused and the use of numerical models should prove beneficial.

5. This report describes a more appropriate open-coast boundary condition and presents results from 11 verification studies. The boundary condition is termed the finite height barrier coast (FHBC) and is incorporated into a two-dimensional model that employs an orthogonal curvilinear coordinate system with telescoping computing cells. This hydrodynamic model with the FHBC is named SSURGE III and uses a slightly different computing scheme than that previously documented.³

6. Similar to the previous model, there are three numerical programs required for staging the production of surge or tide computations. The first numerical program determines the conformal mapping coefficients for the particular study region of the continental shelf. The actual coastline, as seen on National Ocean Survey (NOS) nautical charts, is smoothed relative to portraying small-scale features. This continuous coastline and a deep sea boundary curve (perhaps, following the 300- or 600-ft isobath) are the input to the conformal mapping program. The coefficients are determined and input to the second numerical program which determines the computing grid data relative to a particular design by the user. The grid data are, in part, the input to the SSURGE III program. Other input includes the shelf bathymetry, FHBC data, hydrograph and velocity output locations, and other readily determinable parameters. In actual practice, the entire process is not time-consuming or expensive.

PART II: CONFORMAL MAPPING

7. It is desired to conformally map a spatial region of prototype space of the continental shelf into a rectangle in a mathematical image plane, in which the coastline and deep sea boundary curves are specifically transformed into the image plane as constant values of η .^{*} Figure 1 shows the details of the transformation.

8. It can be shown³ that a conformal transformation satisfying the above constraints is

$$x(\xi, \eta) = \xi + \sum_{n=1}^N (B_n \sinh nk\eta + C_n \cosh nk\eta) \sin nk\xi \quad (1)$$

and

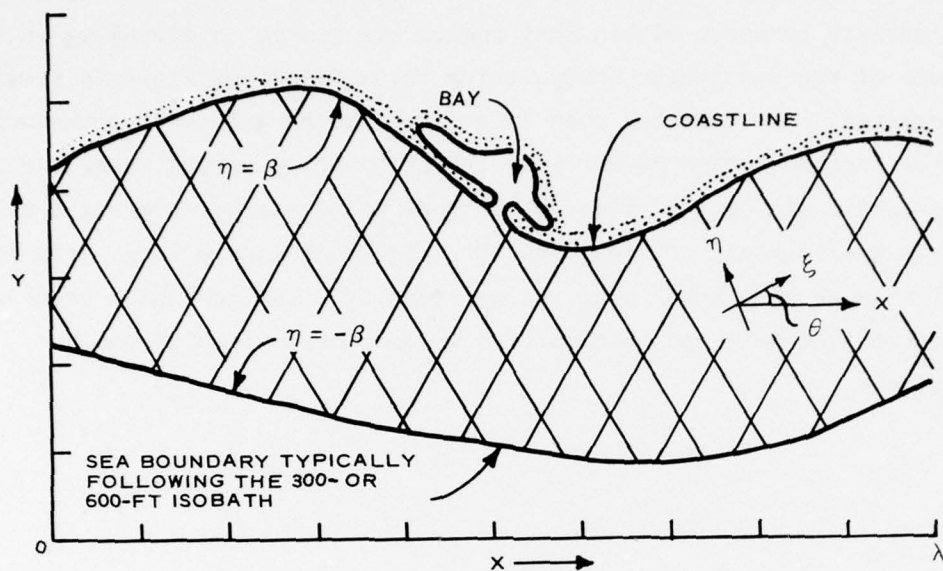
$$y(\xi, \eta) = B_0 + \xi + \sum_{n=1}^N (B_n \cosh nk\eta + C_n \sinh nk\eta) \cos nk\xi \quad (2)$$

where

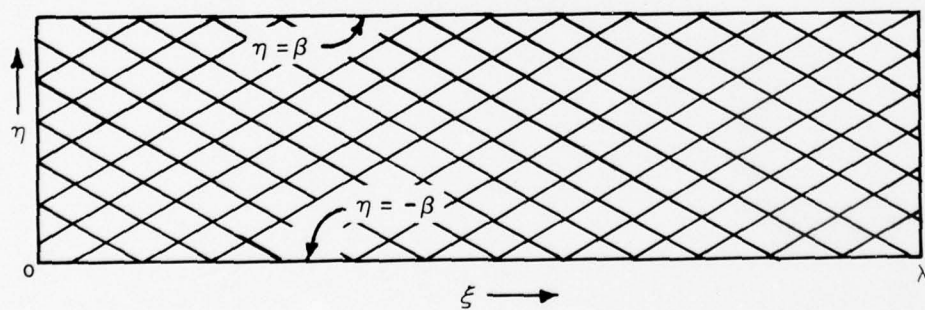
$$\begin{aligned} k &= \pi/\lambda \\ 0 \leq x \leq \lambda ; 0 \leq \xi \leq \lambda \\ -\beta \leq \eta \leq \beta \end{aligned} \quad (3)$$

The N values of B_n and C_n and B_0 constitute the bi-curve fitting conformal mapping coefficients. These coefficients are determined by matching the prototype coastline and sea boundary curves at $\eta = \pm \beta$, respectively, β also being a parameter to be determined. An iterative procedure is required for determining β and the coefficients.³ Essentially, the procedure is terminated after convergence of β and the coefficients or after the transform-generated coastline and sea boundary curves are in good portrayal of those specified (personal view of the user). Typical standard deviation between transform-generated and prototype (slightly smoothed version) over the length of the curve is of the order of 2000 ft. This is achieved with 40 iterations,

* For convenience, symbols and unusual abbreviations are listed and defined in the Notation (Appendix A).



a. PROTOTYPE SPACE



b. IMAGE SPACE

Figure 1. Conformal transformation mapping prototype space into image space

$N = 100$ and at a cost of 9 min of CDC 6600 central processing time. Furthermore, the conformal mapping procedure need only be accomplished once for any large stretch of continental shelf. The computing grids appropriate to areas within that region are generated depending on the nature of the particular study, using the mapping coefficients previously determined. The computer cost in generating the grid is inconsequential to the personnel time required in the grid makeup or assigning the cell aver-aged fluid depth. The cost in generating a grid covering a relatively small extent of coast must be weighed against a large grid of similar high resolution over a long reach of coastline which costs more per prototype hour and even more so when numerous simulations are required.

PART III: MATHEMATICAL MODEL

Stretched Shelf Coordinate System

9. Consider the transform-generated coastline and sea boundary curves shown in Figure 2. The orthogonal curvilinear mesh associated with the (ξ, η) coordinates in prototype space is designated the shelf coordinate system. The display of that system in prototype space is shown in Figure 2a and its image in Figure 2b. Notice that only a portion of the entire shelf mapped area is subsequently employed for long-wave computations. Furthermore, the calculations cannot readily be performed in the image space because the cells are unevenly spaced. Centered computations are a prerequisite for finite differencing of partial differential equations. To provide an evenly spaced computing grid and, at the same time, to obtain the desired spatial resolution with the fewest possible computational points require a second transformation. This transformation preserves the orthogonal property and allows for the independent stretching of ξ and of η . The grid resulting from the second transformation is the evenly spaced computing grid, Figure 2c. The coordinate system is termed the stretched shelf coordinate system (S,T).

10. The stretched shelf coordinate system is generated by independently transforming the ξ and η axes in the following manner:

- a. Given the nearshore region of principal interest, the values of ξ along the coastline are determined which will produce a constant relatively fine increment of coastline arc length, S_p . In this area of prime interest, the line BC in Figure 2a, the constant increment of arc length is equal to ΔS . However, regions AB and CD show that for the same ΔS as above, there is a relative expansion of the increment of the coastline arc length. The functional relation between ξ and S is

$$S = S(S_p(\xi)) \quad (4)$$

where the expansion of S_p with respect to S is specified by an (arbitrary) expression of the form

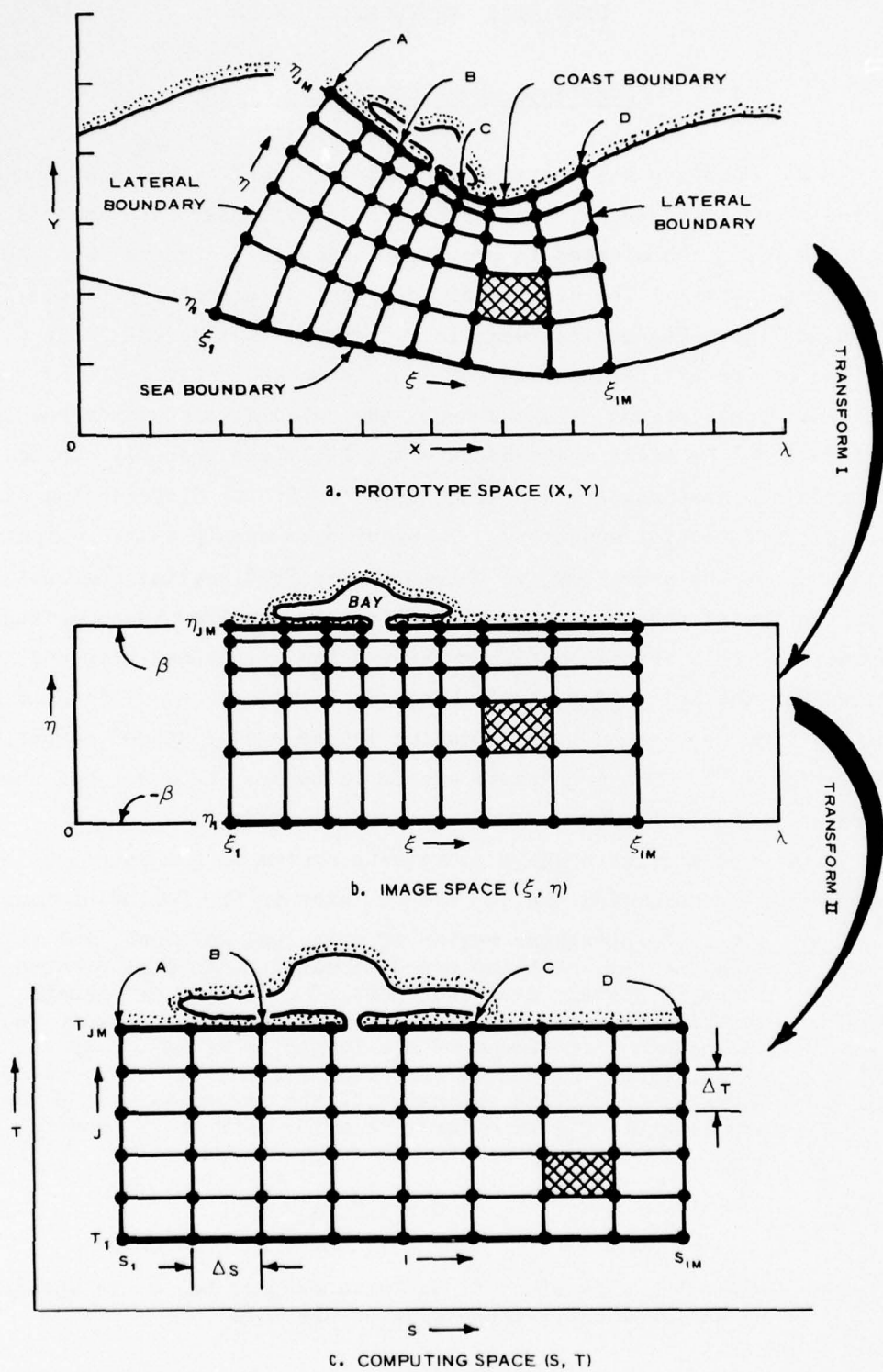


Figure 2. Grid transformations for H computing grid

$$S_p = k_A + k_B (S)^{k_C} \quad (5)$$

where A, B, and C are constants for each expansion region (k). For the example in Figure 2, there are three expansion regions. The ensemble function, $k = 1, 2$, and 3 , is determined such that at interface points the function is continuous and has continuous first derivatives.

- b. Along a particular isoline of ξ, ξ^\dagger , the values of η are determined which will yield a constant change in the time, ΔT , required for a long wave traveling at the local free wave celerity to proceed from the sea boundary ($-\beta$) to the coast (β). The long-wave travel time, T_n , is calculated by

$$T_n = \int_{S_n(\eta)} \frac{ds}{\sqrt{gD_o}} \quad (6)$$

where S_n is the distance along ξ^\dagger , g is the acceleration due to gravity, and D_o is the local depth relative to mean sea level for a standard basin. This procedure provides a fine grid spacing in the nearshore and a coarse grid near the deep sea boundary. The relation between η and T is given by

$$T = T(T_n(S_n(\eta))) \quad (7)$$

The incremental values of T are determined from Equation 6 subject to the (arbitrary) expansion relation of $T(T_n)$ which is the counterpart of Equation 5. Actually, the relation $T(T_n)$ is a convenience (seldom used in applications) which permits an additional degree of freedom in adjusting the relative spacing between isolines of η . In most applications, $T = T_n$ and the value of ΔT is that which divides the total long-wave travel time by an integer number of lines of η . The selection of ΔT relative to the coarse deep sea spacing is based upon a compromise for providing adequate resolution of the hurricane winds and the deepwater surge with a minimum number of points. At first glance, it would appear that the T axis for hydrodynamic long-wave calculations is time; however, this is not the case. Scale factors relating the transformation of η to T are involved in the equations resulting in dimensions of length for the T independent variable.

11. The stretched shelf coordinate system provides a grid system

with a finer resolution near the coast than at the deep sea boundary. The expansion curve, $S(S_p)$, stretches the alongshore reach of the grid while maintaining a finer grid in the area of principal interest. In this manner, an economy is achieved in terms of the number of grid points required for long-wave simulation. However, because the preferred expansion curves dictate the locations (in prototype space) of the fluid depths required for the long-wave calculations, the depth field must be redefined for different combinations of stretching functions.

Governing Equations

12. The vertically integrated form of the quasi-linear long-wave equations in a Cartesian system is well known.¹ The appropriate forms of these equations in the stretched shelf coordinate system are

Transport (momentum) equations

$$\frac{\partial Q_S}{\partial t} - fQ_T + \frac{gD}{F\mu} \frac{\partial}{\partial S} (H - H_B) = \tau_S - \sigma_S \quad (8)$$

$$\frac{\partial Q_T}{\partial t} + fQ_S + \frac{gD}{F\nu} \frac{\partial}{\partial T} (H - H_B) = \tau_T - \sigma_T \quad (9)$$

and

Continuity equation

$$\frac{\partial H}{\partial t} + \frac{1}{F^2} \left[\frac{1}{\mu} \frac{\partial}{\partial S} (FQ_S) + \frac{1}{\nu} \frac{\partial}{\partial T} (FQ_T) \right] = 0 \quad (10)$$

where Q is the volume transport per unit width (units of length²/time), τ is the wind stress divided by water density, σ is the bottom frictional resistance stress divided by water density, f is the Coriolis parameter, g is the acceleration due to gravity, H is the sea surface elevation relative to mean sea level, D is the total

instantaneous depth of water ($=H - D_0$), D_0 the water depth relative to mean sea level, and H_B is the hydrostatic elevation of the sea surface corresponding to the atmospheric pressure anomaly. The independent variables are time (t) and the coordinates (S, T). The terms F , μ and ν are variable scale factors associated with the transformations. It can be shown that F is nondimensional and given by

$$F = \left[\left(\frac{\partial x}{\partial \xi} \right)^2 + \left(\frac{\partial y}{\partial \xi} \right)^2 \right]^{1/2} \quad (11)$$

The μ and ν scale factors are

$$\mu = \frac{\partial \xi}{\partial S_p} \frac{\partial S_p}{\partial S} \quad (12)$$

and

$$\nu = \frac{\partial \eta}{\partial S_n} \frac{\partial S_n}{\partial T_n} \frac{\partial T_n}{\partial T} \quad (13)$$

It can be shown that $\mu(\delta S)$ and $\nu(\delta T)$ have the dimensions of length. Furthermore, $F^2 \mu \nu$ corresponds to the Jacobian of the transformation in the sense that

$$A = \iint_R F^2 \mu \nu \, dS \, dT \quad (14)$$

where A is the area of a closed region in prototype space whose corresponding area in the computing space is R (see Figure 2 for details). This relation assures that all area enclosed by the limits of the curvilinear grid in prototype space is accounted for in the computing space by use of the scale factors.

13. The kinematic wind-stress components τ_S and τ_T are related to their x, y component counterparts (τ_x, τ_y) at a given point in prototype space by

$$\tau_S = \tau_x \cos \theta + \tau_y \sin \theta \quad (15)$$

and

$$\tau_T = -\tau_x \sin \theta + \tau_y \cos \theta \quad (16)$$

where

$$\theta = \tan^{-1} \left(\frac{\partial y / \partial \xi}{\partial x / \partial \xi} \right) \quad (17)$$

The relation between the wind stress and wind speed at a reference anemometer level (usually taken near the water surface) is taken as

$$\tau = K W_{10}^2, \quad K = \frac{\rho_a}{\rho_w} C_d \quad (18)$$

where ρ_a is air density and ρ_w is water density, C_d is a non-dimensional drag coefficient, and W_{10} is the wind speed at an elevation of 10 meters above the water surface. The value of K is taken as

$$K = \begin{cases} 1.1 \times 10^{-6} & , \text{ if } W_{10} \leq 13.58 \text{ knots} \\ \left[1.1 + 2.5 \left(1 - 13.58/W_{10} \right)^2 \right] 10^{-6} & , \text{ if } W_{10} > 13.58 \text{ knots} \end{cases} \quad (19)$$

This form for K was used in previous studies.^{3,5} Recent compilation⁶ of various results relating C_d to the wind speed at 10 meters is shown in Figure 3. As reference, the dashed line in Figure 3 shows the C_d relation based on Equation 19 with $\rho_a/\rho_w = 0.0012$. In the middle to low wind speed range (say, less than 60 knots), Equation 19 is representative of the data. It is this range of wind speeds that were used by Reid and Bodine⁵ in studies of historical storm surges in Galveston Bay. Wanstrath,³ on the other hand, in studying three historical storm surges, each in different coastal regions computed coastal water levels in good agreement with observed conditions using

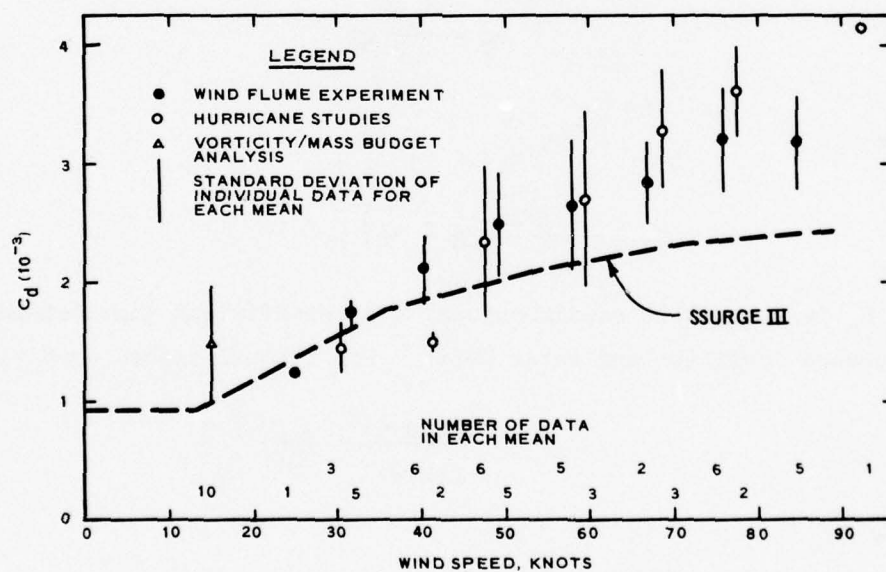
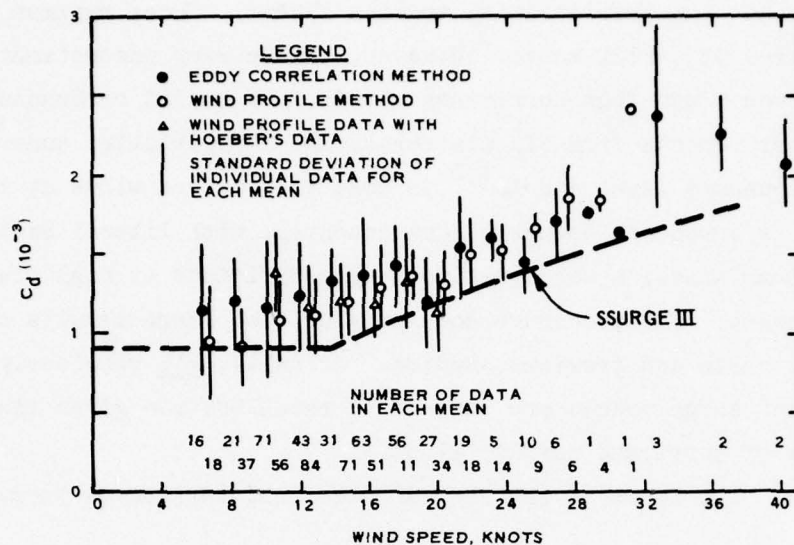


Figure 3. Mean values of the neutral drag coefficient as a function of low and high wind speeds at 10 m height (from Garratt, 1977) and that used in SSURGE III

Equation 19 and estimates of the wind furnished by the Hydrometeorological Section (Hydromet) of the National Weather Service (NWS), National Oceanic and Atmospheric Administration (NOAA). Those maximum winds ranged from 95 to 120 knots. However, the current understanding of the surface winds from hurricanes obtained by aerial reconnaissance, anemometer records from oil platforms, and sophisticated numerical marine boundary layer models^{7,8} is that the surface winds at 10 meters are not as severe as thought. Consequently, with liberal estimates for the maximum winds, a conservative drag coefficient at high wind speeds is necessary. The procedure does provide good surge results as evidenced by these and previous studies. Actually, all previously reported open-coast surge models are subject to recalibration given the recent findings of hurricane surface winds.

14. The forms of the seabed frictional resistance terms are

$$\sigma_S = \frac{K_o Q}{D^2} Q_S \quad (20)$$

and

$$\sigma_T = \frac{K_o Q}{D^2} Q_T \quad (21)$$

where

$$Q = (Q_S^2 + Q_T^2)^{1/2} \quad (22)$$

and K_o is a variable nondimensional drag coefficient that depends on the seabed condition and water depth. For typical seabed conditions,

$$K_o = \frac{0.025^2}{(1.49)^2} (D^*)^{-1/3} \quad (23)$$

where

$$\begin{aligned} D^* &= 0.25, \text{ if } D < 0.5 \\ D^* &= 1.0, \text{ if } 0.5 \leq D < 1.5 \\ D^* &= 2.0, \text{ if } 1.5 \leq D < 2.5 \end{aligned} \quad (24)$$

and all depths D and D^* are in feet.

Recursion Equations

15. The numerical analogs of Equations 8-10 are based on centered difference approximations of all terms. The algorithm treats the time dependency explicitly and employs computing lattices as shown in Figure 4. The recursion equations require two time levels to complete the cycle. H values as well as H_B and τ are computed on the lattice at time level n . This lattice also contains the permanent storage data of D_0 , θ , X_g , and Y_g where X_g and Y_g are the x and y grid coordinates of H points. For a reference index (I,J) , the transports Q_S and Q_T are computed at $\Delta S/2$ and $\Delta T/2$, respectively, from the H point in the positive axes direction. The transports are computed on the lattice at time level $n+1$. For small time steps, Δt , it is inconsequential that τ is computed at n and applied at $n+1$. Furthermore, τ is computed at H point locations and averaged with its neighbor in the S and T directions, respectively, for determination of τ_S and τ_T . These approximations for τ are a result of efficient utilization of computer time and memory considerations and can be shown through numerical experiments to be accurate.

16. Consider that the transports are known at time level $n-1$ and the H field is known at time level $n-2$. The recursion formula for interior grid H points is

$$H(I,J,n) = H(I,J,n-2)$$

$$\begin{aligned}
 & - \frac{2\Delta t [F_U(I,J)Q_S(I,J,n-1) - F_U(I-1,J)Q_S(I-1,J,n-1)]}{M_F \Delta S \mu_H(I) [F_H(I,J)]^2} \\
 & - \frac{2\Delta t [F_V(I,J)Q_T(I,J,n-1) - F_V(I,J-1)Q_T(I,J-1,n-1)]}{M_F \Delta T \nu_H(J) [F_H(I,J)]^2}
 \end{aligned} \tag{25}$$

where I , J , and n indices express the S , T , and time

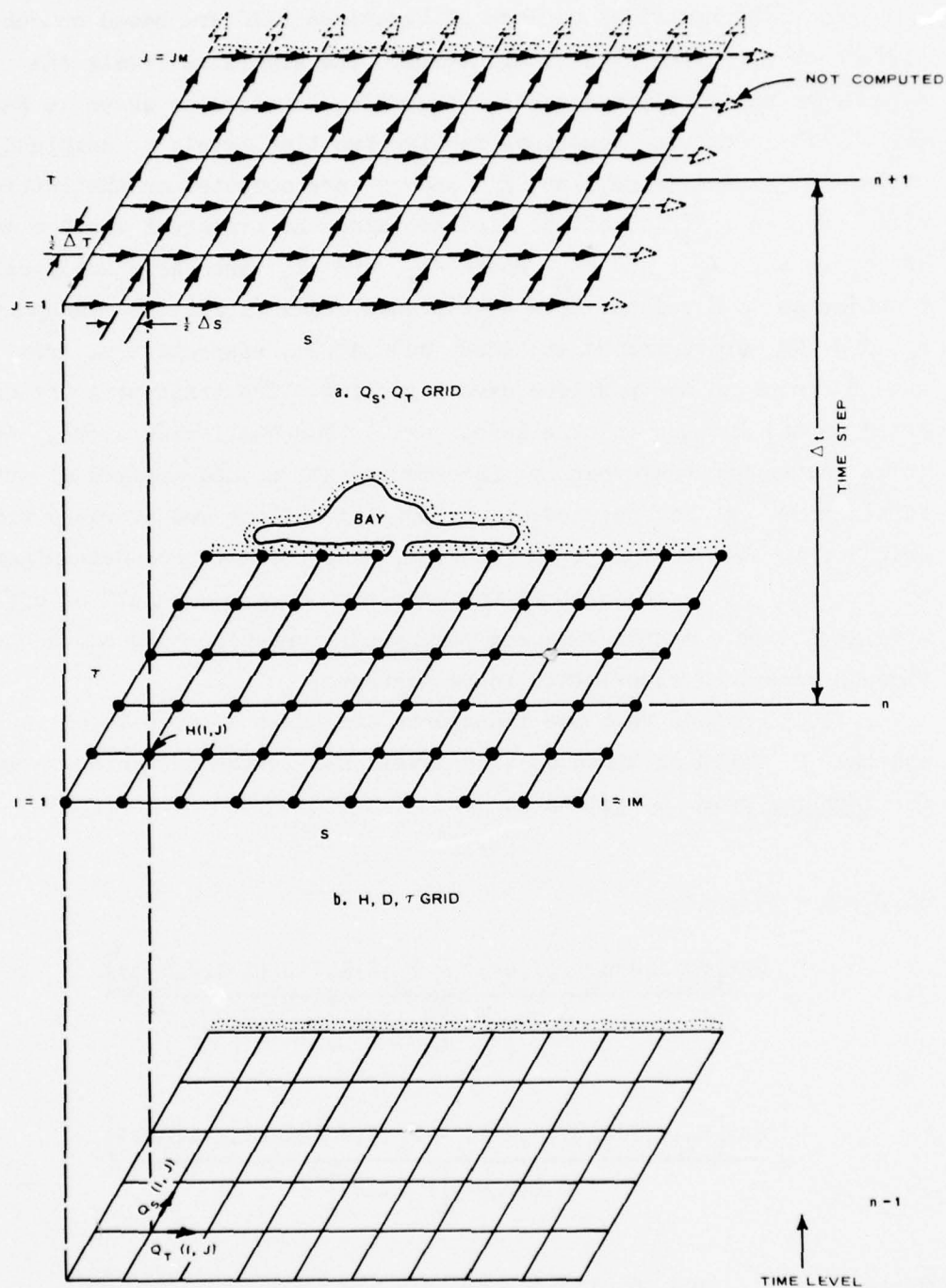


Figure 4. Time-dependent scheme for computed variables

coordinates, respectively, Δt is the numerical time step, F_U , F_V , and F_H are the point values of F from Equation 11 determined at Q_S , and H points, respectively, μ_H is the point value of μ from Equation 12 at S_I (typical H grid points in S direction), v_H is the point value of v from Equation 13 at T_J (typical H grid points in T direction), and M_F is the map factor relating prototype length (feet) to x,y units. The simulation is initiated at $n = 1$ with all transports and previous H field equal to zero.

17. Given the H field just computed at level n and the previous transports, the recursion formulas for interior grid transports are

$$Q_S(I,J,n+1) = \frac{Q_S(I,J,n-1)}{G_S} + \frac{2\Delta t f \bar{Q}_T}{G_S} - \frac{2\Delta t g \bar{D}_S [H(I+1,J,n) - H(I,J,n) - H_B(I+1,J,n) + H_B(I,J,n)]}{M_F \Delta S G_S \mu_U(I) F_U(I,J)} + \frac{\Delta t}{G_S} [\tau_S^H(I,J,n) + \tau_S^H(I+1,J,n)] \quad (26)$$

and

$$Q_T(I,J,n+1) = \frac{Q_T(I,J,n-1)}{G_T} - \frac{2\Delta t f \bar{Q}_S}{G_T} - \frac{2\Delta t g \bar{D}_T [H(I,J+1,n) - H(I,J,n) - H_B(I,J+1,n) + H_B(I,J,n)]}{M_F \Delta T G_T v_V(J) F_V(I,J)} + \frac{\Delta t}{G_T} [\tau_T^H(I,J,n) + \tau_T^H(I,J+1,n)] \quad (27)$$

where

$$\bar{D}_S = 0.5 [H(I+1,J,n) - D_O(I+1,J) + H(I,J,n) - D_O(I,J)] \quad (28)$$

$$\bar{D}_T = 0.5 [H(I, J+1, n) - D_O(I, J+1) + H(I, J, n) - D_O(I, J)] \quad (29)$$

$$\begin{aligned} \bar{Q}_S = 0.25 [& Q_S(I, J+1, n-1) + Q_S(I, J, n-1) \\ & + Q_S(I-1, J-1, n-1) + Q_S(I-1, J, n-1)] \end{aligned} \quad (30)$$

$$\begin{aligned} \bar{Q}_T = 0.25 [& Q_T(I+1, J, n-1) + Q_T(I, J, n-1) \\ & + Q_T(I, J-1, n-1) + Q_T(I+1, J-1, n-1)] \end{aligned} \quad (31)$$

$$G_S = 1 + K_O^S \left\{ [Q_S(I, J, n-1)]^2 + (\bar{Q}_T)^2 \right\}^{1/2} / (\bar{D}_S)^2 \quad (32)$$

$$G_T = 1 + K_O^T \left\{ [Q_T(I, J, n-1)]^2 + (\bar{Q}_S)^2 \right\}^{1/2} / (\bar{D}_T)^2 \quad (33)$$

μ_U , in a similar manner, is the point value of μ from Equation 12 at $S_I + \Delta S/2$ (typical Q_S grid points in the S direction), v_V is the point value of v from Equation 13 at $T_J + \Delta T/2$ (typical Q_T grid points in the T direction), τ_S^H and τ_T^H are the wind stresses in the S, T directions, respectively, which are computed at H points, and K_O^S , K_O^T are the seabed drag coefficients computed from Equation 23 with D in Equation 24 given by \bar{D}_S and \bar{D}_T , respectively.

Boundary Condition

18. For the studies reported in PART IV, two general types of simulations were conducted. Numerical simulations of hydraulic physical model studies require that the lateral boundaries, $I = 1$ and $I = IM$, be portrayed as walls. The sea boundary is specified by time-dependent water elevations, $H(I, 1, n)$, similar to that observed in the physical model. In some of these studies, reference is made to hurricane or surge simulations. To be precise, $H(I, 1, n)$ is a transient response function but no wind stress is applied in either the physical or numerical model. The coast boundary condition is the

Finite Height Barrier Coast (FHBC) which is detailed later.

19. Numerical simulations of hurricane-induced surges require other forms for the lateral boundary conditions. Many different continuum type boundary conditions are reported in the literature. In principle, it should not matter which of these is used. If the computing grid is of sufficiently large extent, the solution in the central part of the grid near the coast should be insensitive to the particular one used. A popular lateral boundary condition which is also used in SSURGE III is

$$\frac{\partial Q_S}{\partial S} = 0 \quad (34)$$

The sea boundary condition is that the water-surface elevation is placed in equilibrium with the atmospheric pressure anomaly

$$H(I,1,n) = H_B(I,1,n) \quad (35)$$

Along the lateral and sea boundaries, the transports are computed using modified forms of Equations 30 and 31. The modification is to compute an average value using only the two adjacent interior points.

20. It has long been recognized that the coast boundary condition plays a major role in the nearshore hydrodynamic solution of the governing equations. Most open-coast shelf models (whether curvilinear, rectilinear, finite element, implicit, or explicit) treat the coast as an infinitely high, continuous wall. The use of numerical models in simulating circulation and water level conditions is made difficult because of application of such a condition. The coast boundary condition developed and incorporated into SSURGE III is the FHBC. The FHBC provides for the overtopping of low-lying land and bay communication with the open sea.

21. The FHBC condition is to allow for potential ponding areas landward of the shoreline. Figure 5 shows the conceptual design of the barrier coast and adjacent bay. The bay is shown to be of several increments of ΔS in length. The coast flooding routine permits a volume of water to be transported across the nominal shoreline which is dependent

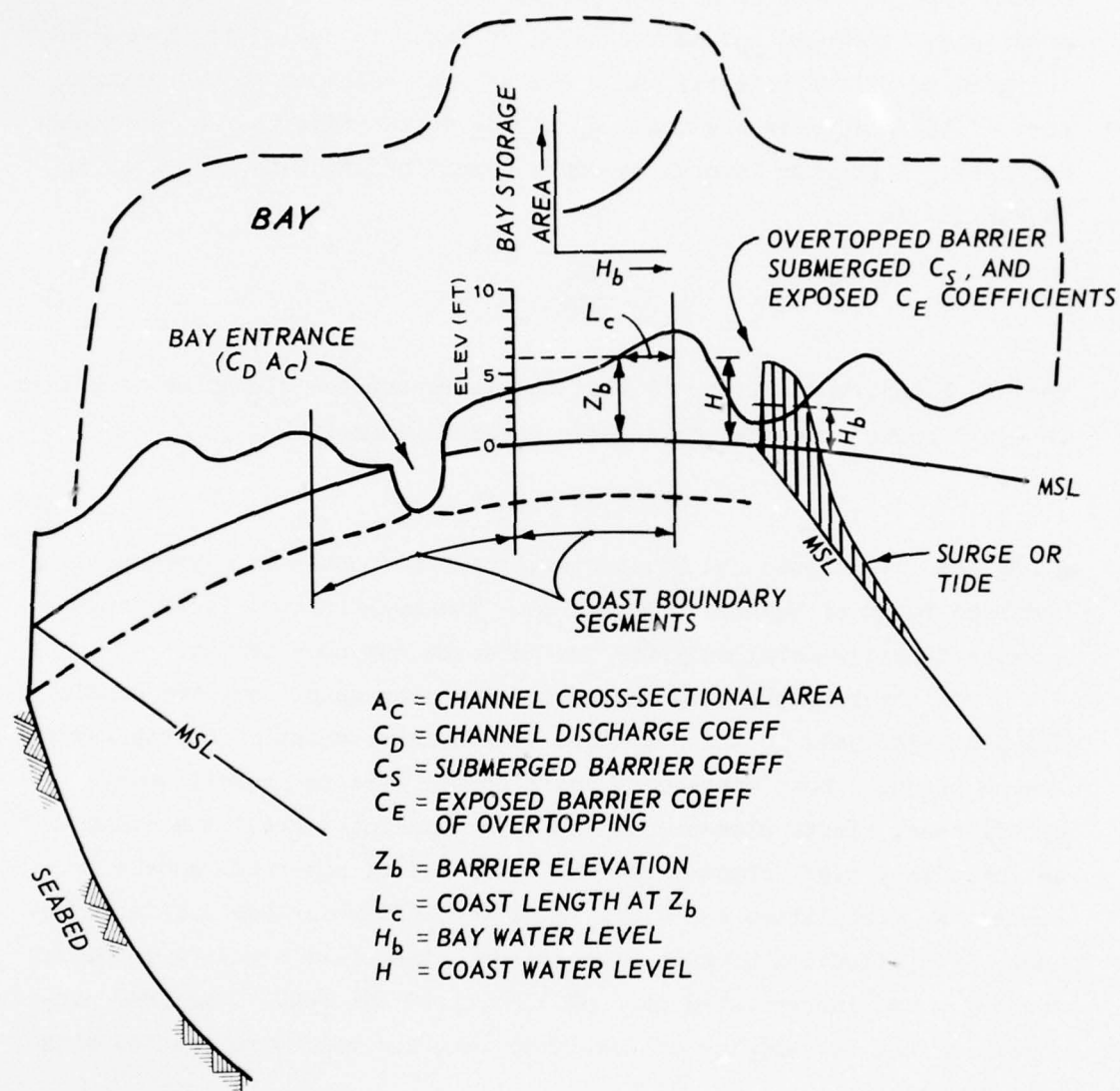


Figure 5. Finite Height Barrier Coast (FHBC) boundary

upon barrier heights, predicted water level at the coast, channel entrance characteristics, and the water level in the ponding area, H_b . The routine is applied at the H time levels as shown in Figure 4.

22. A prediction/correction method is used to compute $H(I, JM, n)$. The philosophy is taken that the coast barrier as viewed by the long wave is essentially a wall over much of the time of surge development, reflecting the majority of the long-wave energy. This results from the consideration that long-wave reflection occurs when the wave experiences a significant change in fluid depth over distances that are small relative to the wavelength.^{9,10} The typical nearshore bathymetry combined with coastal barrier elevations assures that the coast is essentially a wall which leaks water.

23. The prediction/correction method is to first assume total reflection at the boundary and then to correct that prediction of H based on a finite height coast. In this manner, the method provides a smooth transition from the time-dependent circumstances where the boundary is not flooded and no corrections are required to the catastrophic flooding coast. Other relations for predicting H at the coast than that of total reflection were considered. In particular, a water-surface slope projection method was tested. Results of these tests which are presented in PART IV show the method to be inappropriate for surge simulations. Other tests (results not presented) imply that the slope projection method is applicable to tidal (free wave) simulations.

24. At time level n , the water level at the coast, H^+ , is predicted. If the water levels, H^+ and H_b , exceed the minimum height of the coast, then a volume of water is transported across the nominal coast for the time interval, $n-1$ to $n+1$,

Submerged Barrier

$$V_A^k = 2C_{S_h} \Delta t \Delta L_c^k \sqrt{g|D_h|} \quad (35)$$

where

$$D_h = H^+ - H_b \quad (36)$$

$$\Delta L_c^k = |L_c^k - L_c^{k+1}| \quad (37)$$

C_S is a nondimensional submerged barrier coefficient taken as 0.4, L_c^k and L_c^{k+1} are lengths of the coast at elevations Z_b^k and Z_b^{k+1} , respectively, and the direction of the flow is determined by the sign of D_h (positive means water is removed from the coastal cell and placed in the ponding area). Barrier heights per ΔS section centered on H points are discretized into unit elevations (k). The length of the coast at each elevation is obtained from topographic maps, beach surveys, etc. The total volume of water crossing the submerged coast is the summation of Equation 35 for $k = 0, 1, \dots, K$ where K is the integer of the lesser of H^+ or H_b . Considering large ponding areas and high minimum coastal heights, this volume is generally small compared with that which is transported through channels or which overtopped the exposed (on one side) section of the barrier. These submerged barrier equations reflect the assumption that frictional effects are dominant in the bottom layer which is continuous across the boundary.

25. For the overtopped barrier, the volume of water crossing the coast is

Exposed (on one side) Barrier

$$V_B^k = 2C_E D_b^k \Delta t \Delta L_c^k \sqrt{g |D_b^k|} \quad (38)$$

where

$$D_b^k = \begin{cases} Z_b^k - H_b, & \text{if } H^+ < Z_b^k \leq H_b \\ H^+ - Z_b^k, & \text{if } H_b < Z_b^k \leq H^+ \end{cases} \quad (39)$$

C_E is a nondimensional exposed barrier coefficient taken as 0.2 and the direction of flow is determined by the sign of D_b . The total volume of water overtopping the coast is the summation of Equation 38 for $k = 0, 1, \dots, M$ where M is the integer of the greater of H^+ or H_b .

26. The volume of water associated with channel communication is

$$V_C = \pm 2\Delta t \left(C_D A_c \sqrt{g|H^+ - H_b|} + W_c D_c \sqrt{gD_c} \right) \quad (40)$$

where

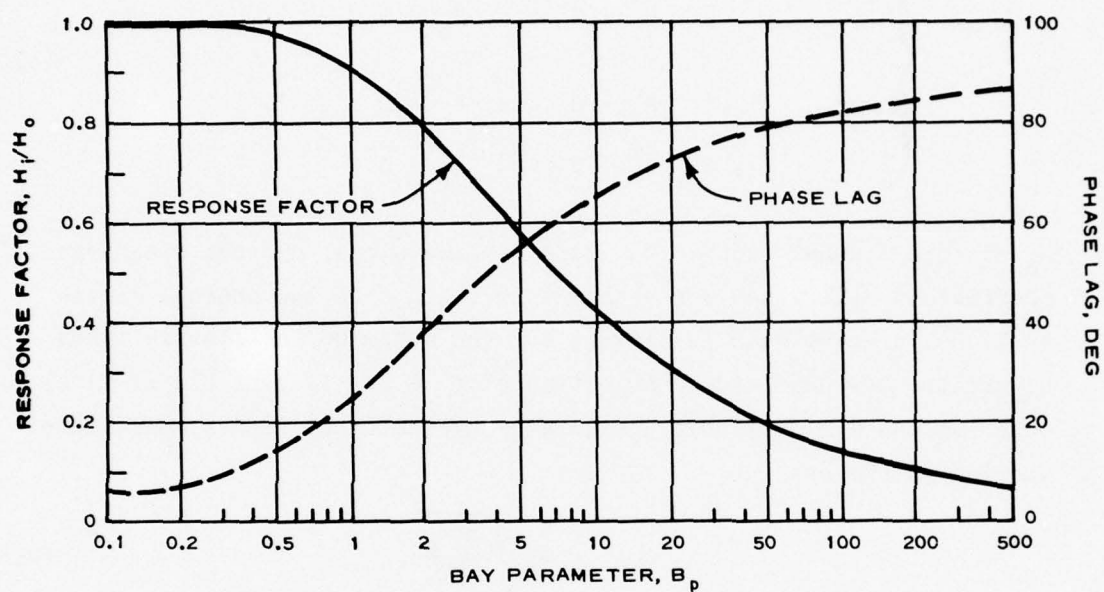
$$D_c = \begin{cases} |H^+ - H_b|, & \text{if } H^+ > 0 \text{ and } H_b > 0 \\ H^+, & \text{if } H^+ > 0 \text{ and } H_b < 0 \\ H_b, & \text{if } H^+ < 0 \text{ and } H_b > 0 \\ 0, & \text{if } H^+ < 0 \text{ and } H_b < 0 \end{cases} \quad (41)$$

W_c is the channel width, C_D is a nondimensional channel discharge coefficient determined for each entrance, A_c is the channel cross-sectional area at mean sea level, and the sense of the flow is taken toward the low head side. An estimate of $C_D A_c$ is possible if tidal observations are available inside and outside a bay with a constricted opening to the sea

$$C_D A_c = \frac{A_s}{T} \sqrt{\frac{32\pi H_o}{3gB_p}} \quad (42)$$

where A_s is the surface area of the bay at mean sea level, T is the tidal period, H_o is the tidal range outside the bay, and B_p is a nondimensional bay parameter that is dependent on the response (H_o/H_i) or phase lag. H_i is the tidal range inside the bay. The bay parameter as a function of response or phase lag is shown in Figure 6.¹¹

27. Consider that H^+ values along the coast (uncorrected for flooding) are known at time level n and H_b and A_b are known at level $n-2$ where A_b is the bay storage area. The volume of water entering (or leaving) the ponding area is determined for each segment by the appropriate sum of V_A^k , V_B^k , and V_C . The ratio of that volume to the surface area of the grid block representative of H^+ , A_I , provides the incremental correction to the predicted coastal water level to conserve mass. This value is stored in $H(I, JM, n)$ for use in



NOTE: H_i = TIDAL RANGE
INSIDE THE BAY
 H_o = TIDAL RANGE
OUTSIDE THE BAY

Figure 6. Bay parameter B_p as a function of response factor or phase lag

the transport computations at level $n+1$. The new value of H_b at time level n is H_b at $n-2$ plus the incremental water level change from the instantaneous and even distribution of the entering volume (the sum for all appropriate ΔS segments) on A_b at level $n-2$. From H_b at n , a new bay storage area is obtained. The above is repeated for each ponding area and its designated coastal segments.

Hurricane Wind and Atmospheric Pressure Models

28. The hurricane wind and atmospheric pressure models as given by Jelesnianski¹² are employed in the surge studies with some minor additions. The x,y-wind components for a stationary storm at the H grid points are

$$w_x = \frac{W_R}{r_H} \left[-(X_g - X_e) \sin \phi - (Y_g - Y_e) \cos \phi \right] F(r_H) \quad (43)$$

and

$$w_y = \frac{W_R}{r_H} \left[(X_g - X_e) \cos \phi - (Y_g - Y_e) \sin \phi \right] F(r_H)$$

where

$$r_H = [(X_g - X_e)^2 + (Y_g - Y_e)^2]^{1/2} \quad (44)$$

$$F(r_H) = \begin{cases} \left(\frac{r_H}{R_H} \right)^{3/2} & , \text{ if } r_H < R_H \\ \left(\frac{R_H}{r_H} \right)^{1/2} & , \text{ if } r_H \geq R_H \end{cases} \quad (45)$$

W_R is the stationary storm maximum wind, ϕ is the wind ingress angle reflecting the inward flow relative to that wind vector tangent to the isovel, R_H is the distance from the storm center (X_e, Y_e) to region of maximum winds, and X_g and Y_g are the (x,y) coordinates of H grid

points. The translation of the storm provides an alteration in the wind field. The x,y supplemental wind components due to storm translation are

$$t_x = (T_x \cos \psi + T_y \sin \psi)G(r_H) \quad (46)$$

and

$$t_y = (-T_x \sin \psi + T_y \cos \psi)G(r_H) \quad (47)$$

where

$$\psi = \alpha - \phi - 90 \quad (48)$$

$$G(r_H) = \begin{cases} \frac{r_H}{r_H + R_H} & , \text{ if } r_H < R_H \\ \frac{R_H}{R_H + r_H} & , \text{ if } r_H \geq R_H \end{cases} \quad (49)$$

T_x and T_y are x,y components of the forward speed of the storm and α is a rotation angle used, primarily, to fine tune the alignment of maximum winds. For standard operation of the wind model, α is set equal to $90^\circ + \phi$. The x,y-wind stress components for a moving storm are

$$\tau_x = K \left(W_x^2 + W_y^2 \right)^{1/2} W_x \quad (50)$$

and

$$\tau_y = K \left(W_x^2 + W_y^2 \right)^{1/2} W_y \quad (51)$$

where

$$W_x = w_x + t_x \quad (52)$$

$$W_y = w_y + t_y \quad (53)$$

and K is given by Equation 19. The stress components in the stretched shelf coordinate system are determined by applying Equations 50 and 51 in Equations 15 and 16. In an alternate manner,

$$W_S = W_x \cos \theta + W_y \sin \theta \quad (54)$$

and

$$W_T = -W_x \sin \theta + W_y \cos \theta \quad (55)$$

where θ is given by Equation 17 and W_S and W_T are the wind components in the (S,T) system. The stress components are

$$\tau_S = K \left(W_S^2 + W_T^2 \right)^{1/2} W_S \quad (56)$$

and

$$\tau_T = K \left(W_S^2 + W_T^2 \right)^{1/2} W_T \quad (57)$$

29. The surface atmospheric pressure field associated (but not dynamically coupled) with the hurricane wind is

$$P = P_O + (P_\infty - P_O) e^{-R_H/r_H} \quad (58)$$

where P_O is the central pressure and P_∞ is the far-field pressure. It is often observed that relatively high winds remain along the coast after the storm has proceeded inland. Through numerical experiments, it is found that reasonably good comparison between observed (Hydromet) and computed winds is obtained by setting R_H to be the distance the storm center is from the coast, specifying W_R to be desired winds at the coast and setting α (measured clockwise from the storm movement) such that the maximum wind region is along the coast. This procedure allows slightly longer simulations to be performed after landfall than

would be permitted otherwise due to poor wind field portrayal. However, R_H in the pressure expression (Equation 58) is not allowed to increase. If this procedure is followed in the numerical program (it is optional), R_H is held constant at a value R_{HIT} in nautical miles (n.mi.) after the time of storm landfall (THIT) which is input in hours after the start of the simulation.

30. The various program parameters that are used to generate the wind and atmospheric pressure fields for Hurricanes Donna, Flossy,¹³ Hilda,¹⁴ Betsy,¹⁵ and Carmen are given in Tables 1-5. Only for the postlandfall winds from Hurricanes Hilda, Betsy, and Carmen were the normal routines modified in the above manner. This is seen by noting the number for THIT.

31. The term H_B in Equations 8, 9, 26, 27, and 35 is computed in feet of water by

$$H_B = 0.0328(P_\infty - P) \quad (59)$$

where P_∞ , named PINF in Tables 1-5, and P_0 are in pressures of millibars.

32. For historical storms, all necessary input parameters can be determined if Hydromet has assessed the maximum winds W_R following the same procedures. This procedure probably results in a liberal estimate for W_R . Storm surge simulations for forecasting purposes typically involve storm parameters of track, P_∞ , P_0 , and R_H . The only other necessary input for this wind model is W_R . This can be determined from the correlation of a few severe historical storms where Hydromet has estimated W_R and that value which is predicted by the Standard Project Hurricane (SPH) method¹⁶ using only the required forecast storm parameters. A cursory examination shows that the ratio W_R to $W_{max}(SPH)$ is probably in the range 1.2 to 1.3. This approach is suggested only as a temporary solution. Actually, a dynamic marine boundary layer hurricane model is needed that is independently calibrated to several storms of record and verified against even more historical storms. This wind model is comparable to the treatment of the physics of the atmosphere as SSURGE III is to the hydrodynamics.

PART IV: MATHEMATICAL MODEL APPLICATIONS

33. The results of five studies are reported. In all but one study, simulations of different events were performed to assess the behavior of the FHBC under varying conditions. Two studies, the Galveston Bay and Murrells Inlet studies, compare the free wave solution as observed in the physical model and computed in the mathematical model. Furthermore, the solutions are for the nearshore, open sea waters and not, per se, for the interior of the bay or inlet. In some cases, the prototype data used to calibrate the physical model are used. The plates, reflecting the results of these studies, refer to "surge" or "hurricane" simulations. As noted previously, the sea boundary water level is specified as a transient response function and no wind stress is applied in either the physical or numerical model.

34. The remaining three studies deal with a computing grid sensitivity study and actual hurricane surge simulations from historical storms. The grid sensitivity study compares the surge results obtained from variable spaced and evenly spaced rectilinear computing grids. The storm surge from Hurricane Donna is simulated along the west coast of Florida for a wall and flooding coast conditions. The final study is of the storm surges from Hurricanes Flossy, Hilda, Betsy, and Carmen which affected the Louisiana coast from Atchafalaya Bay to the Mississippi River.

Galveston Bay Physical Model Study

35. The Galveston Bay physical model¹⁷ was constructed for study of hurricane surge routing. The physical model results or observed (prototype) data are from that report. The general computing grid, location map of tide or velocity gages, particular computing grid points, and channel entrance details are presented in Plate 1. The FHBC data are given in Table 6.

36. The procedures used in both the numerical and physical models were to input a water level at the respective sea boundaries such that

the hydrograph at Pleasure Pier, sta 1, is reproduced. This procedure is followed for the astronomical tide, Hurricane Carla and large radius, high translation (LRHT) hurricane simulations. The hydrograph at Pleasure Pier from the numerical model and the prototype (essentially, that recorded in the physical model) is presented in Plate 2. Having achieved the proper input, the numerical portrayals for the flow in the nearshore, channel entrance velocity, and H_b hydrograph are obtained. Plates 3 and 4 show the depth-averaged velocity fields, as determined by SSURGE III, in the Galveston Channel entrance region for the flood and ebb stages, respectively. For the tide simulation, the numerical program was specially altered to crudely portray the north and south entrance jetties. By doing this, better agreement in the comparison between the prototype and numerical model entrance channel velocity is accomplished. This velocity comparison is shown in Plate 5 where, in addition, the velocity at Rollover Pass is present. For the tide range, Rollover Pass is essentially a wall. Consequently, one can conclude that if a wall were placed across the main entrance--not following the FHBC--an inappropriate simulation would result. The response of Galveston Bay at selected "mean" stations and the computed H_b are shown in Plate 6. Although the velocity fields shown in Plates 3 and 4 are seemingly very representative of what one should expect to occur, the detailed entrance velocity comparison shows that the FHBC overreacts to the small semidiurnal component. This should be expected in such cases because the numerical solution does not contain the inertia of Galveston Bay. Considering that the computer cost for a simulation is about a couple of dollars, reasonable results are obtained.

37. The hydrographs at Pleasure Pier for the Hurricane Carla simulation are shown in Plate 7. The FHBC solution at the grid boundary for the channel (Plate 8) shows a small 0.4-ft drawdown relative to the peak of sta 1. The computed peak elevation occurs nearly in phase with sta 1. For comparison, the hydrograph at sta 4 is presented and shows it to lag that of the open-coast records. Consequently, it is thought that the numerical solution at the boundary does follow that expected for the nearshore open-coast waters. No physical model entrance

channel velocities were recorded. The numerical model velocities of the Galveston Entrance Channel and Rollover Pass are presented in Plate 9 for comparative purposes with the tidal results and the LRHT hurricane results. The computed H_b is in reasonable agreement with the bay hydrograph at sta 7 shown in Plate 10.

38. The special procedure for numerically simulating the jetties was not included in the program for this or the LRHT case because the jetties were readily overtopped at these water levels. It is not known if the channel velocity should be amplified in accord with that found for the tidal simulation. It is recommended that the numerical program be generalized such that it can treat open-coast structures of finite height. In the study of Murrells Inlet, it is difficult to assess the model's behavior because of the lack of such program features.

39. Plates 11-14 are for the LRHT simulation and follow in similar designation those for the Hurricane Carla simulation. Again, it is noted that the FHBC solution at the grid boundary shows a drawdown of 0.7 ft relative to the peak at sta 1. The phase of the peak occurs nearly midway between sta 1 and 4 (Plate 12). However, relative to the amplitudes, the FHBC boundary solution would appear to follow that of the expected entrance condition. The comparison of Plates 9 and 13 provides qualitative assurance that the model is responding in accord with expected conditions. Although the agreement between H_b and sta 7 in phasing and amplitude is not as good as in the other simulations, H_b is representative of the bay water elevations (Plate 14).

Murrells Inlet Physical Model Study

40. The physical model study of Murrells Inlet¹⁸ was recently completed. The physical model results for the astronomical tide simulation are from that report. The same entrance details (Plan 1H) were used for the tide and physical model surge simulations. The two surge experiments were conducted by this author with assistance from others in the Hydraulics Laboratory.

41. The computing grid and location map of tide gages are

presented in Plate 15. The FHBC data are shown in Table 7. The physical model entrance details and the computing grid for that area are shown in Plate 16. The numerical program was not specially altered to reflect these finite height open sea structures (jetties, weirs, or training dikes). As noted previously, the program can readily be generalized for proper treatment of such situations. The results comparing the physical and numerical models are presented here for two reasons. First, Murrells Inlet offers a contrasting study to the much larger Galveston Bay; second, data will exist for a subsequent study with an improved model.

42. Tide sta 10 provides the sea boundary forcing condition to the mathematical model (Plate 17). Essentially, it is also the control hydrograph for the physical model where water is added or removed at the head bay (approximately, $Y = -10$, Plate 15) such that the control hydrograph is followed. The flood and ebb stages of the depth-averaged velocity fields for the numerical tide simulation are shown in Plates 18 and 19, respectively. The velocity fields are illustrative and representative for the portrayed situation. The time history of the numerical entrance velocity located in close proximity to velocity sta 1 (Plate 16) is compared in Plate 20 with that recorded from the physical model. The flood velocity from the numerical simulation agrees, probably fortuitously, with the physical model results; however, the ebb velocity comparison does not. It is noted that these results for the flood and ebb velocity comparison also follow for the two surge simulations. Plate 21 compares the observed interior hydrographs and computed H_b . Clearly, a representative time-dependent transport of water into the bay is achieved through the FHBC procedure.

43. Plates 22-25 compare the results for a 9-ft surge simulation. The sea boundary hydrograph is presented in Plate 22 where the surge height is actually 9.8 ft relative to mean low water (mlw). The name, 9-ft surge simulation, is carried for convenience. The comparison of the numerical and physical models' water levels at the entrance is shown in Plate 23. The drawdown through the entrance channel is represented in the results of the numerical model. The velocity comparison (Plate 24) shows fair agreement in the flood and poor agreement

in the ebb. Plate 25 shows that the computed peak bay water level is in agreement with several peak water levels at selected stations; but H_b decreases too rapidly relative to observed conditions.

44. Plates 26-29 show the results for 12-ft surge experiments. The coastal and inland topographies of the physical model were accurately portrayed to an elevation of +10 ft (relative to mlw). Flooding in excess of 10 ft is constrained by the walls of the physical model.

45. The sea boundary hydrograph (Plate 26) shows the results of a numerical experiment which in addition to specifying the (known) forcing condition (H_{10}), allows that input to be instantaneously adjusted for the outward transport of water at the boundary. This numerical boundary condition is in close analog with that of the physical model controller which adds or removes water given the control hydrograph and that continuously sensed at the gage. The sea boundary condition is

$$H(I,1,n) = \begin{cases} H_{10}(n) & , \text{ if } Q_T \geq 0 \text{ (inward flow)} \\ H_{10}(n) + \frac{|Q_T(I,1,n-1)|}{\sqrt{gD_S}} & , \text{ if } Q_T < 0 \text{ (outward flow)} \end{cases} \quad (60)$$

where H_{10} is the observed hydrograph at sta 10 and $(gD_S)^{1/2}$ is a constant wave speed appropriate for deep water. For this application, D_S is taken as 500 ft. The second term in Equation 60 represents an additional rise in the water level from the outward propagating wave energy. The homogeneous form of Equation 60 is most pleasing since it involves both the water level and the local computed transport. In fact, without applying this condition the computations were unstable in the decreasing stage of the surge where the time step was taken at 10 sec. Pseudostable computations resulted when the time step was reduced to 6 sec as shown by the dashed line in Plate 27. The solid line in Plate 27 shows the results with Equation 60 and the larger time step of 10 sec. It is seen that without the radiation-type sea boundary condition, significant trapping of wave energy occurs between

the coast and sea boundary. The energy directed toward the sea boundary in the decreasing stage is much greater in this experiment than in the 9-ft surge experiment because of the overtopping of the entire coastline. For this reason, there was found to be no practical difference in the 9-ft surge results using Equation 60 and those previously presented. More testing of the radiation condition is required before it can be accepted for general use.

46. Similar results concerning the drawdown through the entrance channel as shown in Plate 23 are obtained in the 12-ft surge simulations. The previous discussions comparing the entrance channel velocities and inland hydrographs for the 9-ft surge experiments are applicable also in this case. Plate 28, which compares the entrance channel velocities for the physical and numerical models, shows fair agreement in the flood stage and poor agreement in the ebb stage. Plate 29 shows the computed H_b and selected inland hydrograph stations. As before, H_b decreases too rapidly relative to observed conditions.

Variable Grid Spacing Study

47. Two hypothetical storms, Hurricanes A and B, are employed to induce surges in a standard (or fixed) basin of specified length, width, and bathymetry. Hurricane A is an onshore moving storm while the track of Hurricane B is parallel to the coast. A variety of rectilinear computing grids are used to portray the standard basin. Grids A, B, and C are unevenly spaced in x and y, but they all have the same number and alignment of points in the x-direction. Each of these grids have different numbers of points in the y-direction since the same basin width is used. Grid D is an evenly spaced grid in both the x- and y-directions. Plate 30 shows the standard basin, the various grids, the storm parameters, and hurricane tracks. In particular, grids A, B, and C have identical computing points at $y = 82$ n.mi (or, 8 n.mi. from the coast).

48. There are no analytical or known solutions such that an assessment can be performed of the accuracy of the results from one grid

relative to the results from another grid. Rather, the approach taken here is to show that the same results are obtained from the variable spaced grids which involve the stretching functions (μ, ν) and the evenly spaced grid. Results from grids B, C, and D are presented in Plate 31 for an onshore storm and in Plate 32 for an alongshore storm. The results from the unevenly spaced grids for each type track are equivalent to that from the evenly spaced grid. The equivalent computations from grids B and C should not be generalized to typical open-coast surge conditions where varying bathymetry and coastal configurations will play a role in the calculations. The term "coastal surge envelope" refers to the peak surge water elevations along the coast without regard to the time of its occurrence. All simulations are for a 22-hr period of time with landfall for Hurricane A at 18 hr. Hurricane B, on the other hand, is located only 30 n.mi. from the right lateral boundary where, at the start of computations, hurricane force winds are imparted to the basin (initial basin water conditions are H , Q_S , and $Q_T = 0$). This procedure is not recommended for general surge modeling since the basin water is not permitted an initial transition period for spin-up. Consequently, transient conditions cause the surge envelope bubble exhibited in Plate 32 for all grids at $x = 340$ n.mi. The envelope is representative of that expected (that is, a constant) in the range $x = 120$ n.mi. to $x = 270$ n.mi. This stretch of coastal surge development corresponds to the last 10 hr of the surge simulation. It may be possible to minimize the initial model spin-up period and, at the same time, reduce the transient bubble. Development of such procedures would result in significant computer cost savings.

49. For the linear, free wave simulation in an enclosed, constant depth body of water, it can be shown that the numerical analogs of the governing equations of motion conserve mass and energy. As noted in PART III, the coastal water level is first predicted (and subsequently corrected for flooding) by assuming total energy reflection at the boundary. This condition is also used in the above-mentioned free wave seiche simulations. An alternate coastal water level prediction method is studied which linearly projects the water level to the coast boundary

from the slope of the water surface. This boundary condition does not guarantee conservation of mass. Comparison of surge results from grids A, B, and C using the slope projection boundary condition and grid B using the mass continuity (total energy reflection) method are presented in Plates 33 and 34 for Hurricanes A and B, respectively. Even for grid A, which has a very small spacing in the y-direction at the coast, the slope method proves inappropriate for surge computations. Not only are poor results computed at the coast in the principal surge development area but, since the equations of motion are integrated in time, poor agreement in the hydrographs is observed at 8 n.mi. from the coast as shown in Plate 35. However, in other applications the slope projection boundary condition did yield results (not presented) similar to those previously shown for the Galveston Bay studies. Qualitatively, reasonable results are seen to occur when the flooding coast is used with the slope projection method in grid B for the onshore storm (Plate 36) and the alongshore hurricane (Plate 37). Further testing of projection method is warranted centering on nonlinear, quadratic, or cubic projections. The method may prove useful in other applications where projection to a boundary is required.

West Coast of Florida, Hurricane Donna Surge Study

50. Hurricane Donna, which occurred in September 1960, paralleled the southwest coast of Florida, crossing the Florida Keys and landfalling near Cape Sable. Table 1 presents the storm parameters. Plate 38 shows the location map of the storm track for the last 18 hr of the 30-hr simulation and the computing grid. The Florida Keys are portrayed as a wall (Plate 38) because of the land and the highway elevations of U.S. 1. From the surge results and observed conditions, portions of the highway in the central keys were washed out or overtopped; but no attempt is made to account for this.

51. The FHBC condition is applied to the coast from 10 n.mi. north of Cape Romano to the end of the grid in Florida Bay. Table 8 presents the FHBC data. Particular to this coastal region is the

Everglades National Park and the dense population of both red and black mangroves. These trees, essentially, are the coastal barrier rather than sand dunes, sea walls etc. They are described in many studies^{19,20} and were described through personal communications with Mr. Ben McPherson, Aquatic Biologist, U. S. Department of Interior, Geologic Survey, Water Resources Division, Miami, Fla. The typical widths of the mangrove stand are from 1 to 10 miles and the minimum heights range from 10 to 15 ft, increasing to 25 ft in more inland areas. The red mangrove has a thick tangle of prop roots which act to catch and hold sediment. An agile, 6-ft tall person can supposedly move about on these roots, traversing the mangrove stand from the coast inland to the large relatively flat swamp and prairie. Above this is a thick, interweaving canopy of tree limbs, branches, and leaves. Since the mangrove characteristics relative to long-wave attenuation are not known, though it would appear that little or no attenuation should exist for the trunk portion of the tree stand,²¹ the approach taken in this study is to assume a standard tree barrier coast. This tree coast is a barrier from msl to 3 ft (a nominal beach berm plus the prop root system), from 3 to 9 ft is the trunk portion where no attenuation is assumed, and from 9 to 12 ft is another barrier portraying the canopy. Only a small length of coastline on Cape Sable is free of the mangrove as seen in Table 8. The normal FHBC routine, including barrier coefficients, was followed except in the situation where if the predicted coastal water level opposite a tree barrier exceeds 9 ft, the water level was taken as 9 ft for flooding computations appropriate to the trunk portion. For example, if the predicted coastal water level is 13.5 ft, only 9 ft is used for flooding the trunk portion of the tree barrier and 1.5 ft is used for overtopping the canopy.

52. There are four discrete ponding areas whose storage area information is presented in Table 8. Flood Region I is from Naples, Fla., to Marco Island and bounded inland by highways U.S. 41 and Fla. 92. Flood Region II is from Marco Island to Everglades City, Fla., and bounded inland by highways Fla. 92, U.S. 41, and Fla. 29. Flood Region III is from Everglades City to Flamingo, Fla., and bounded

inland by highways U.S. 41 and Fla. 27. This region is the major part of the Everglades National Park. The last flood region, IV, is the remaining portion of the park bounded by Florida Bay and highways Fla. 29 and U.S. 1.

53. Plate 39 compares the coastal surge envelope for a wall and the flooding coast boundary conditions. The maximum surge for both simulations occurs at the coast, seaward of Everglades City. The difference between the maximum surges is about 2 to 3 ft. This difference in surge envelopes, however, also occurs over the entire length of the coast boundary, reflecting a significant flooding condition. In proper perspective, the volume of water flooding the coast is inconsequential to that volume entrained in the nearshore open sea circulation. Consequently, water can be removed from the coast and be almost instantaneously replaced without significant effect on the nearshore water level. The circulation pattern, however, is greatly changed due to the flooding. The water-surface topography together with the depth-averaged velocity field for a wall and the flooding coast boundary conditions are presented in Plates 40, 41, and 42. In the early surge development (Plate 40), Florida Bay is practically drained of its water. As the storm center passed Cape Sable, the surge began to rapidly develop in Florida Bay (Plate 41). The effect of flooding is yet to be noticed in the nearshore water levels and velocity fields. However, Plate 42 which is a snapshot 6 hr after Plate 41, clearly shows a very different solution in the nearshore and not-to-nearshore conditions resulting from the flooding coast. Of note is the enhancement of the onshore velocity component which, as a result, must transport more sea sediment to (and over) the coast than previously computed with nonflooding open-coast models. Furthermore, as the mound of high water that follows the storm upcoast is reduced by flooding, that effect must have an influence along adjacent nonflooding coastal segments. This occurs at Naples where no local flooding was considered, yet flooding that occurred many miles away results in a difference of 0.5 ft in the peak surge level. Certainly, nonflooding open-coast models are inappropriate for the

study of Florida Bay or the Everglades area. One should also question their use at Naples.

54. Table 9 compares the computed water level envelope and that observed for various coastal locations. The water level envelope is the peak water level from the time-record made by the superposition of the expected tide at a coastal location and the surge hydrograph without regard to the time of its occurrence. It is seen that the model results are in good agreement with the observed water level. It is more difficult to compare computed H_b and observed inland high-water levels because the tide cannot be simply added to the computed. Furthermore, H_b loses some meaning in surge simulations where for inland locations, the local wind setup is of major importance. Consider a surge of 5 ft occurring at a time of low tide which is expected to be -5 ft relative to msl. The surge model would compute flooding relative to barrier elevations based on msl and surge levels (rel msl). The result is an erroneous computation for H_b and, to a lesser degree, also for the coastal surge. However, for small tide ranges such as exist in the Gulf of Mexico, the computations for the open-coast water level are representative of the superposition of tide and surge. This problem can be avoided if the tide function is input at the sea boundary and dynamically computed along with the surge. It is recommended that this should be pursued when a generalized predictive tide function appropriate to the edge of the continental shelf becomes available. Subject to the above comments, Table 10 shows the computed (not adjusted for the tide) and observed high-water levels at inland locations. The observed data are taken from a poststorm survey²² which are presented in Plates 43-45.

Louisiana Coast, Hurricanes Flossy, Hilda, Betsy,
and Carmen Surge Study

55. Hurricanes Flossy, Hilda, Betsy, and Carmen affected the Louisiana coast from Atchafalaya Bay to the Mississippi River. Hurricane Flossy is the only storm in this study that paralleled this coastal region with subsequent landfall near Pensacola, Fla. Tables 2-5 present the storm parameters for these hurricanes. Plate 46 shows the

location map, the four storm tracks, and the computing grid. The Mississippi River delta region and the adjacent levees are simulated as nonovertopping barriers protruding from the coast in the manner shown in Plate 46. For three of these hurricanes, Hydromet has estimated the surface wind fields at various storm locations.^{13,14,15} Information about Hurricane Carmen is from personal communication with Dr. Joe Pellissier, National Hurricane Center (NHC), NOAA, Miami, Fla. It is noted that the storm track as observed from Hydromet, other weather bureau offices as noted in poststorm damage survey reports of the U. S. Army Engineer District, New Orleans (NOD), and from the NHC in-house historical storm track record are, in most cases, somewhat different-- in particular, the track of Hurricane Flossy as it crossed the Mississippi River delta and Hurricane Carmen as it approached Lake Charles, La., in which the storm was decaying (filling) rapidly. The storm tracks presented in this report are from the NHC record except that the track of Hurricane Hilda prior to landfall is moved 6 n.mi. to the east and the track of Hurricane Flossy in the Mississippi River region is a compromise between the NOD report and NHC.

56. Six discrete ponding areas with storage area information and FHBC data are presented in Table 11. Flood Region I is from Marsh Is. to Point Au Fer Is. and bounded inland by elevated railroads or highways, spoil banks of canals, bayous, or other waterways. Flood Region II is from the terminal point of Flood Region I to Wine Is. and bounded inland by the spoil banks of the Houma Navigation Canal to the west and Bayou Chene to the east and highway U.S. 90 to the north. Flood Region III is from Wine Is. to Belle Pass and bounded inland by the Houma Navigation Canal, Bayou Lafourche to the east, and Bayou Blue and portion of U.S. 90 to the north. Flood Region IV is from Belle Pass to Barataria Pass and bounded inland by Bayou Lafourche, Barataria Bay Waterway, and U.S. 90 to the north. Flood Region V is from Barataria Pass to the west bank of the Mississippi River levee and bounded inland by the Barataria Bay Waterway which closes with the levee near New Orleans, La. Flood Region VI is from the east bank of the Mississippi River levee to the entrance of Lake Borgne following the seaward extent

of the marsh area and bounded inland by New Orleans and U.S. 90. All the above-mentioned bayous, canals, etc., have spoil banks associated with them that would have the tendency to limit flows from one flood region to another.

57. For Hurricane Flossy which occurred in September 1956, the coastal surge envelope for a wall and flooding coast boundary conditions is presented in Plate 47. The comparison of computed water level envelope and observed high-water conditions is presented in Table 12 for coastal areas. Table 13 shows the peak value of H_b and the observed conditions for each flood region. The observed conditions are taken for the NOD poststorm survey²³ which is presented in Plate 48. The comparison of computed and observed conditions is not as good as should be expected. Although the surge model could be in error, more probably it is either the winds or poor field survey of high-water conditions.

58. Hurricane Hilda occurred in October 1964. Plates 49-54 show the water-surface topography together with the depth-averaged velocity field for a wall and flooding coast boundary in 6-hr intervals over a 30-hr period. The role of the Mississippi River delta in limiting the free transport in the continental shelf waters is clearly seen in the series of the above snapshots. The effect of a flooding boundary relative to a wall is, again, seen to enhance the onshore-directed transport of water. The principal surge area occurs at Caillou Bay as seen in Plates 51 and 55, which show the surge envelope. The coastal barrier in this area is typically a beach berm, generally less than 3 ft in height (msl). Consequently, significant flooding occurred from 1800Z (Z referring to Greenwich Mean Time), 3 October, to approximately 0300Z the next day. The winds at 0300Z, 4 October, are directed more alongshore, forcing the inland surge to the east. The highest observed water level of 9.8 ft occurred inland, to the east of Caillou Bay along the Houma Navigation Canal.

59. Tables 14 and 15, as before, compare the computed and observed high-water levels for coastal and inland regions, respectively. The observed water level record and that computed (superposition of

surge and expected tide as determined from the National Ocean Survey tide table) at various coastal locations are presented in Plates 56-58. An oscillation of 8 hr in period is shown in the computed hydrograph at Biloxi, Miss. (Plate 58). The period of oscillation is characteristic of an edge wave. Multioscillations occur from the trapping of energy between the right lateral boundary and the protruding Mississippi River levee. However, other computed water levels in this region do not exhibit such oscillations as shown in Plates 57 and 59. Plate 56 shows another typical problem in open-coast surge computations--that of proper wind specification. Before storm landfall, the analytically computed winds at Eugene Is. are always directed offshore, resulting in the enhanced drawdown of the water. Moreover, the island is on the leeward side of the coast and land frictional influence on the wind is not considered in the hurricane model. Further complication occurs in light of recent developments which shows that the surface winds in the forward section of the storm may be outflowing (a negative ingress angle).²⁴ The results presented in the comparison tables and in Plates 56-58 are in good agreement with the observed; however, improvement should be expected with a better wind model. Plate 60 presents the observed high-water levels as reported in the poststorm survey.²⁵

60. Hurricane Betsy occurred in September 1965. The water-surface topography and velocity field comparing a wall and flooding coast boundary are shown in Plates 61-65. The effects of the flooding boundary on the nearshore water levels and currents are most dramatically demonstrated in Plate 62. Without overtopping, the wall condition is trapping water in excess of 18 ft at the corner between the east Mississippi levee and coastal wall. With flooding of the marsh area, only 12 ft of water is computed along the levee. The coastal surge envelope (Plate 66) clearly shows the effect of a flooding boundary versus that with a wall. The velocity fields are considerably different with, again, the enhancement of the onshore velocity for the flooding boundary. Plate 62 also shows that the surge is just beginning to develop on the western side of the Mississippi River levee. Plate 63, 3 hr later than that snapshot in Plate 62, shows the developed

surge in this area while to the east, sustained relatively high water is continuing. Plates 64 and 65 show the decreasing surge, whereas Plate 65 shows the reentrance of the water from the ponding areas.

61. Tables 16 and 17 compare the computed and observed high-water levels for coastal and inland regions, respectively. Furthermore, observed and computed hydrographs at two coastal locations are presented in Plates 67 and 68. The hydrograph location in Plate 67 is to the left of landfall. The problems associated with the computed large drawdown have been discussed previously. No presurge water level anomaly is added to any of the computed results in any study reported herein, although after viewing the observed hydrograph at Biloxi, it may seem appropriate. The results from this surge simulation, more than in any other presented in this report, show the necessity in treating the coast as a finite barrier. The comparison of the computed and observed water level conditions are in excellent accord. Plate 69 presents the observed high-water levels as reported in the poststorm survey.²⁶

62. Hurricane Carmen occurred in September 1974. Snapshots of the water-surface topography, together with the depth-averaged velocity field for a wall and flooding coast, are shown in Plates 70-72. The principal surge developed between Caillou Bay and the entrance to Terrebonne Bay, as shown in the surge envelope (Plate 73), at approximately 0900Z, 8 September (between the time of Plates 70 and 81). The surge does not develop in Atchafalaya Bay until 1800Z. After this time, the forward motion and location of the storm are in question due to its rapid decay. Since the surge developed in East Cote Blanche Bay during the decay stage of the storm, it is viewed as fortuitous that the peak computed and observed water level are in good agreement (Plate 74). The phasing of the peak water levels at Luke's Landing, La., is in poor agreement probably due to the storm proceeding faster on the track than that used in the simulation.

63. Plates 75-77 present computed and observed hydrographs at other coastal locations. The observed hydrographs in the region to the east of the Mississippi River (Plates 76 and 77) show a considerable initial water elevation at the start of computations. This

elevation is not totally a presurge condition because the action of the wind is seen to reflect the observed peak levels some 20 hr later. On the other hand, this initial condition, especially at the Gulf Outlet Canal, is not due to the hurricane since the winds on the continental shelf are very weak at the start of computations; that is, if the surge simulation had begun at 1200Z, 6 September (24 hr in advance of the starting time in Plate 76), the model would not have shown over 4 ft of water at the canal entrance at 1200Z, 7 September. Other processes are occurring, presumably not assignable to the storm surge, for whatever caused the transient water level bump at 1700Z, 7 September (Plate 76) is probably responsible for a similar, well-correlated bump at 2200Z, 7 September, at Biloxi (Plate 77).

64. Tables 18 and 19 compare the computed and observed high-water levels for coastal and inland regions, respectively. There are no observations along the coast in the principal surge area for comparison with the computed value. In other places and subject to the above discussion, the comparison between computed and observed water levels is in good agreement. Plate 78 presents the observed high-water levels as reported in the poststorm survey.²⁷

PART V: CONCLUSIONS AND RECOMMENDATIONS

65. The development of a two-dimensional, time-dependent, curvilinear, open-coast storm surge and tidal model is presented. In particular, the model treats the coast boundary as a finite height barrier which is broken with bay entrances. The flooding coast routine in its treatment of submerged and exposed (on one side) barriers is considered conservative. The results from the model compare most favorably with those obtained from two hydraulic physical models involving tidal or pseudosurge simulations. These experiments revealed that the model could be improved in its treatment of open sea, finite height structures such as weirs or jetties.

66. The results of five storm surge simulations are presented in which observed and computed conditions are compared. These simulations employed two separate stretches of coastline, each of different coastal characteristics. Again, the model results compare most favorably with those observed. However, from currently available data, a relatively low value for the wind drag coefficient at high wind speeds is used. This is necessary to compensate for the liberal estimate for the maximum winds. In hindcasting situations, it is not guaranteed that the same procedure is used for estimating the maximum wind. The wind model employed in these surge simulations from historical storms requires input of the maximum wind. The problem can be resolved by using a wind model based on the physics of the marine boundary layer that will provide a wind field as a result of dynamic meteorological computations. It is recommended that such a model be obtained (as they do exist) and incorporated into the hydrodynamic flooding coast model. The resulting composite model, therefore, would be appropriate for both forecasting and hindcasting and involve a drag coefficient reflective of the currently available data.

67. The following recommendations are secondary to that of incorporating a dynamic wind model in SSURGE III. It can be shown that the astronomical tide does distort the predicted coastal and inland flood water levels when it is not incorporated into the dynamic

computations; that is, equivalent results are not obtained by the superposition of surge and tide and that simulation where the tide is included in the sea boundary forcing condition. For the east coast of the United States where there are large tidal ranges, the tide should be included in the computation. The results of the five storm surge simulations are considered sufficiently accurate using superposition as they occurred in Gulf of Mexico waters where the tidal range is small. It is recommended that a generalized tide prediction function which is appropriate to the edge of the continental shelf be incorporated into the surge computations.

68. It is recognized that other approaches, equations, and coefficients are reported or can be developed for the treatment of a flooding, finite height barrier coast. These should be investigated and the more promising approach tested against the one reported herein.

REFERENCES

1. Welander, P., "Numerical Prediction of Storm Surges," Advances in Geophysics, Vol 8, Academic Press, New York, 1961.
2. Jelesnianski, C. P., "A Sheared Coordinate System for Storm Surge Equations of Motion with a Mildly Curved Coast," Technical Memorandum NWS TDL-61, Jul 1976, Techniques Development Laboratory, National Oceanic and Atmospheric Administration, Silver Spring, Md.
3. Wanstrath, J. J. et al., "Storm Surge Simulation in Transformed Coordinates; Vol 1: Theory and Application," Technical Report 76-3, Nov 1976, U. S. Army Coastal Engineering Research Center, Fort Belvoir, Va.
4. Wang, J. D. and Connor, J. J., "Mathematical Modeling of Near Coastal Circulation," Report No. 200, Apr 1975, Ralph M. Parsons Laboratory, Department of Civil Engineering, Massachusetts Institute of Technology, Cambridge, Mass.
5. Reid, R. O. and Bodine, B. R., "Numerical Model for Storm Surges in Galveston Bay," Journal, Waterways and Harbor Division, American Society of Civil Engineering, Vol 94, No. WW1, Feb 1968, pp 33-57.
6. Garratt, J. R., "Review of Drag Coefficients over Oceans and Continents," Monthly Weather Review, Vol 105, Jul 1977, pp 915-929.
7. Cardone, V. J. and Ross, D., "Forecasting Hurricane Winds and Waves--A Pilot Study," Final Report, 1976, Institute of Marine and Atmospheric Sciences, City University of New York, New York, N. Y.
8. Cardone, V. J., Pierson, W. J., and Ward, E. C., "Hindcasting the Directional Spectrum of Hurricane Generated Waves," Journal, Petroleum Technology, Vol 28, Apr 1976, pp 385-394.
9. Wanstrath, J. J., Reflection and Transmission of a Monochromatic Gravity Wave at Oblique Incidence to a Step, M.S. Thesis, Texas A&M University, College Station, Tex., 1971.
10. Cochrane, J. D. and Arthur, R. S., "Reflections of Tsunamis," Journal, Marine Research, Vol 7, No. 3, 1948, pp 239-251.
11. Love, R. W., Tidal Response of a Bay with a Constricted Opening to the Sea, M.S. Thesis, Texas A&M University, College Station, Tex., 1959.
12. Jelesnianski, C. P., "A Numerical Calculation of Storm Tides Induced by a Tropical Storm Impinging on a Continental Shelf," Monthly Weather Review, Vol 93, 1965, pp 343-358.

13. Environmental Science Services Administration, "Pressure and Winds over the Gulf of Mexico in Hurricane Flossy, September 23-24, 1956," Memorandum HUR 7-53, Jun 19, 1958, U. S. Department of Commerce, Weather Bureau, Hydrometeorological Section, Washington, D. C.
14. _____, "Preliminary Analysis of Surface Winds in Hurricane Hilda, October 2-4, 1964," Memorandum HUR 7-82, Jun 8, 1965, U. S. Department of Commerce, Weather Bureau, Hydrometeorological Branch, Washington, D. C.
15. _____, "Surface Winds (30 ft) over the Gulf of Mexico in Hurricane Betsy, September 9 and 10, 1965," Memorandum HUR 7-87, Dec 20, 1965, U. S. Department of Commerce, Weather Bureau, Hydrometeorological Branch, Washington, D. C.
16. National Oceanic and Atmospheric Administration, "Revised Standard Project Hurricane Criteria for the Atlantic and Gulf Coasts," Memorandum HUR 7-120, Jun 1972, U. S. Department of Commerce, National Weather Service, Hydrometeorological Branch, Washington, D. C.
17. Brogdon, N. J., "Galveston Bay Hurricane Surge Study; Effects of Proposed Barriers on Hurricane Surge Heights, Hydraulic Model Investigation," Technical Report H-69-12, Report 1, Sep 1969, U. S. Army Engineer Waterways Experiment Station, CE, Vicksburg, Miss.
18. Seabergh, W. C., Lane, E. F., and Perry, F. C., "Improvements for Murrells Inlet, South Carolina, Hydraulic Model Investigation" (in preparation), U. S. Army Engineer Waterways Experiment Station, CE, Vicksburg, Miss.
19. Marshall University, "Quantitative Physiognomic Analysis of the Vegetation of the Florida Everglades," Huntington, W. Va.; Prepared for U. S. Army Engineer Waterways Experiment Station, CE, Vicksburg, Miss., under Contract No. DA-22-079-eng-322.
20. Davis, J. H., "The Natural Features of Southern Florida Especially the Vegetation, and the Everglades," Geological Bulletin No. 25, 1943, State of Florida, Department of Conservation, Florida Geological Survey, Tallahassee, Fla.
21. Markle, D. and Davidson, D. D., "Levee Wave Wash Protection by Trees" (in preparation), U. S. Army Engineer Waterways Experiment Station, CE, Vicksburg, Miss.
22. U. S. Army Engineer District, Jacksonville, "Report on Storms and Floods in Florida, July-September 1960; (Including Hurricane "Donna" and Tropical Disturbance "Florence")," Feb 1961, Jacksonville, Fla.
23. U. S. Army Engineer District, New Orleans, "Report on Hurricane Flossy--23-24 September 1956, Southeastern Louisiana," Aug 1957, New Orleans, La.

24. Shea, D. J. and Gray, W. M., "The Hurricanes Inner Core Region I, Symmetric and Asymmetric Structure," Journal, Atmospheric Science, Vol 30, 1973, pp 1544-1564.
25. U. S. Army Engineer District, New Orleans, "Report on Hurricane Hilda, 3-5 October 1964," May 1966, New Orleans, La.
26. _____, "Report on Hurricane Betsy, September 8-11, 1965," Nov 1965, New Orleans, La.
27. _____, "Report on Hurricane Carmen, 7-8 September 1974," Oct 1975, New Orleans, La.

Table 1

Program SSURGE III Wind Data for Hurricane Donna Surge Simulation

PHI = 25.
 THIT = 9999.
 RHIT = 9999.
 PINF = 1014.56

Program Time hr	Track Location			Rotation o	Radius To Maximum Winds n. mi.	Stationary Storm Maximum Wind, knots	Central Pressure mb
	Lat. ON	Long. OW	X e	Y e			
0.*	23°42'	79°24'	266.8	200.7	17.4	110.	947.
6.	24°12'	80°6'	234.1	178.5	18.2	105.	947.
12.	24°42'	80°42'	202.3	160.2	20.0	105.	952.
18.	25°18'	81°18'	165.8	144.0	20.8	105.	952.
24.	26°12'	81°42'	117.5	140.7	21.7	100.	957.
30.	27°18'	81°54'	62.3	149.4	21.7	90.	957.

* Program Time of 0 hr = 1800 GMT, 9 Sept 1960.

Table 2

Program SSURGE III Wind Data for Hurricane Flossy Surge Simulation

PHI = 25.0
 THIT = 9999.
 RHIT = 9999.
 PINF = 1014.56

Program Time hrs	Track Location				Rotation °	Radius To Maximum Wind n. mi.	Stationary Storm Maximum Wind, knots	Central Pressure mb
	Lat. °N	Long. °W	X _e	Y _e				
0*	25°50.2'	90°59.8'	282.2	-196.5	115.0	22.0	60.0	984.0
6	27°9.3'	90°54.5'	290.1	-69.5	115.0	22.0	60.0	984.0
12	27°58.8'	90°34.5'	318.0	8.5	115.0	22.0	60.0	984.0
15	28°22.9'	90°12.3'	349.0	46.5	115.0	22.0	65.0	982.0
18	28°44.8'	89°48.5'	382.0	81.5	115.0	22.0	70.0	979.0
21	29°4.0'	89°25.6'	414.0	112.0	115.0	22.0	75.0	975.0
24	29°21.5'	89°3.3'	445.0	140.0	115.0	22.0	75.0	975.0
27	29°41.6'	88°31.9'	489.0	172.5	115.0	22.0	75.0	974.0
30	29°48.0'	87°39.1'	562.0	182.5	115.0	22.0	75.0	974.0

* Program Time of 0 hr = 1230 GMT, 23 Sept 1959.

Table 3

Program SSURGE III Wind Data for Hurricane Hilda Surge Simulation

PHI = 25.0
 THIT = 23.0
 RHIT = 24.0
 PINF = 1014.56

Program Time hrs	Track Location			Rotation °	Radius To Maximum Wind n. mi.	Stationary Storm Maximum Wind, knots	Central Pressure mb
	Lat. ON	Long. OW	X _e Y _e				
0*	27°11.7'	91°12.2'	265.0 -65.6	115.0	22.0	100.0	956.3
6	27°43.4'	91°9.4'	269.0 -15.3	115.0	22.0	98.0	958.0
12	28°16.4'	91°9.4'	269.0 36.5	115.0	23.0	92.0	959.4
18	28°54.5'	91°19.5'	255.0 97.0	115.0	24.0	92.0	960.7
24	29°35.8'	91°23.0'	250.0 162.7	135.0	24.0	90.0	961.7
30	30°16.7'	91°0.8'	281.5 228.8	150.0	50.0	60.0	970.5
36	30°35.5'	90°5.8'	358.3 259.0	70.0	50.0	60.0	985.4
42	30°43.8'	88°58.4'	452.0 272.0	60.0	22.0	65.0	990.2

* Program Time of 0 hr = 0000 GMT, 3 Oct 1964.

Table 4

Program SSURGE III Wind Data for Hurricane Betsy Surge Simulation

PHI = 30.0
 THIT = 16.0
 RHIT = 32.0
 PINF = 1014.56

Program Time hrs	Track Location				Rotation °	Radius To Maximum Wind n. mi.	Stationary Storm Maximum Wind, knots	Central Pressure mb
	Lat. °N	Long. °W	X e	Y e				
0*	26°21.3'	86°45.5'	639.0	-145.9	75.0	23.5	90.0	951.0
6	27°8.3'	88°3.5'	529.0	-71.5	75.0	27.0	90.0	949.0
9	27°43.8'	88°34.6'	485.6	-15.7	75.0	28.5	94.0	944.0
12	28°20.4'	89°10'	436.0	42.2	75.0	30.0	96.0	941.0
15	28°56.4'	89°50.5'	379.3	99.5	75.0	32.0	96.0	941.0
18	29°35.5'	90°31.8'	321.5	161.8	215.0	32.0	88.0	948.0
21	30°4.2'	91°3.9'	276.3	208.0	245.0	45.0	75.0	955.0
24	30°38.1'	91°33.2'	235.5	262.5	220.0	65.0	60.0	965.0
27	31°11.6'	91°55.9'	203.3	315.9	230.0	105.0	40.0	975.0

* Program Time of 0 hr = 1200 GMT, 9 Sept 1965.

Table 5

Program SSURGE III Wind Data for Hurricane Carmen Surge Simulation

PHI = 25.0
 THIT = 24.0
 RHIT = 20.0
 PINF = 1014.56

Program Time hrs	Track Location			Rotation °	Radius To Maximum Wind		Stationary Storm Maximum Wind, knots	Central Pressure mb
	Lat. °N	Long. °W	X _e Y _e		n. mi.			
0*	25°43.2'	90°13.0'	340.8 -207.6	115.0	17.0		90.0	950.0
6	26°52.5'	90°13.0'	340.8 -103.0	115.0	17.0		100.0	950.0
12	27°48.0'	90°24.1'	332.4 -8.8	115.0	17.0		100.0	944.0
18	28°41.6'	90°48.3'	298.6 76.0	115.0	17.0		110.0	937.0
24	29°24.0'	91°8.3'	256.8 144.0	115.0	20.0		90.0	960.0
30	30°0.0'	92°6.3'	189.3 201.3	115.0	24.0		70.0	982.0
36	30°24.0'	92°41.7'	140.0 240.0	115.0	30.0		45.0	993.0

* Program Time of 0 hr = 1200 GMT, 7 Sept 1974.

Table 8

SSURGE III Finite Height Coast Boundary Data for the West Coast of Florida - Hurricane Donna Surge Study

Coast H Grid Point	Values of Coastal Barrier Length L_c (x 500 ft) at Various Barrier Elevations Z_b (ft REL MSL)																			Entrance Channel		Coastal Water Surface Area at MLLW		Flood Region	
	1-13 NO FLOODING CONSIDERED																			Width W_c (ft)	Discharge Coeff Times Cross Sectional Area $C_D A_c$ (ft ²)	Representative of $H(1, JM)$ A_1 (ft ² x 10 ⁶)	Num- ber	Storage Area A_b (ft ² x 10 ⁹)	Elevation H_b (ft REL MSL)
	0	1	2	3	4	5	6	7	8	9	10	11	12	13	14	15	16	17	18	19	20				
1	49	49	49	49	0	0	0	0	0	0	0	0	0	0	0	0	0	0	0	0	0	0	0	0	0
14	49	49	49	49	0	0	0	0	0	0	49	49	49	49	0	0	0	0	0	0	0	160.0	I	0.650	0
15	49	49	49	49	0	0	0	0	0	0	49	49	49	49	0	0	0	0	0	0	0	130.0		0.697	2
16	49	49	49	49	0	0	0	0	0	0	0	0	0	0	0	0	0	0	0	0	0	130.0		2.181	>5
17	51	51	51	51	0	0	0	0	0	0	49	49	49	49	0	0	0	0	0	0	0	150.0		1.900	0
18	54	54	54	54	0	0	0	0	0	0	51	51	51	51	0	0	0	0	0	0	0	260.0	II	2.091	2
19	57	57	57	57	0	0	0	0	0	0	54	54	54	54	0	0	0	0	0	0	0	340.0		4.279	>5
20	60	60	60	60	0	0	0	0	0	0	57	57	57	57	0	0	0	0	0	0	0	390.0			
21	63	63	63	63	0	0	0	0	0	0	60	60	60	60	0	0	0	0	0	0	0	410.0			
22	66	66	66	66	0	0	0	0	0	0	63	63	63	63	0	0	0	0	0	0	0	430.0		10.000	0
23	69	69	69	69	0	0	0	0	0	0	66	66	66	66	0	0	0	0	0	0	0	460.0	III	10.454	2
24	73	73	73	73	0	0	0	0	0	0	69	69	69	69	0	0	0	0	0	0	0	430.0		32.106	>6
25	76	76	76	76	0	0	0	0	0	0	73	73	73	73	0	0	0	0	0	0	0	460.0			
26	79	79	79	79	0	0	0	0	0	0	76	76	76	76	0	0	0	0	0	0	0	500.0			
27	83	83	83	83	83	0	0	0	0	0	79	79	79	79	0	0	0	0	0	0	0	290.0			
28	87	87	87	87	87	0	0	0	0	0	0	0	0	0	0	0	0	0	0	0	0	230.0			
29	90	90	90	90	0	0	0	0	0	0	0	0	0	0	0	0	0	0	0	0	0	370.0			
30	94	94	94	94	0	0	0	0	0	0	90	90	90	90	0	0	0	0	0	0	0	700.0		4.000	0
31	98	98	98	98	0	0	0	0	0	0	94	94	94	94	0	0	0	0	0	0	0	1220.0	IV	4.182	2
											98	98	98	98	0	0	0	0	0	0	0	1760.0		10.947	>6

Table 9

Comparison of Computed and Observed Coastal
High-Water Levels for Hurricane Donna

<u>Coastal Location</u>	<u>Computed* High-Water Level (ft)</u>	<u>Observed High-Water Level (ft)</u>	<u>Average</u>
Estero Bay	8.5	7.4, 7.7, 7.8, 8.1, 9.5	8.1
	10.5	9.7, 10.4	10.1
	11.0	9.8, 10.2, 10.4, 11.1	10.4
8.3 n.mi. North of Naples, FL	11.2	8.1, 10.2, 11.9	10.1
3.3 n. mi. North of Naples, FL	10.2	10.0	10.0
Naples, FL	9.8 (w/o flood- ing coast, 10.4)	8.1, 9.4, 10.0, 11.3, 11.6	10.1
Marco I. (1.2 n.mi. inland)	9.5	10.2	10.2
3.8 n.mi. East of Cape Romano (1.5 n.mi. inland)	11.7	7.8, 11.7	9.8
Everglades City, FL	15.0	N/A	
Shark River	9.3	N/A	
Flamingo, FL, on Cape Sable	11.0 (w/o flood- ing coast, 12.5)	12.0	12.0

(Continued)

* Adjusted for astronomical tide.

Table 9 (Concluded)

<u>Coastal Location</u>	<u>Computed* High-Water Level (ft)</u>	<u>Observed High-Water Level (ft)</u>	<u>Average</u>
<u>Florida Keys</u>			
Rock Harbor, FL	10.1	5.6, 7.0, 8.9	7.2
Plantation Key Upper Mat. Key	8.2	4.0, 4.8, 6.3, 9.0, 10.0, 10.6	7.5
Craig, FL	7.3	8.5	8.5
Long Key	6.4	6.0	6.0
Grassy Key	8.3	7.0, 7.4	7.2
Vaca Key	9.9	7.5, 8.0, 8.0, 8.5, 8.8	8.2
Torch Key	7.0	3.4	3.4
Sugarloaf Key	5.1	6.6	6.6
10.0 n.mi. East of Key West, FL	4.4	4.9	4.9
5.5 n.mi. East of Key West, FL	3.5	4.7	4.7
Key West, FL	2.3	1.9	1.9

* Adjusted for astronomical tide.

Table 10
Comparison of Computed and Observed Inland
High-Water Levels for Hurricane Donna

<u>Inland Location</u>	<u>Computed* Ponding Region Level (ft)</u>	<u>Observed High-Water Level (ft)</u>
Marco Is. (1.2 n.mi. inland), Flood Region I	5.9	5.3 (7.7 n.mi. inland near FL 41)
Everglades City, FL Flood Region II	7.1	6.2 (7.0 n.mi. inland) 8.5, 9.7 (5.1 n.mi. inland)
Shark River, Flood Region III	6.4	6-6.5 (4.2 n.mi. inland and 0.5 n.mi. from river)
Flamingo, FL, on Cape Sable, Flood Region IV	7.0	N/A

* Not adjusted for astronomical tide.

Table 12
Comparison of Computed and Observed Coastal
High-Water Levels for Hurricane Flossy

<u>Coastal Location</u>	<u>Computed* High-Water Level (ft)</u>	<u>Observed High-Water Level (ft)</u>
6.1 n.mi. East of East Timbalier I. at Bay Champagne	2.3	3.7 (EST**)
Southwest Pass Ent.	2.0	3.7
Quarantine Bay	9.6	10.8, 11.9, 12.1
Pointe A La Hache, LA to Point Pleasant, LA	8.9	10.3, 10.5 (EST) 10.7, 11.0 (EST)
Breton I.	6.0	7 to 8 (EST)

* Adjusted for astronomical tide.

** Furnished by various oil companies and by the Freeport Sulphur Co.

Table 13
Comparison of Computed and Observed Inland
High-Water Levels for Hurricane Flossy

<u>Inland Location</u>	<u>Computed* High-Water Level (ft)</u>	<u>Observed High-Water Level (ft)</u>
Barataria Bay to Mississippi River Levee, Flood Region 5	0.4	3.6**, 3.6**, 5.2**, 5.5**, 6.9**, 7.3**, 8.0**
Lake Borgne, Flood Region 6	2.5	4.0, 5.2, 6.3, 8.5, 6.2†, 6.4†, 6.9†, 7.7†, 8.1†, 8.6†, 9.4†, 10.9†

NOTE: Flood Regions 1 - 4 not affected.

* Not adjusted for astronomical tide.

** Observations were located along landward side of coastal barrier.

† Observations were located along southwest side of Lake Borgne.

Table 14
Comparison of Computed and Observed Coastal
High-Water Levels for Hurricane Hilda

<u>Coastal Location</u>	<u>Computed* High-Water Level (ft)</u>	<u>Observed High-Water Level (ft)</u>
Gulf Ent., Freshwater Bayou	1.5	2.3
East Cote Blanche Bay at Lukes Landing, LA	2.5	4.4
Atchafalaya Bay at Eugene I.	3.8 (w/o flooding coast, 4.3)	3.3
Lake Pelto, 2.4 n.mi. Landward from Ent. to Terrebonne Bay	6.8 (w/o flooding coast, 7.2)	7.4
Grand I.	3.2 (w/o flooding coast, 3.2)	4.0
East Side Barataria Bay near Gulf Ent.	5.0	5.5
Southwest Pass, Mississippi River	1.5	3.2, 3.5
Quarantine Bay at Ostrica, LA	4.0 (w/o flooding coast, 4.4)	4.6
Ent. Mississippi River - Gulf Outlet Canal	4.0 (w/o flooding coast, 4.4)	4.6
Biloxi, MS	5.2 (w/o flooding coast, 5.2)	4.6

* Adjusted for astronomical tide.

Table 15
Comparison of Computed and Observed Inland
High-Water Levels for Hurricane Hilda

<u>Inland Location</u>	<u>Computed* High-Water Level (ft)</u>	<u>Observed High-Water Level (ft)</u>
Atchafalaya Bay, Flood Region I	0.	3.8, 5.1
Atchafalaya River to Houma Canal, Flood Region II	3.8	None
Terrebonne-Timbalier Bay, Flood Region III	3.4	3.0, 3.8, 4.0, 4.7, 5.4, 6.6, 6.9, 6.9, 7.0, 7.4, 9.8
Bayou Lafourche to Barataria Bay, Flood Region IV	0.5	None
Barataria Bay to Mississippi River Levee, Flood Region V	1.6	4.0
Lake Borgne, Flood Region VI	3.3	3.8, 4.5, 4.7, 5.0, 5.2, 5.3

* Not adjusted for astronomical tide.

Table 16
Comparison of Computed and Observed Coastal
High-Water Levels for Hurricane Betsy

<u>Coastal Location</u>	<u>Computed* High-Water Level (ft)</u>	<u>Observed High-Water Level (ft)</u>
East Cote Blanche Bay at Lukes Landing, LA	4.5	3.8
Grand I.	7.2 (w/o flooding 7.4)	8.8
East Side Barataria Bay near Gulf Ent.	8.5 (w/o flooding coast, 9.8)	7.6
West Side Mississippi River Levee; Empire, LA, to Venice, LA	6.2 to 12.2 (w/o flooding coast, 6.2 to 16.1)	5.7, 7.4, 7.7, 8.8, 9.2, 10.4
East Side Mississippi River Levee; Pointe A La Hache, LA, to Ostrica (Brenton Sound), LA	12.4 to 15.2 (w/o flooding coast, 12.8 to 23.1)	13.6, 13.7, 14.4, 14.5, 15.7
Gulfport, MS	9.0 (Approx.)	10.7
Biloxi, MS	7.6	8.6

* Adjusted for astronomical tide.

Table 17
Comparison of Computed and Observed Inland
High-Water Levels for Hurricane Betsy

<u>Inland Location</u>	<u>Computed* High-Water Level (ft)</u>	<u>Observed High-Water Level (ft)</u>
Atchafalaya Bay, Flood Region I	0.	2.9, 3.9
Atchafalaya River to Houma Canal, Flood Region II	0.9	3.0, 4.3 (along Houma Canal)
Terrebonne-Timbalier Bay, Flood Region III	1.8	2.8, 3.0, 4.3
Bayou Lafourche to Barataria Bay, Flood Region IV	0.5	3.4, 5.4
Barataria Bay to Mississippi River Levee, Flood Region V	2.1	3.4, 5.0, 5.3
Lake Borgne, Flood Region VI	7.1	6.4, 8.3, 8.8, 9.1, 9.3, 9.8, 10.1, 10.7, 11.0, 11.7, 14.4

* Not adjusted for astronomical tide.

Table 18
Comparison of Computed and Observed Coastal
High-Water Levels for Hurricane Carmen

<u>Coastal Location</u>	<u>Computed* High-Water Level (ft)</u>	<u>Observed High-Water Level (ft)</u>
East Cote Blanche Bay at Lukes Landing, LA	4.3**	4.5
Atchafalaya Bay at Lower Atchafalaya River	4.5**	4.9
Atchafalaya Bay at Eugene I.	3.8 (w/o flooding coast, 4.0)	3.7
Grand I.	4.7 (w/o flooding coast, 4.8)	4.2
Ent. Mississippi River - Gulf Outlet Canal	5.1 (w/o flooding coast, 5.4)	5.7
Biloxi, MS	4.0 (w/o flooding coast, no change)	4.5
Caillou Bay	9.2 (w/o flooding coast, 11.6)	None
Ent. Terrebonne Bay	8.7 (w/o flooding coast, 11.1)	None

* Adjusted for astronomical tide.

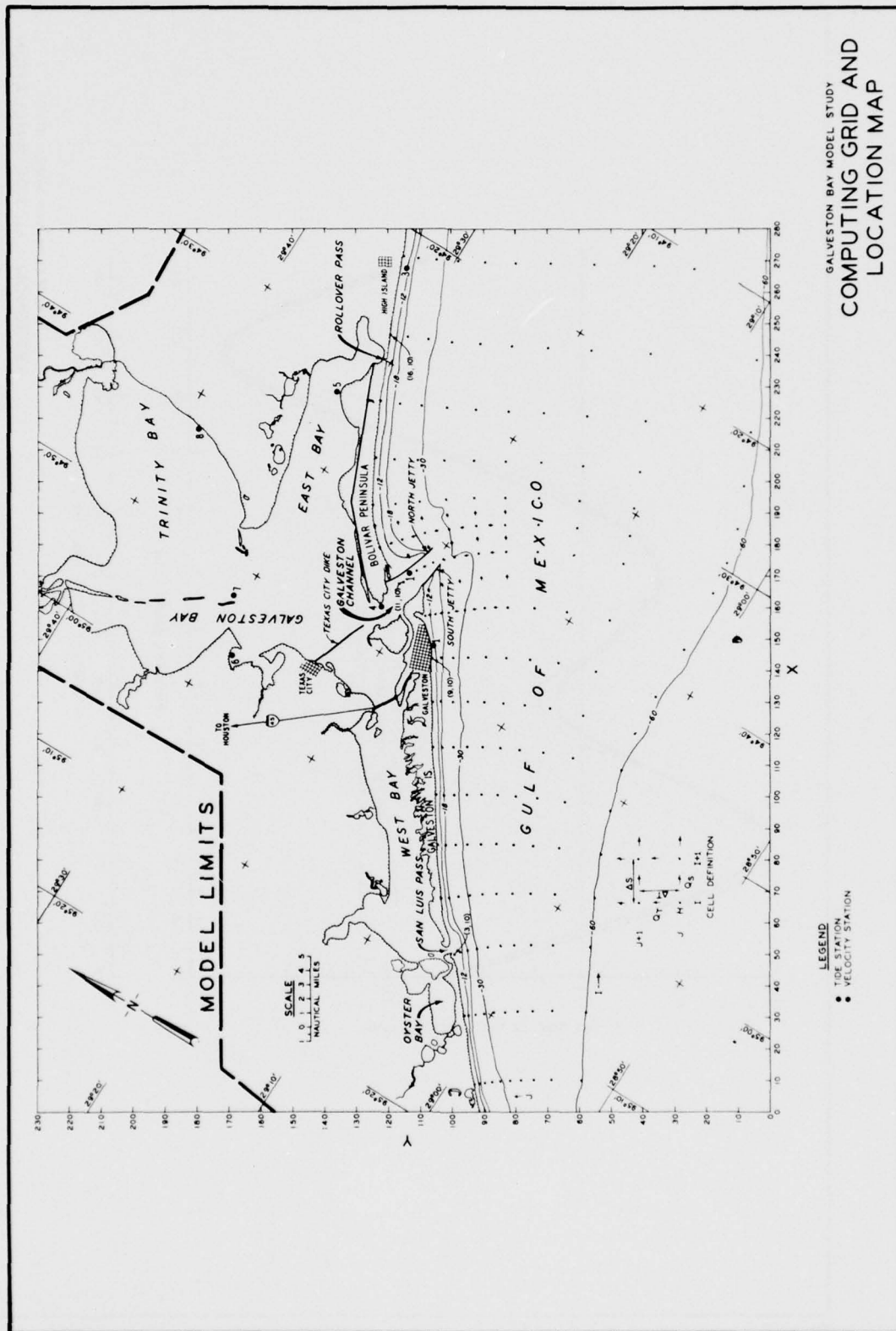
** The time of high water occurred after 1200 CST 8 Sept 1974. The water level is approximate because the structure of the storm after 1200 CST is uncertain due to its rapid decay. Computations ended at 1800 CST 8 Sept.

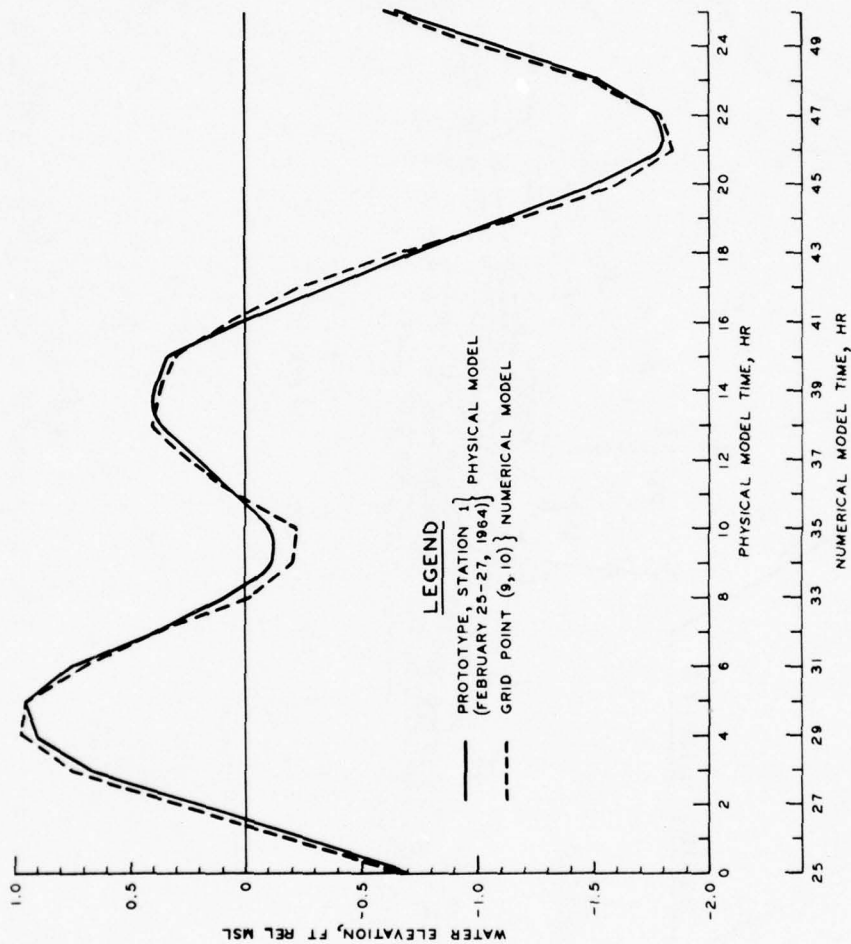
Table 19
Comparison of Computed and Observed Inland
High-Water Levels for Hurricane Carmen

<u>Inland Location</u>	<u>Computed* High-Water Level (ft)</u>	<u>Observed High-Water Level (ft)</u>
Atchafalaya Bay, Flood Region I	0.6**	2.8, 3.2, 3.8, 4.0, 4.8
Atchafalaya River to Houma Canal, Flood Region II	3.8	3.3
Terrebonne-Timbalier Bay, Flood Region III	4.4	2.9, 3.8, 4.6, 5.9, 11.6
Bayou Lafourche to Barataria Bay, Flood Region IV	0.5	None
Barataria Bay to Mississippi River Levee, Flood Region V	1.4	3.1
Lake Borgne, Flood Region VI	3.4	5.0, 6.0

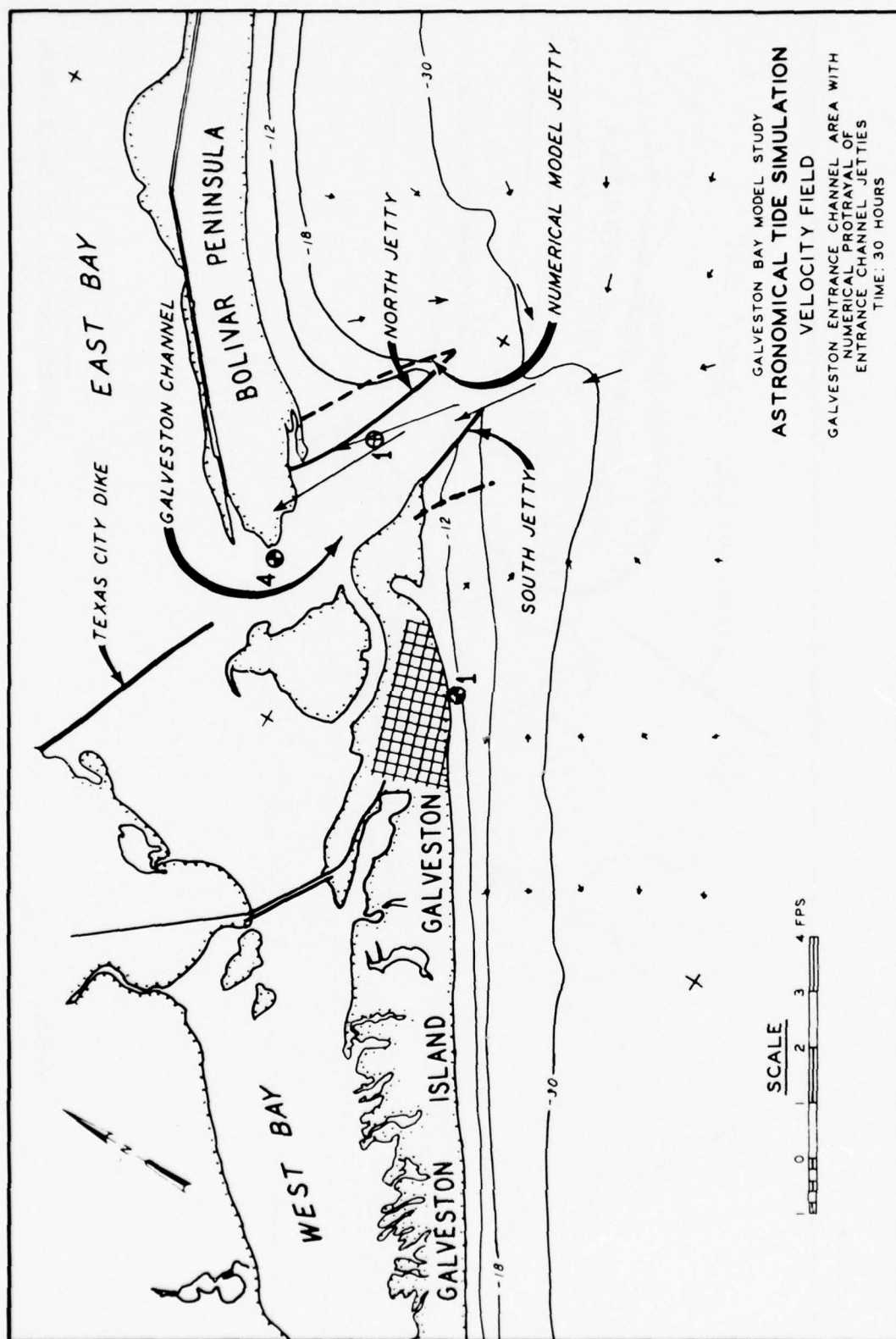
* Not adjusted for astronomical tide.

** Computed bay level rising at end of computation. See footnote **, Table 18.





GALVESTON BAY MODEL STUDY
ASTRONOMICAL TIDE SIMULATION
 HYDROGRAPH
 PLEASURE PIER, GALVESTON, TEXAS



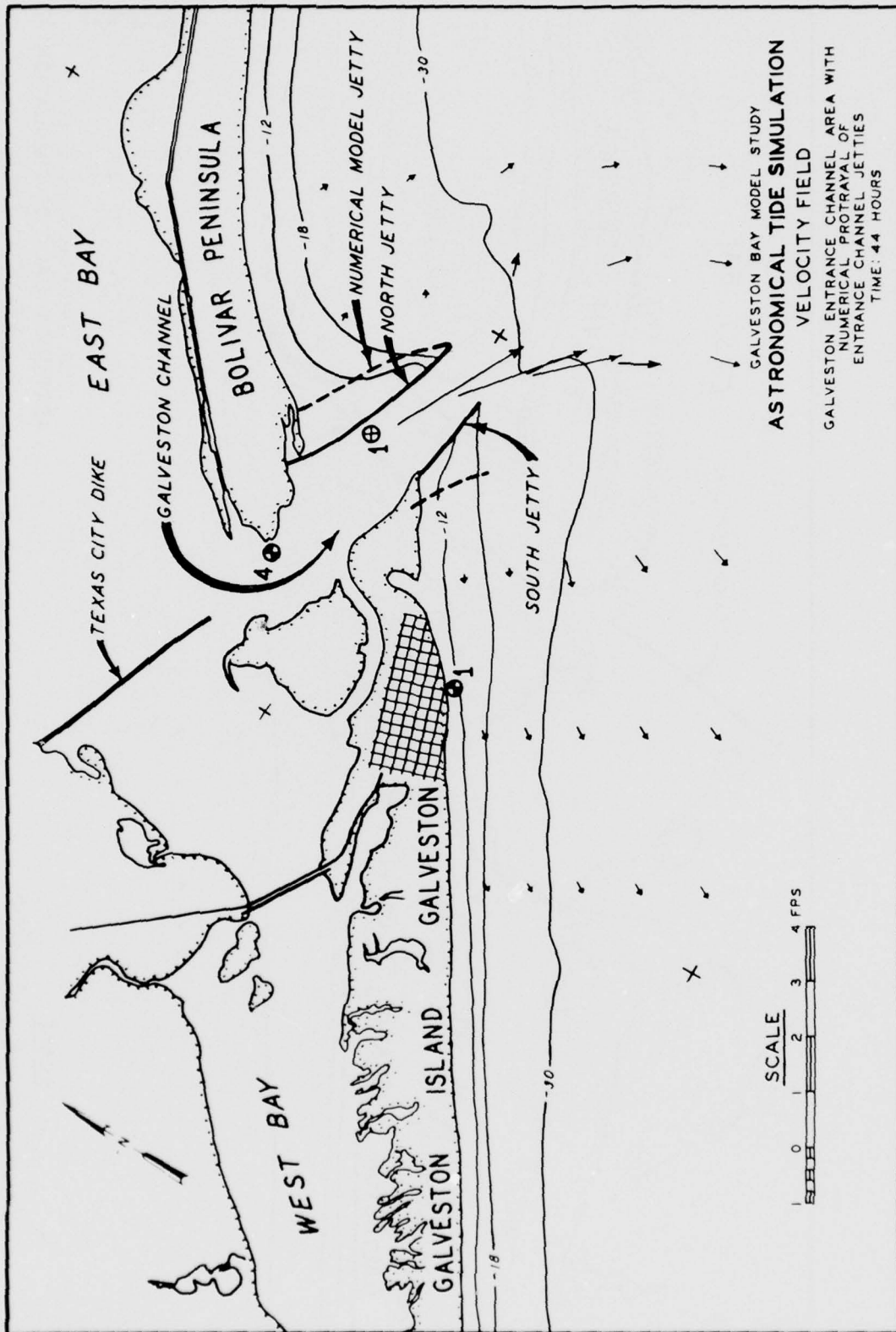


PLATE 4

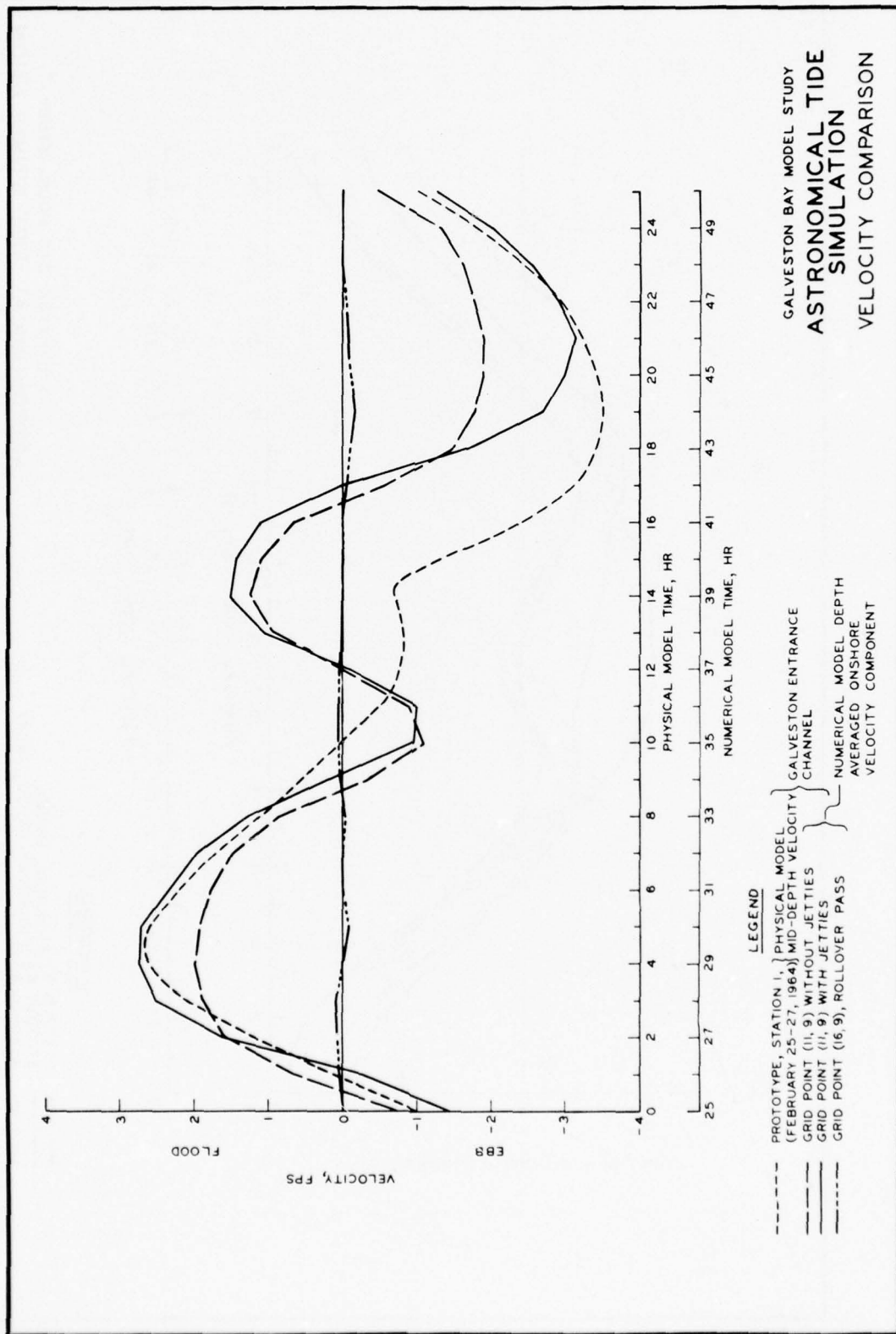
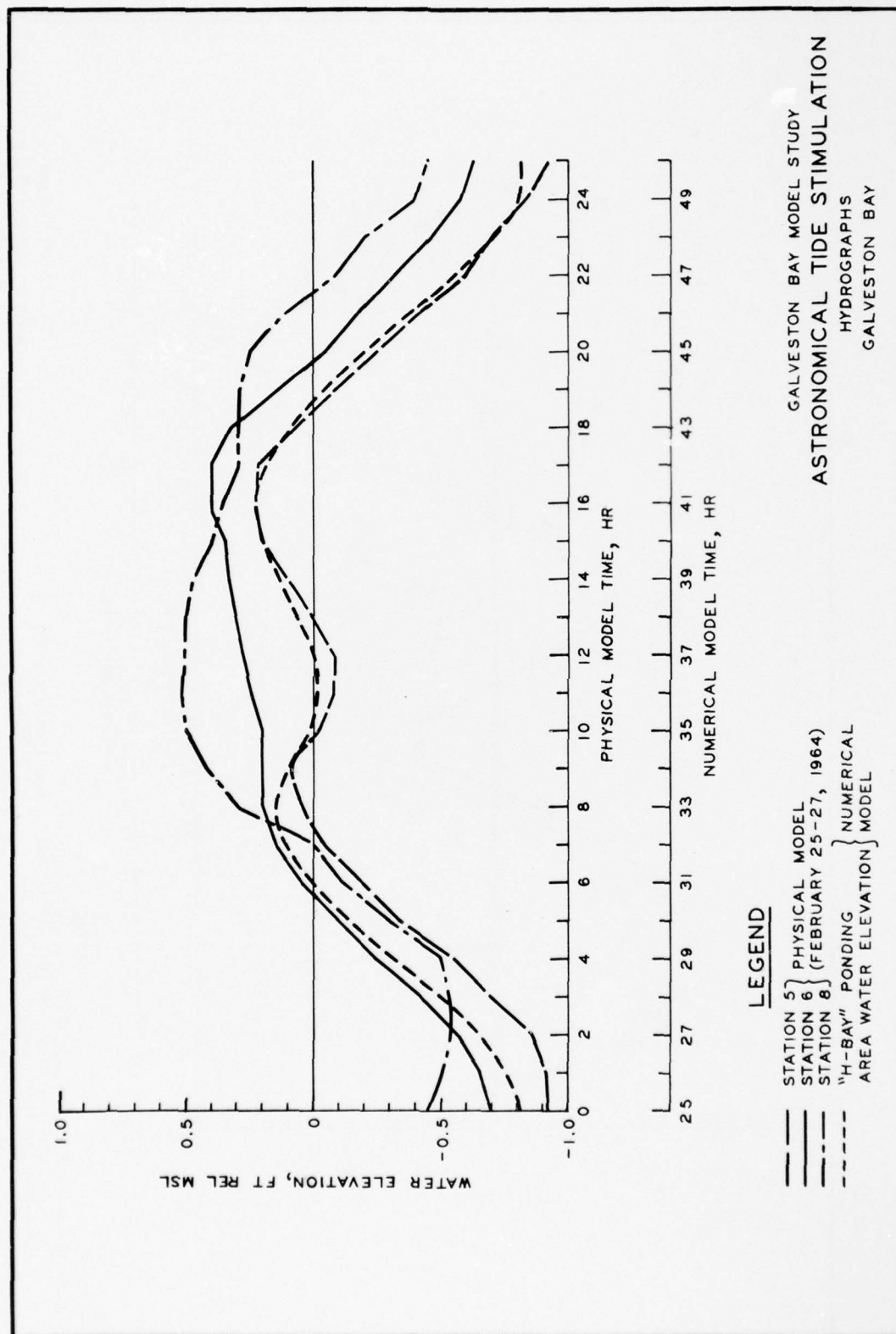
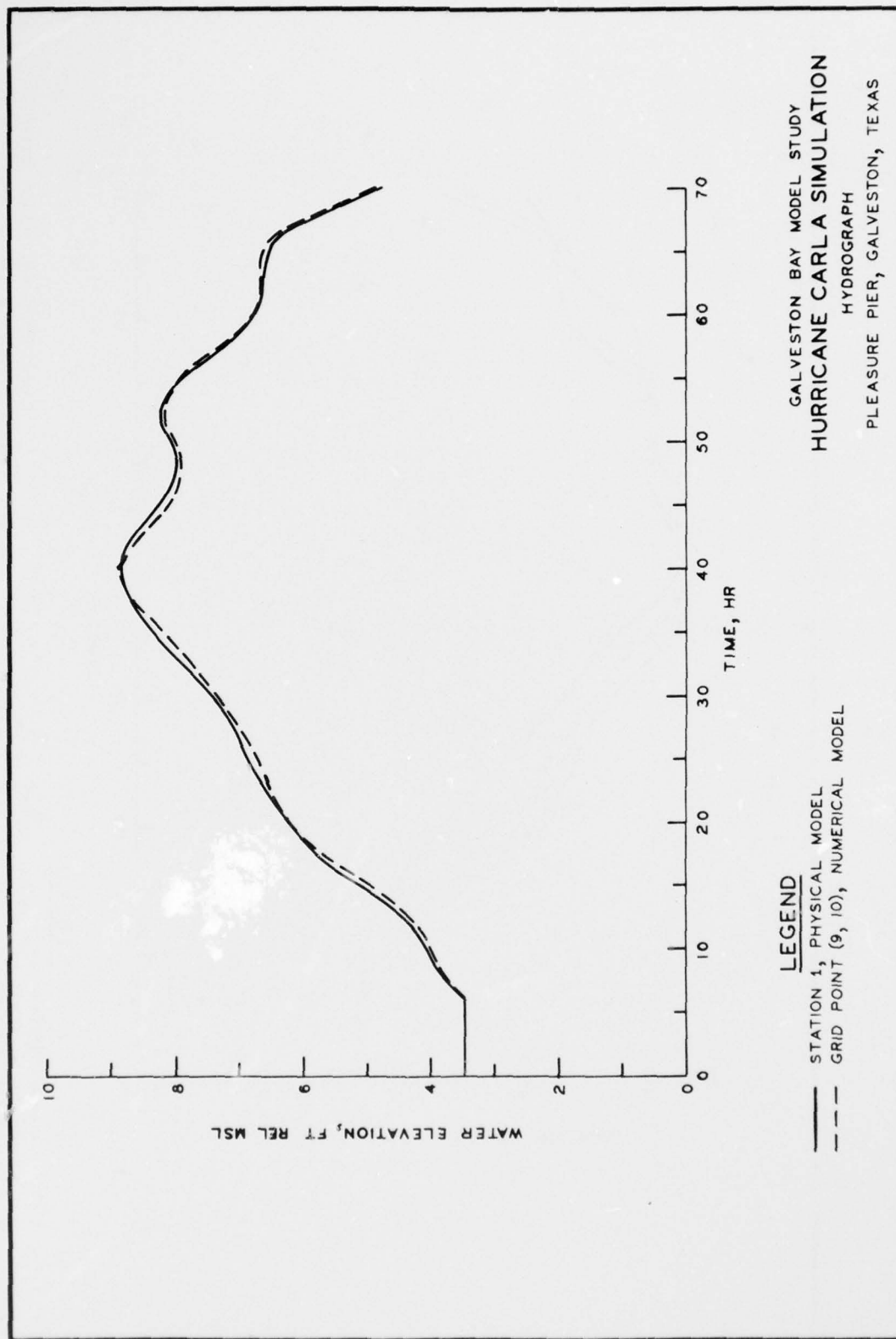


PLATE 6





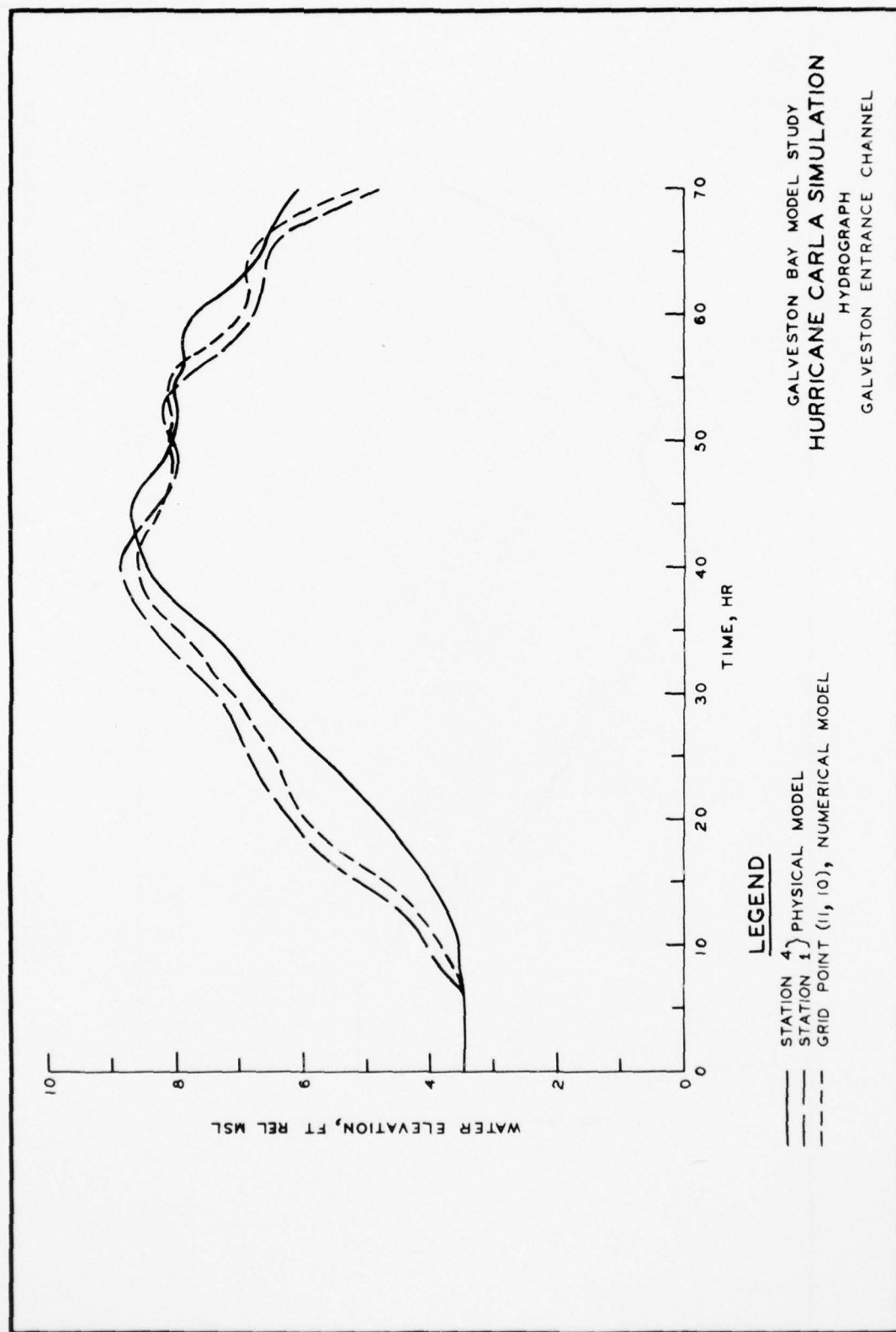
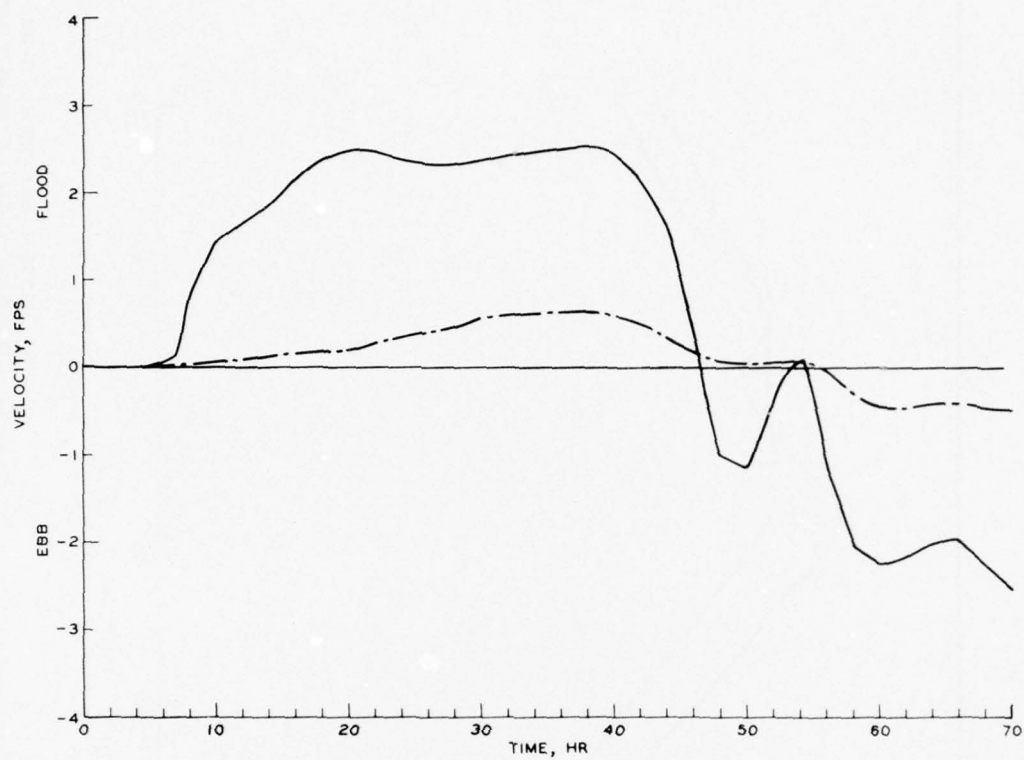


PLATE 8



LEGEND

—	GRID POINT (11, 9), GALVESTON ENTRANCE CHANNEL	} NUMERICAL MODEL DEPTH AVERAGED ONSHORE VELOCITY COMPONENT
- - -	GRID POINT (16, 9), ROLLOVER PASS	

GALVESTON BAY MODEL STUDY
HURRICANE CARLA
 SIMULATION
 VELOCITY

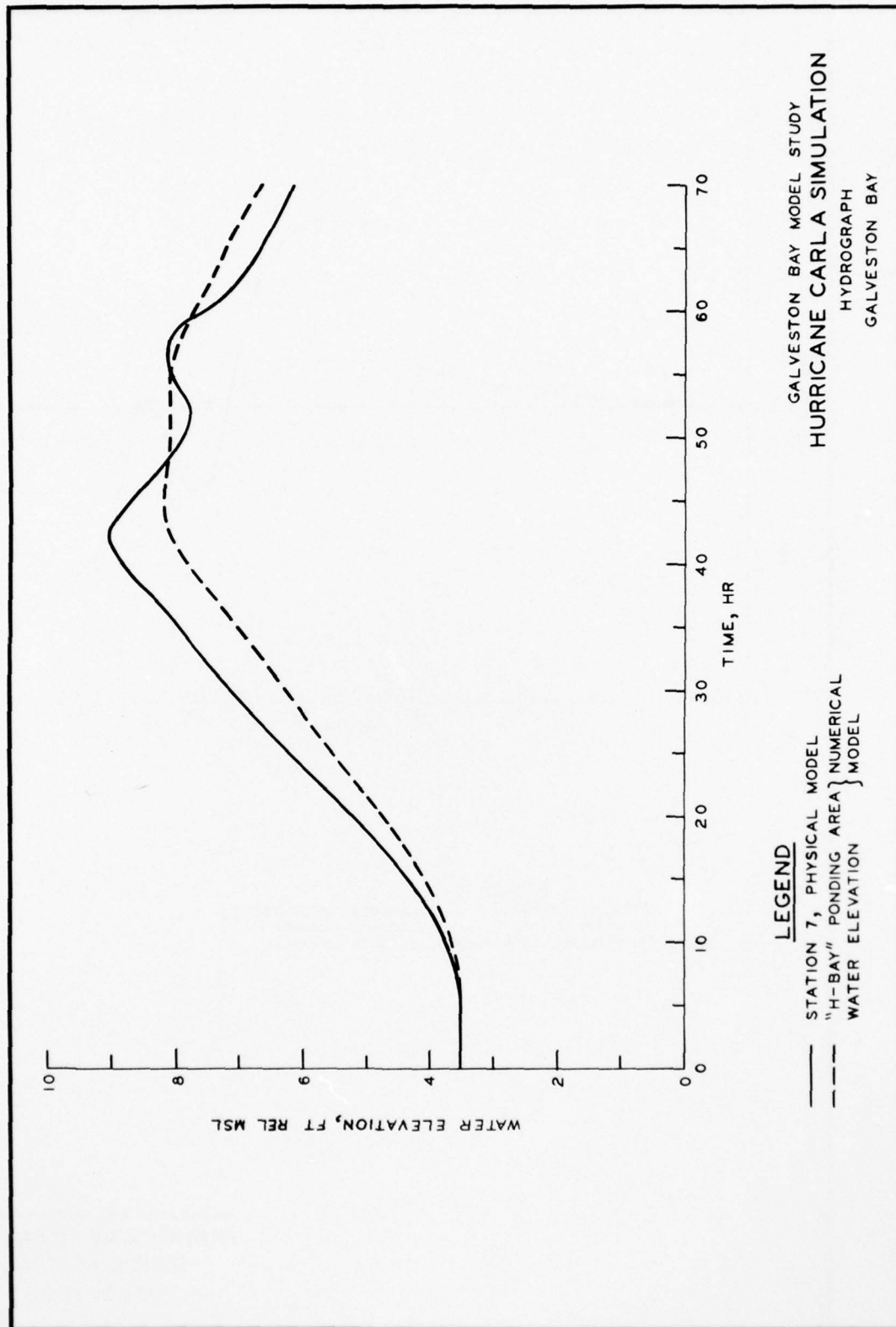
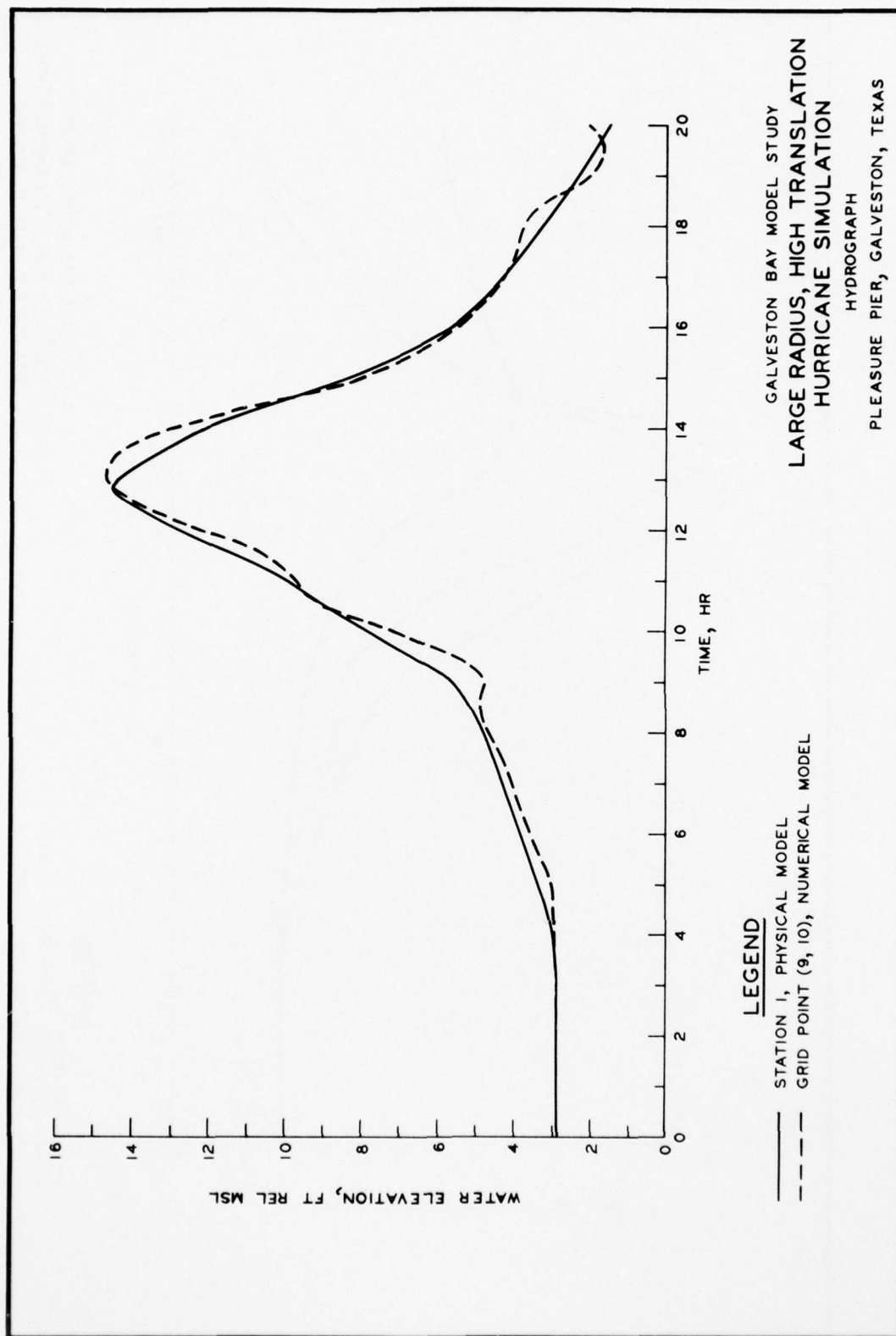


PLATE 10



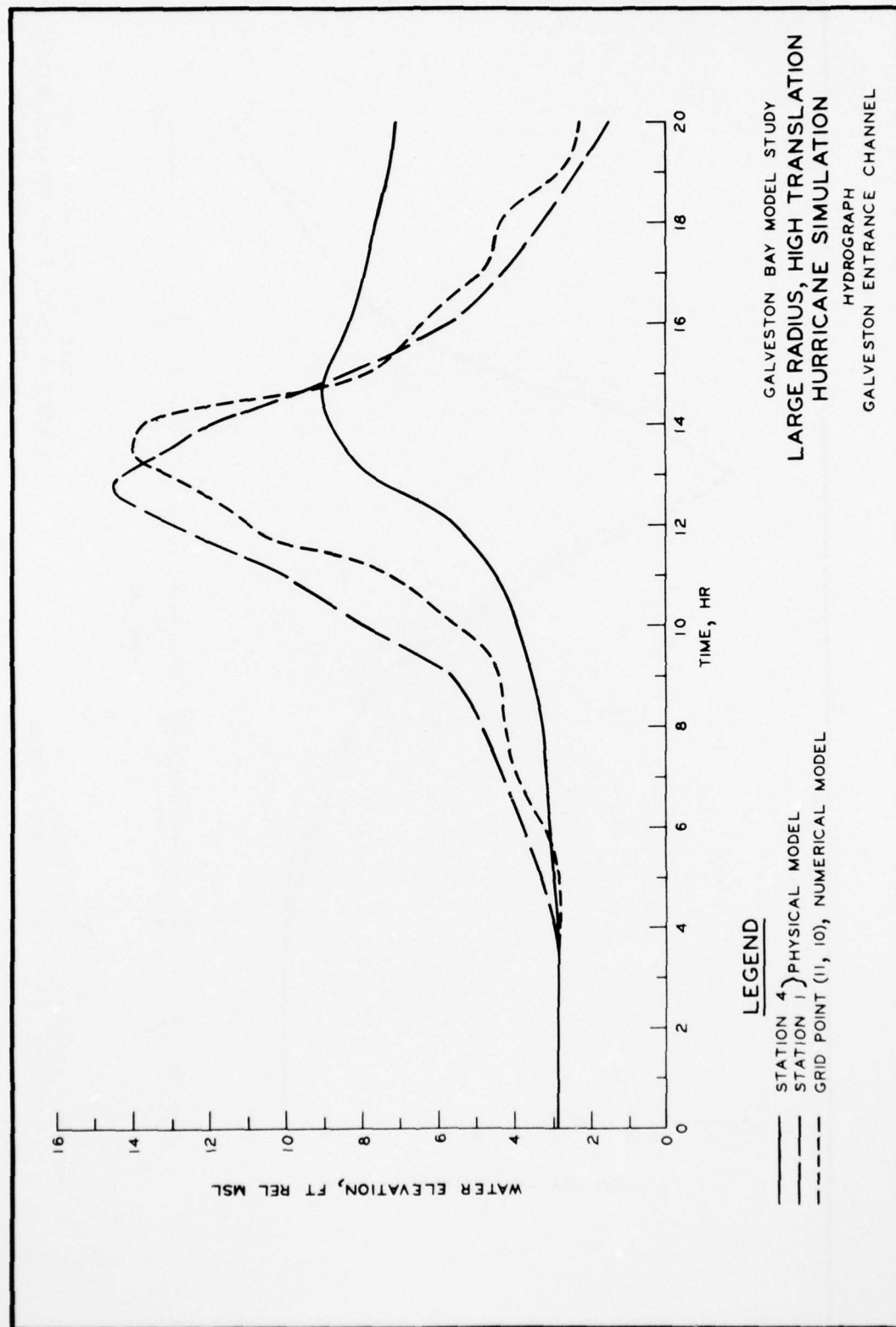
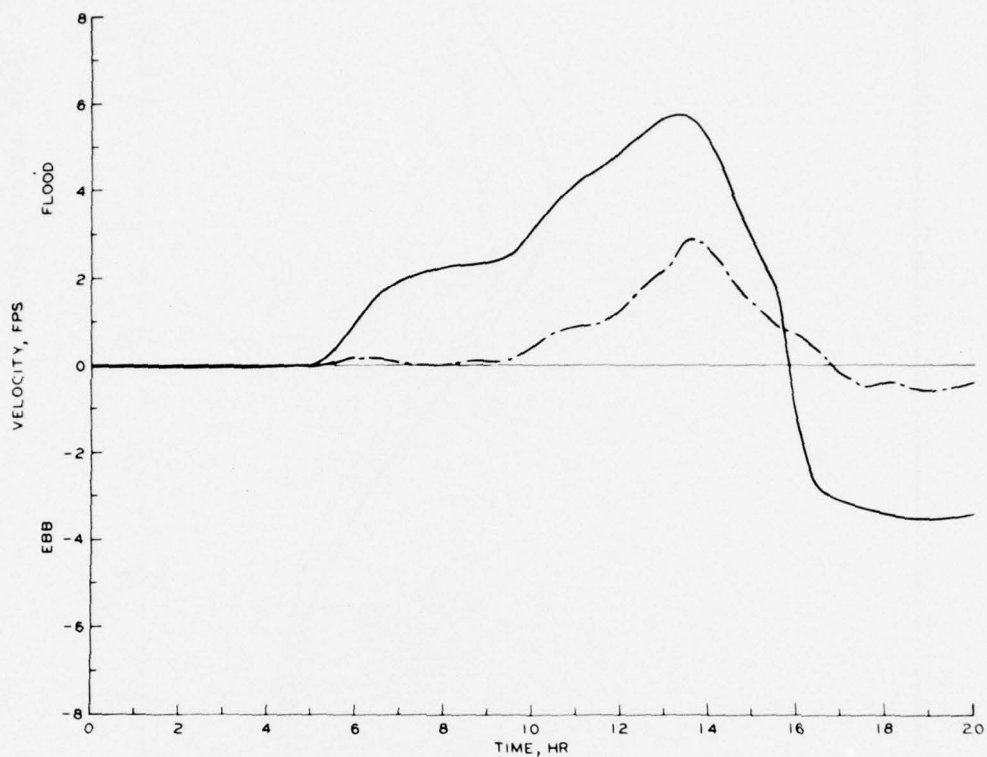


PLATE 12



LEGEND

<p>— GRID POINT (11, 9), GALVESTON ENTRANCE CHANNEL</p> <p>- - - GRID POINT (16, 9), ROLLOVER PASS</p>	<p>}</p>	<p>NUMERICAL MODEL DEPTH</p> <p>AVERAGED ONSHORE</p> <p>VELOCITY COMPONENT</p>
--	----------	--

GALVESTON BAY MODEL STUDY
**LARGE RADIUS,
 HIGH TRANSLATION
 HURRICANE SIMULATION
 VELOCITY**

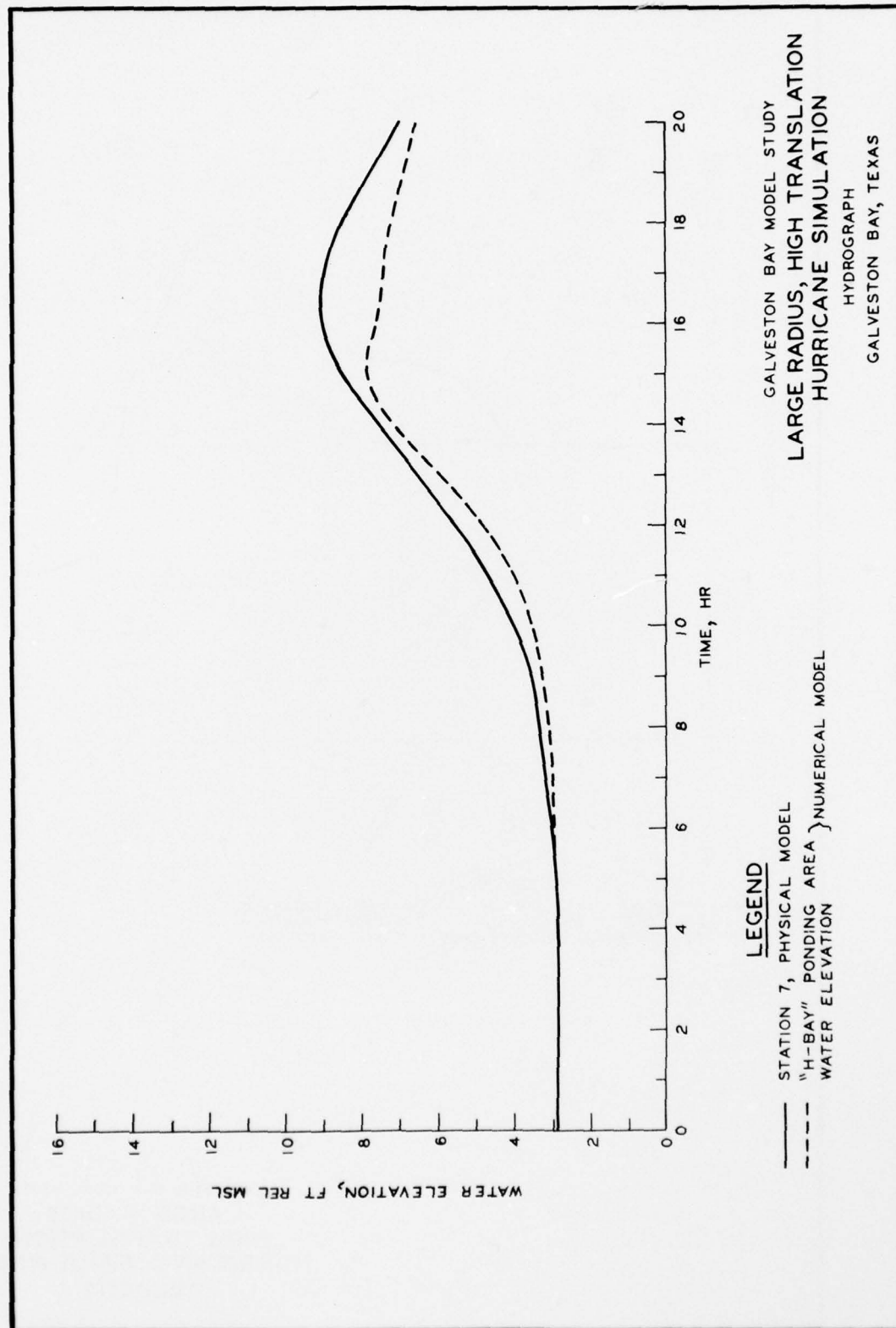
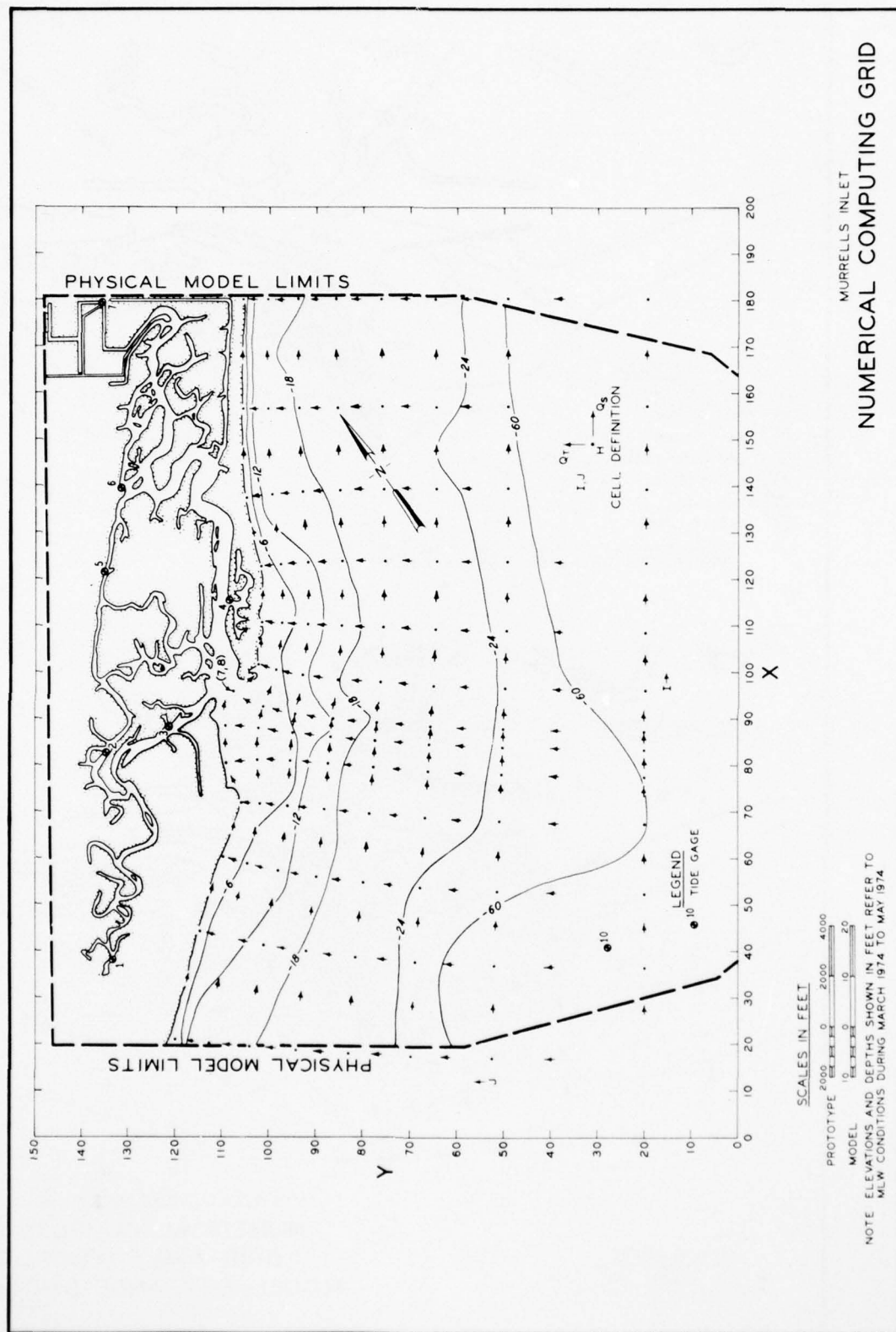


PLATE 14



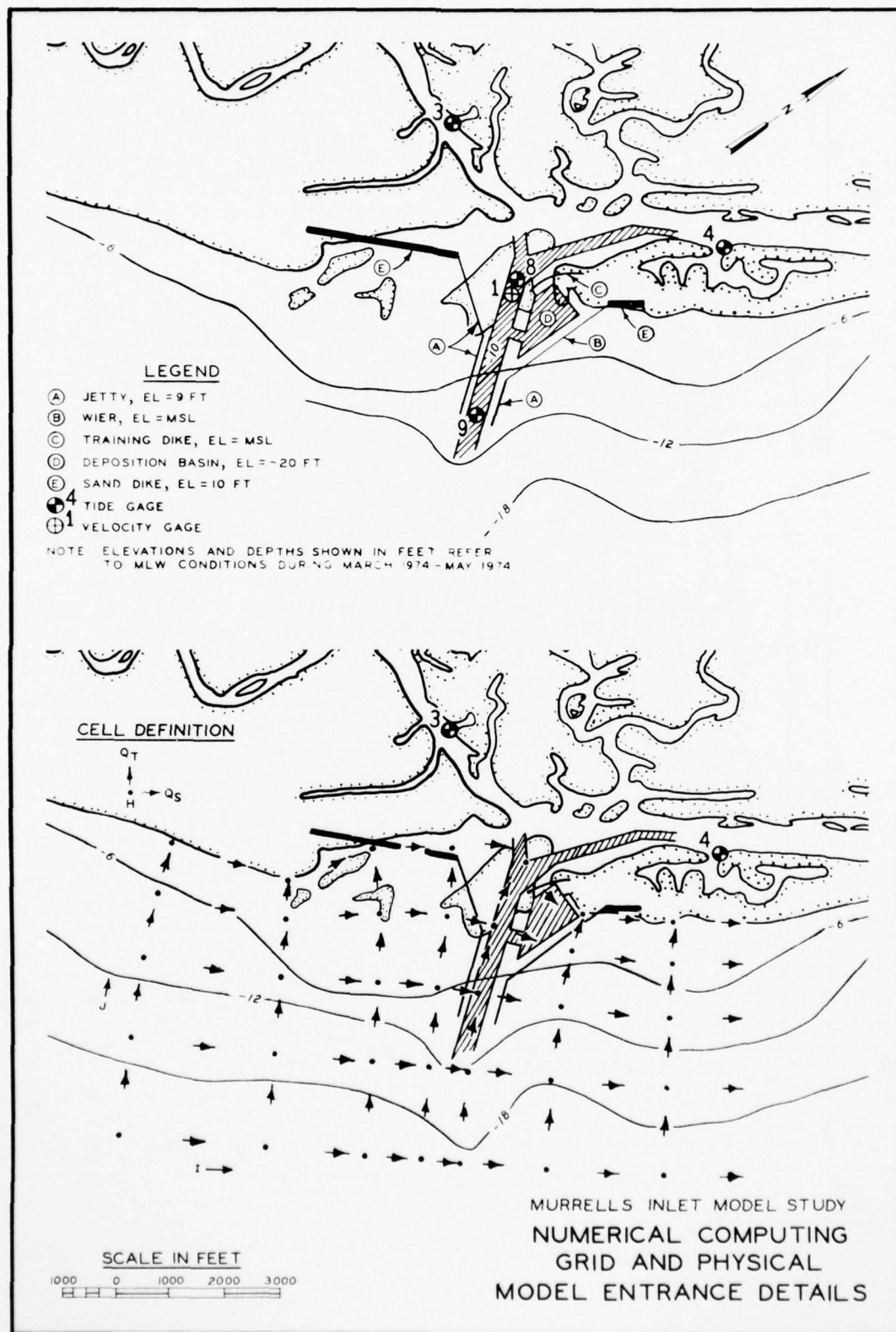
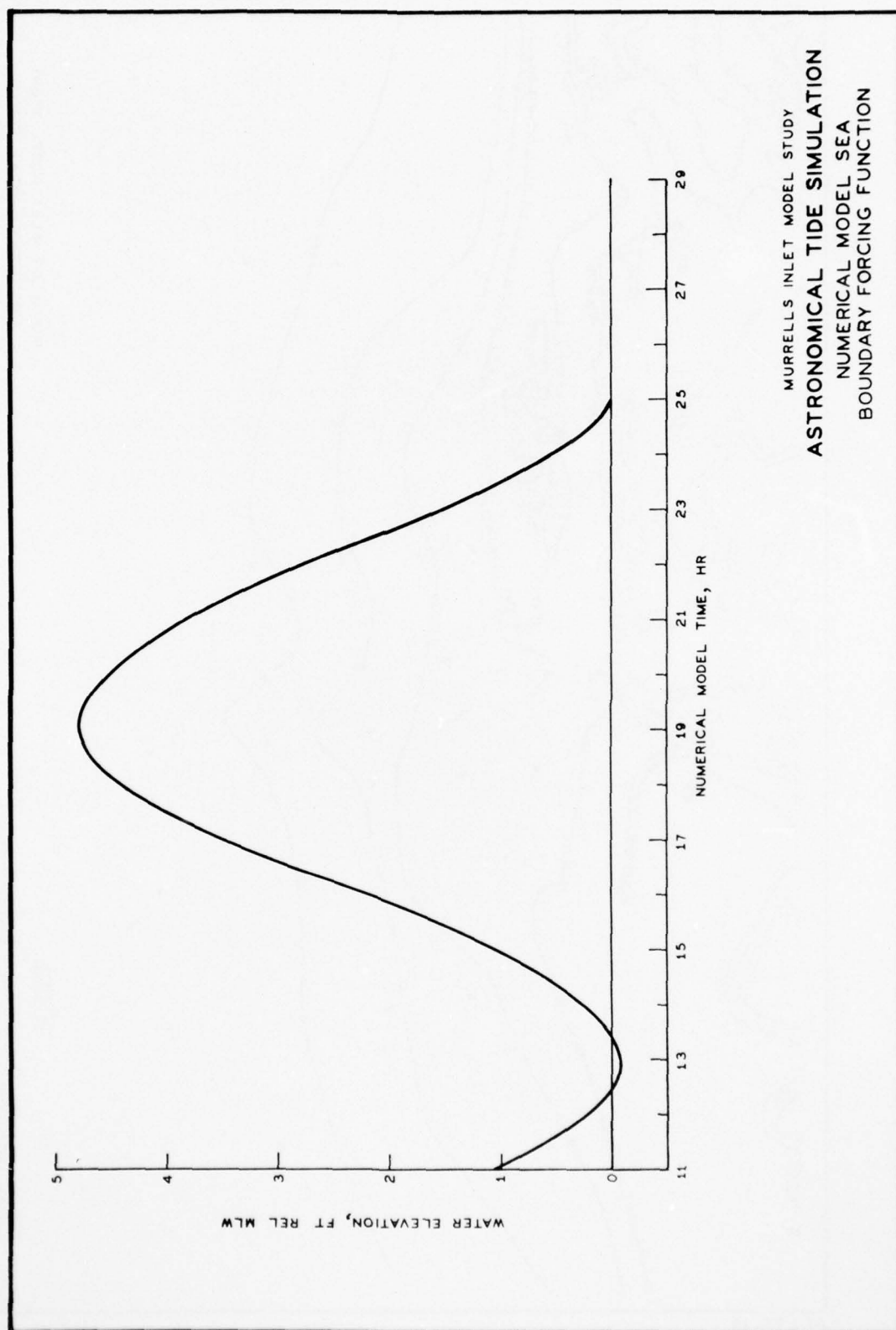


PLATE 16



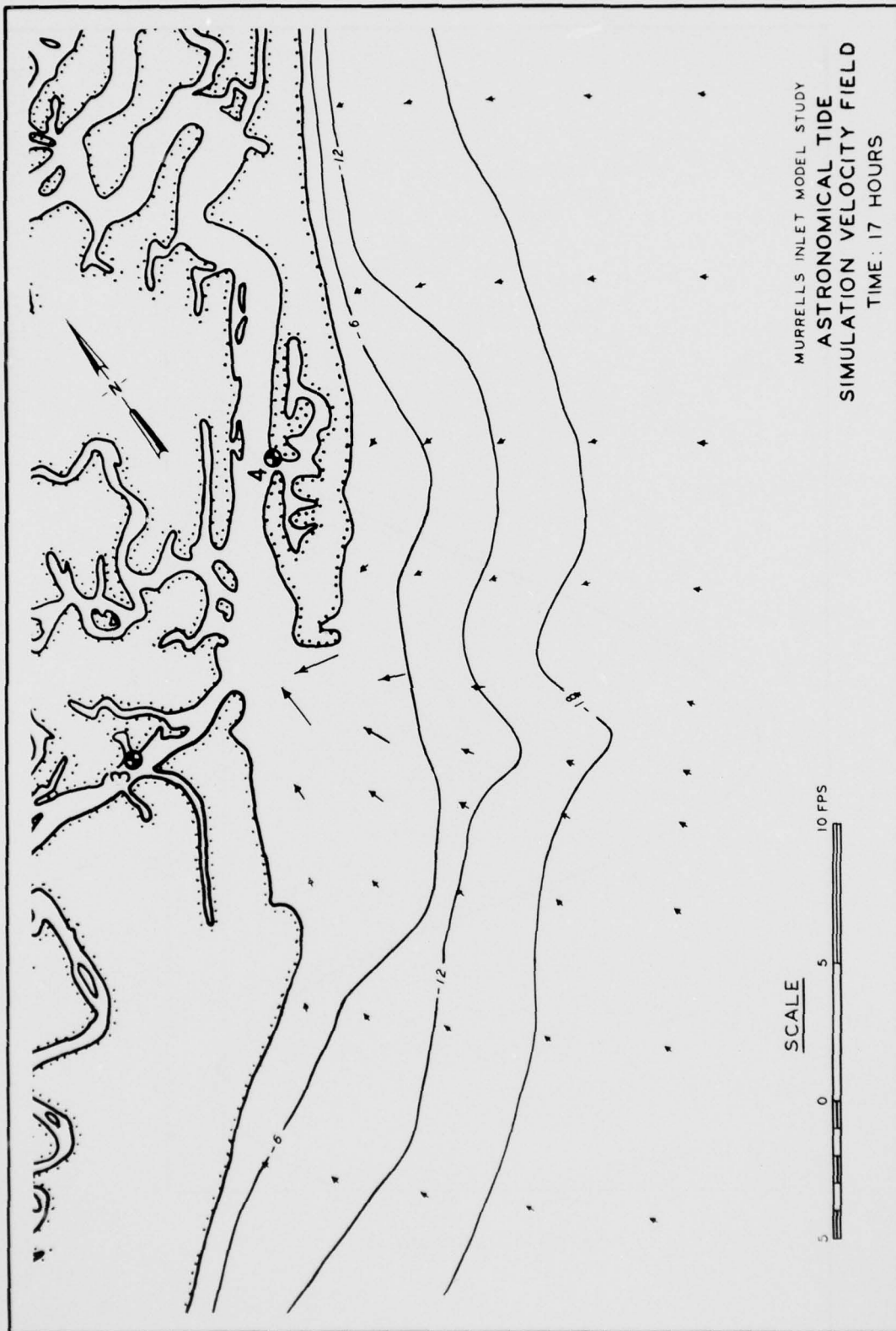
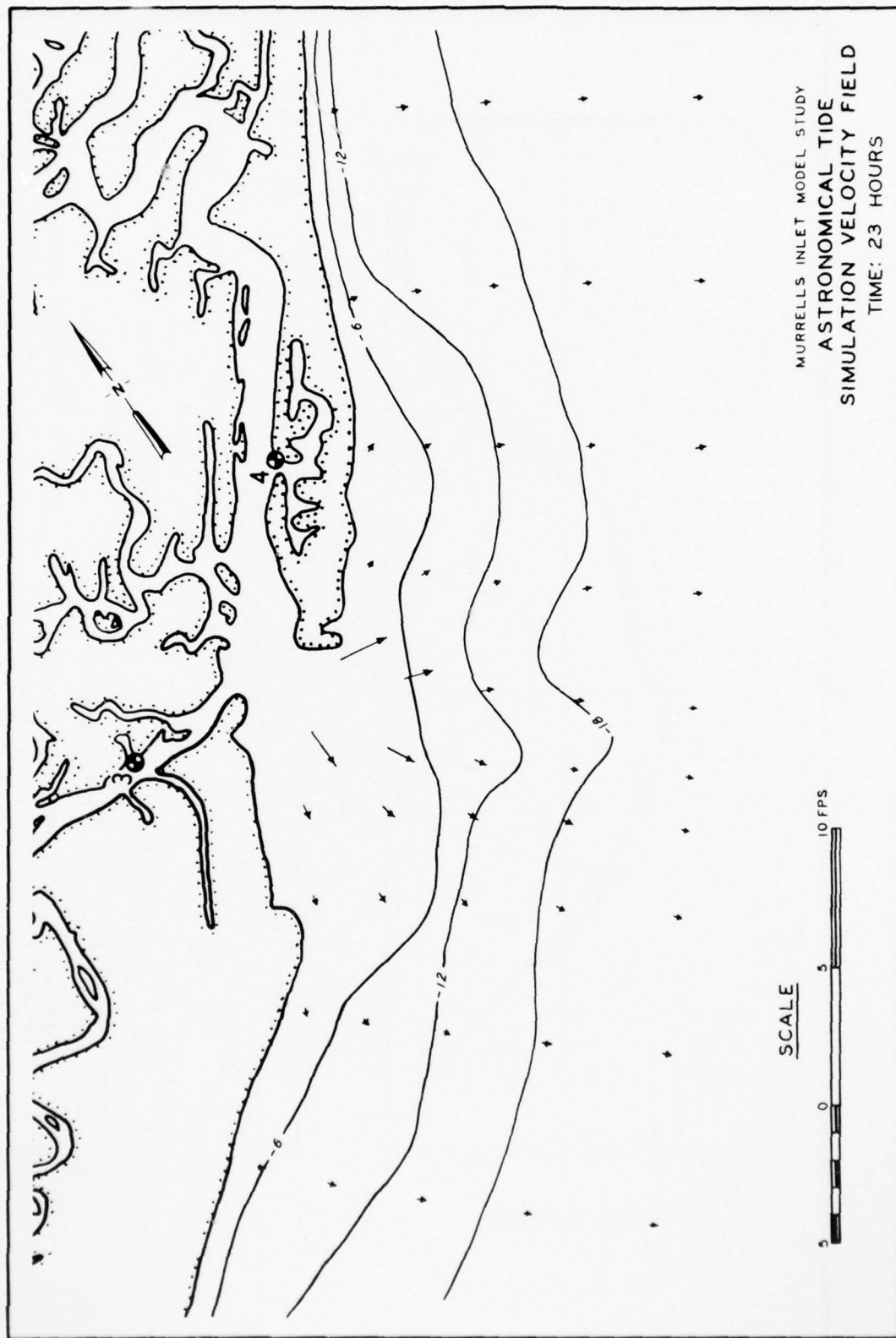
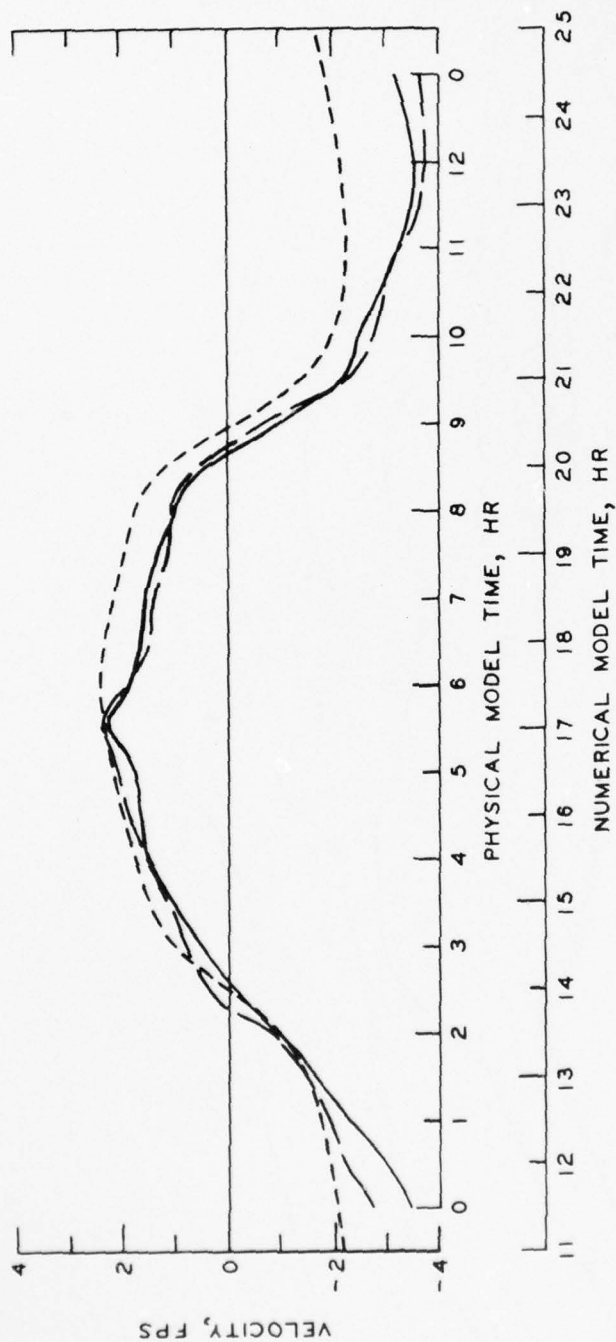


PLATE 18





LEGEND

- SURFACE, STATION 1
- BOTTOM, STATION 1
- DEPTH-AVERAGED, ONSHORE
- VELOCITY AT GRID PT (7, 7)

MURRELLS INLET MODEL STUDY
ASTRONOMICAL TIDE
SIMULATION
VELOCITY COMPARISON

AD-AU47 994

ARMY ENGINEER WATERWAYS EXPERIMENT STATION VICKSBURG MISS F/G 4/2
NEARSHORE NUMERICAL STORM SURGE AND TIDAL SIMULATION.(U)
SEP 77 J J WANSTRATH

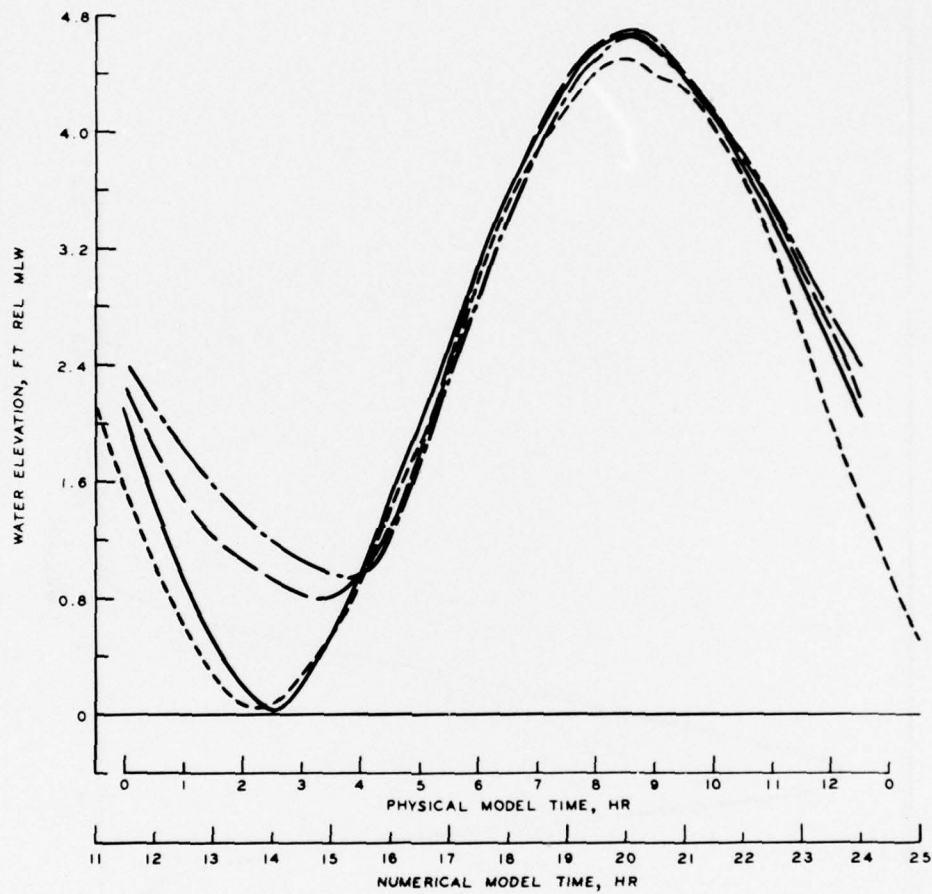
UNCLASSIFIED

WES-TR-H-77-17

NL

20f 2
ADAO47994

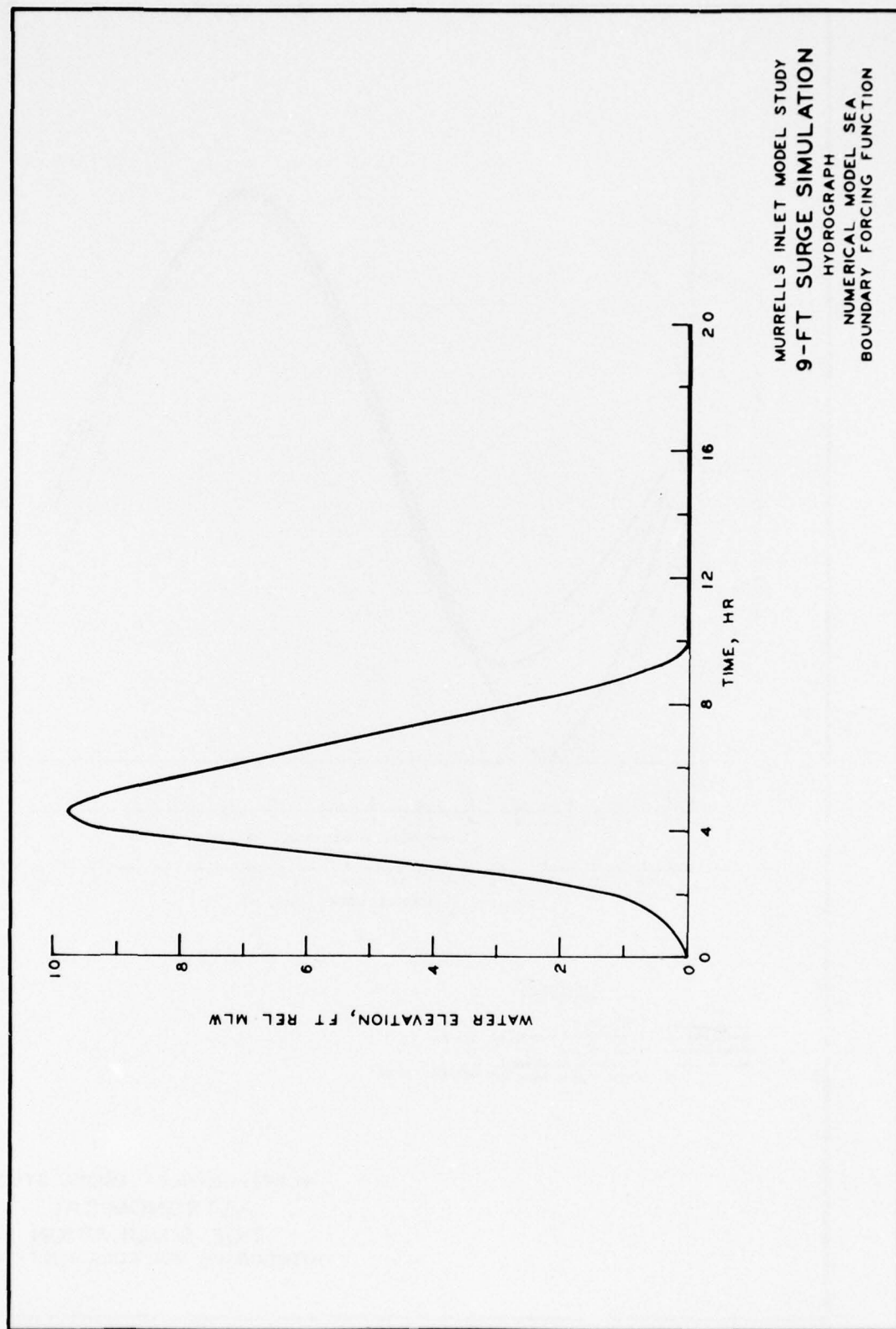


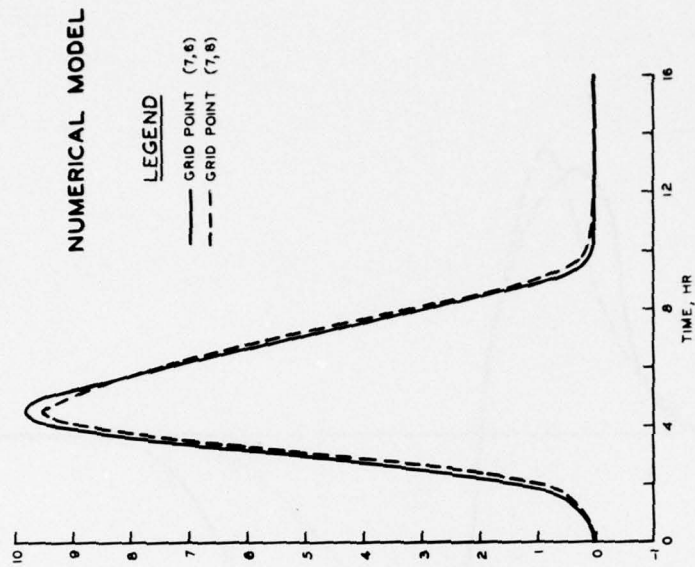
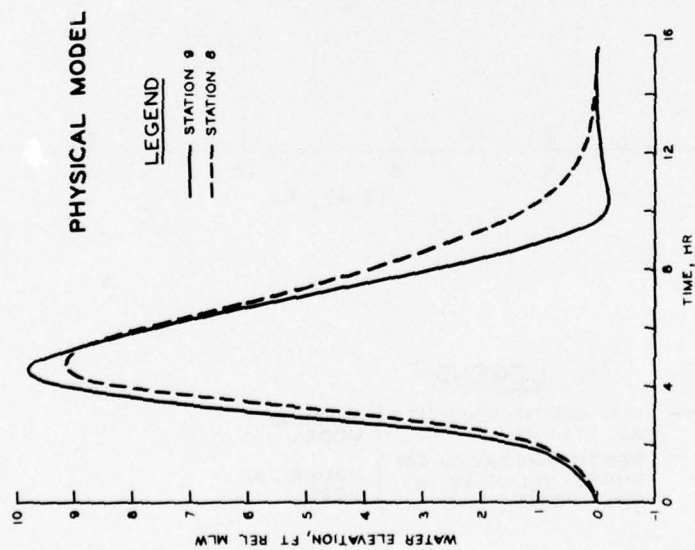


LEGEND

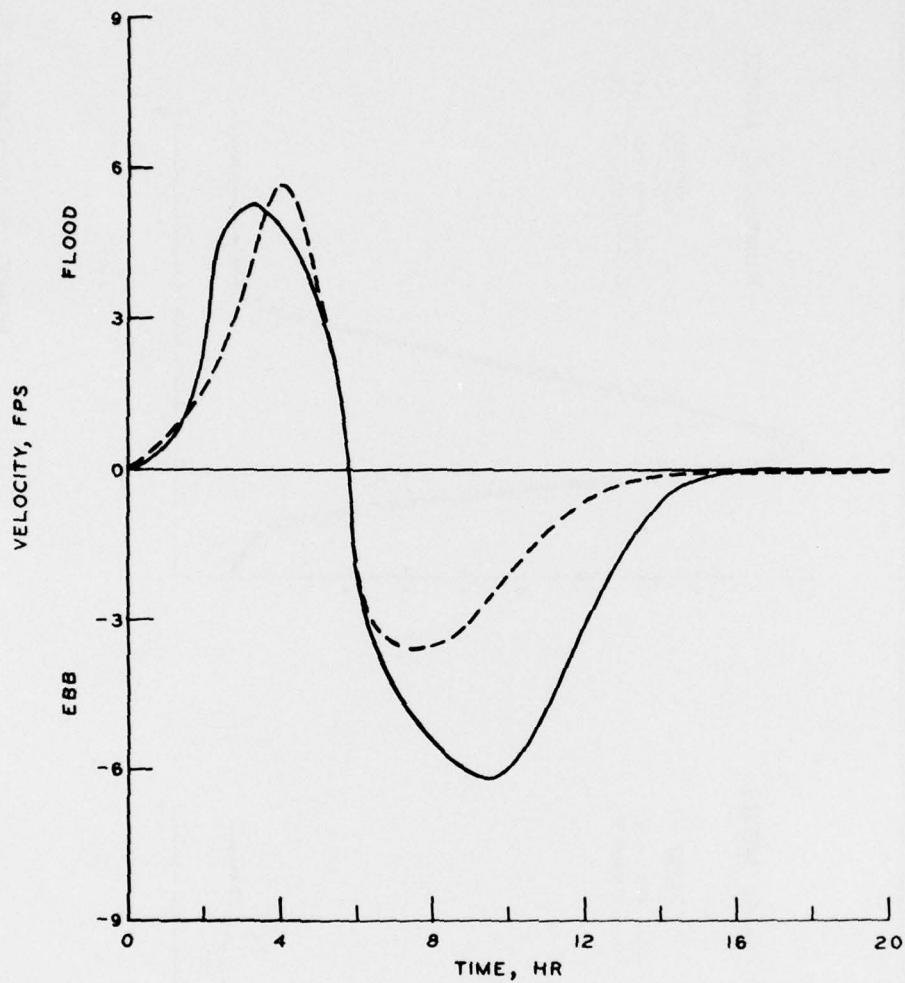
=====	STATION 6	} PHYSICAL MODEL
-----	STATION 5	
- - - - -	STATION 2	
- . - . -	"H-BAY" PONDING	} NUMERICAL MODEL
-----	AREA ELEVATION	

MURRELLS INLET MODEL STUDY
**ASTRONOMICAL
TIDE SIMULATION**
HYDROGRAPH, MURRELLS INLET-BAY





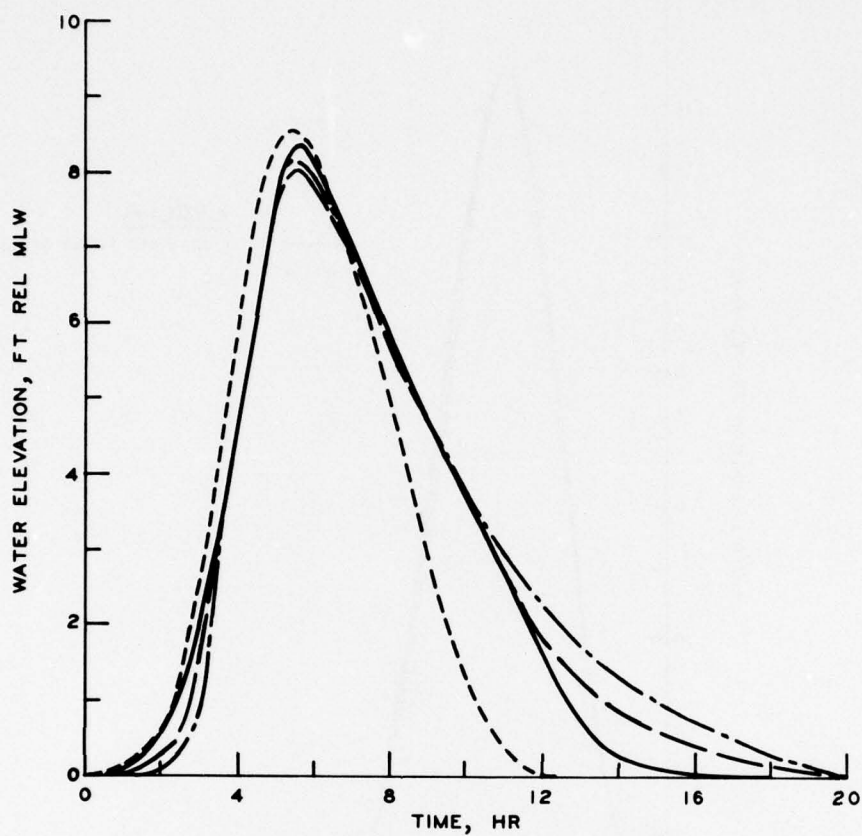
MURRELLS INLET MODEL STUDY
9-FT SURGE SIMULATION
HYDROGRAPH COMPARISON
MURRELLS INLET ENTRANCE



LEGEND

—	MID DEPTH VELOCITY AT STATION 1	} PHYSICAL MODEL
- - -	DEPTH AVERAGED ON SHORE VELOCITY AT GRID POINT (7, 7)	
		} NUMERICAL MODEL

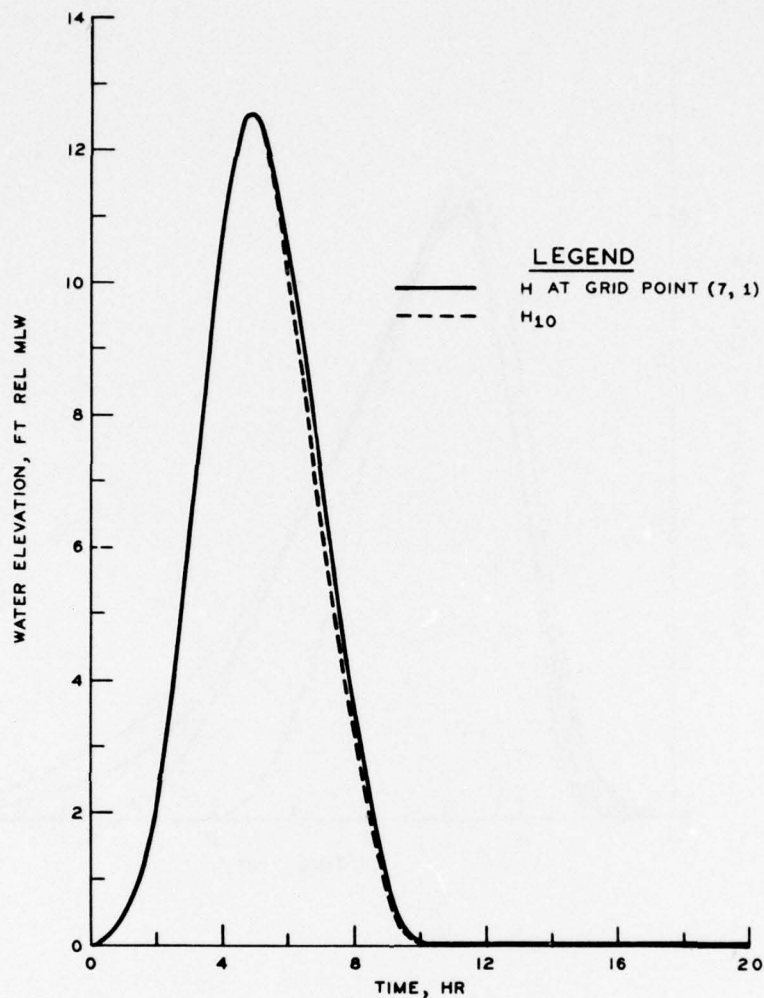
MURRELLS INLET MODEL STUDY
9-FT SURGE SIMULATION
VELOCITY COMPARISON



LEGEND

————	STATION 6	} PHYSICAL MODEL
————	STATION 5	
————	STATION 2	
- - - -	"H-BAY" PONDING	} NUMERICAL MODEL
- - - -	AREA ELEVATION	

MURRELLS INLET MODEL STUDY
9-FT SURGE SIMULATION
HYDROGRAPH, MURRELLS INLET-BAY



NUMERICAL MODEL SEA BOUNDARY FORCING FUNCTION

$$H = H_{10} + H_r$$

H_{10} = PHYSICAL MODEL HYDROGRAPH AT STATION 10
AND APPLIED TO ALL H-GRID POINTS ALONG $J=1$
 H_r = WATER ELEVATION DUE TO RADIATION COMPONENT

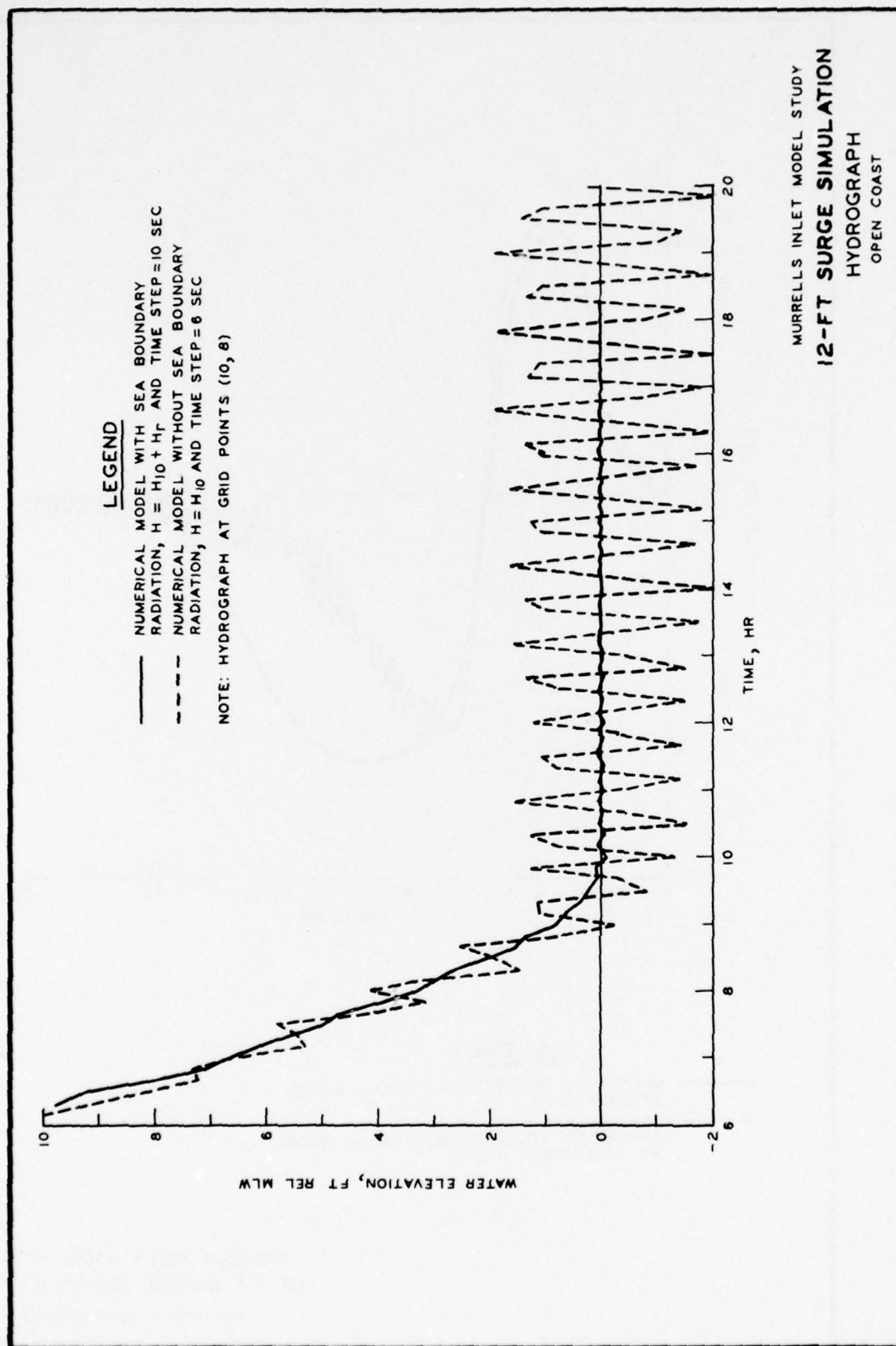
TIME ≤ 10 HR:

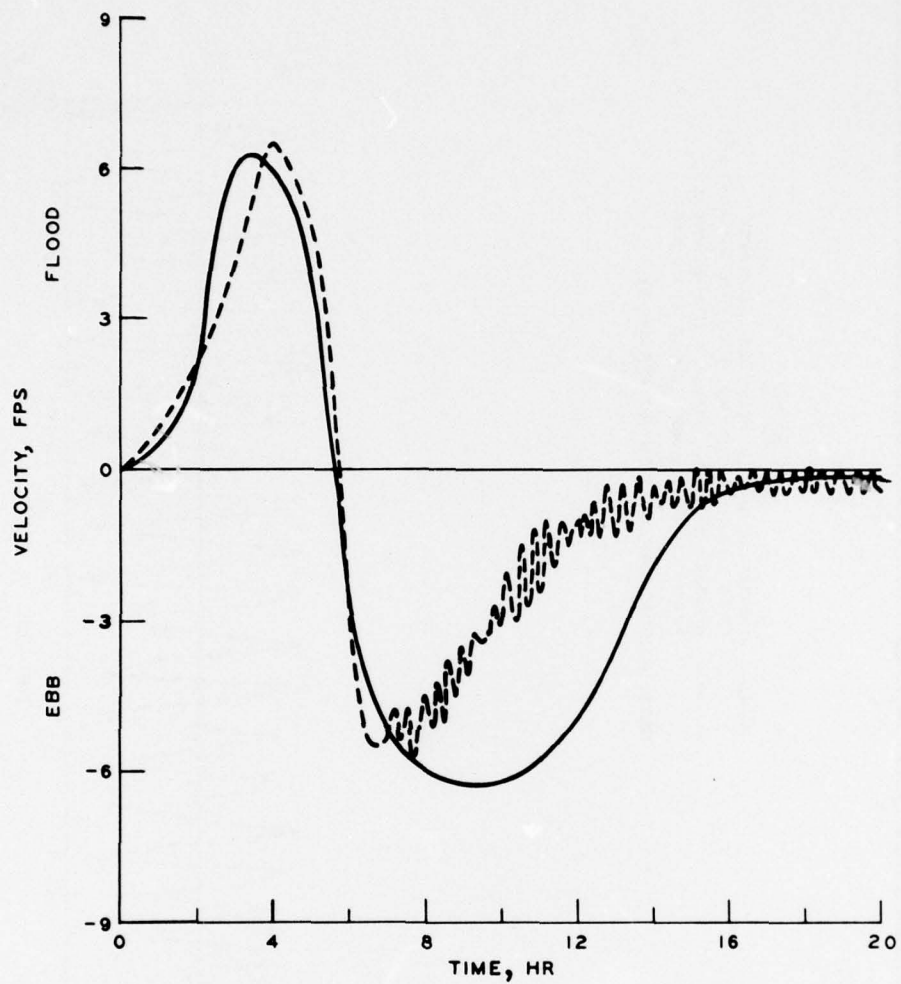
$$H_{10} = A_0 + \sum_{K=1}^4 A_K \cos\left(\frac{2\pi t}{T_K} - \phi_K\right)$$

A = AMPLITUDE, FT	K	A_K	T_K	ϕ_K
T = PERIOD, HR	0	5.26	—	—
t = TIME	1	6.12	10.0	-177
ϕ = PHASE, DEGREES	2	0.98	5.0	-20
	3	0.30	3.3	114
	4	0.05	2.5	35

TIME > 10 HR, $H_{10} = 0$

MURRELLS INLET MODEL STUDY
12-FT SURGE SIMULATION
HYDROGRAPH
NUMERICAL MODEL SEA
BOUNDARY FORCING FUNCTION

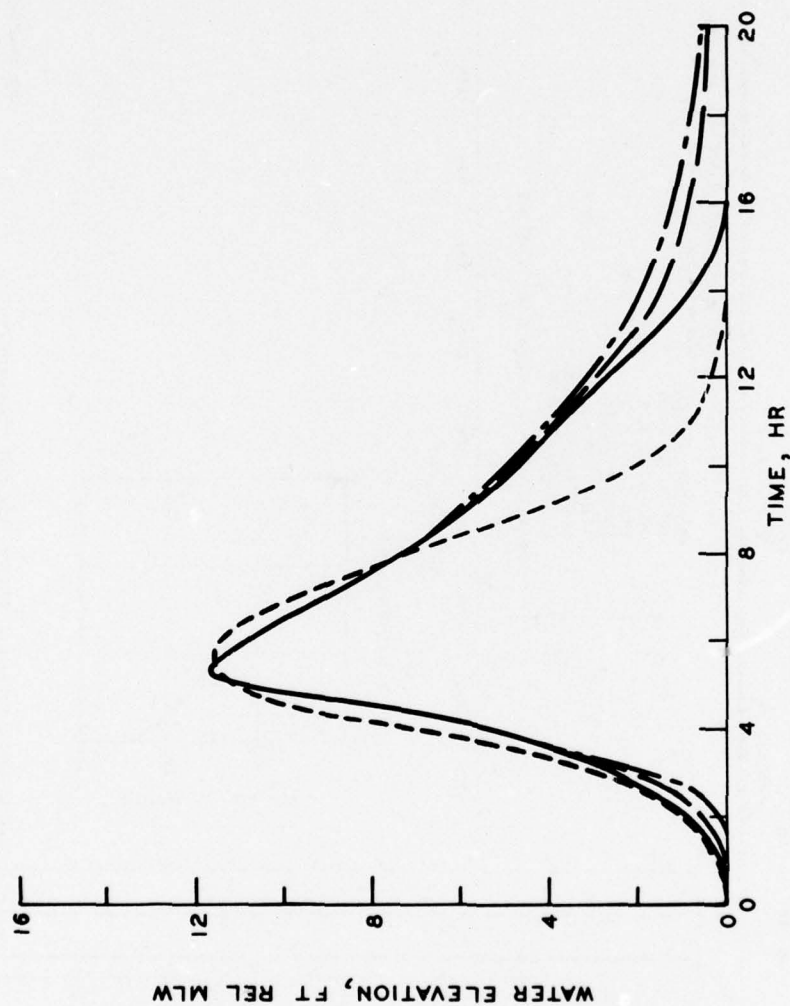




LEGEND

- | | | |
|-------|---|-------------------|
| ———— | MIDDEPTH VELOCITY
AT STATION 1 | } PHYSICAL MODEL |
| ----- | DEPTH-AVERAGED
ON-SHORE VELOCITY
AT GRID POINT (7, 7) | |
| | | } NUMERICAL MODEL |

MURRELS INLET MODEL STUDY
12-FT SURGE SIMULATION
VELOCITY COMPARISON



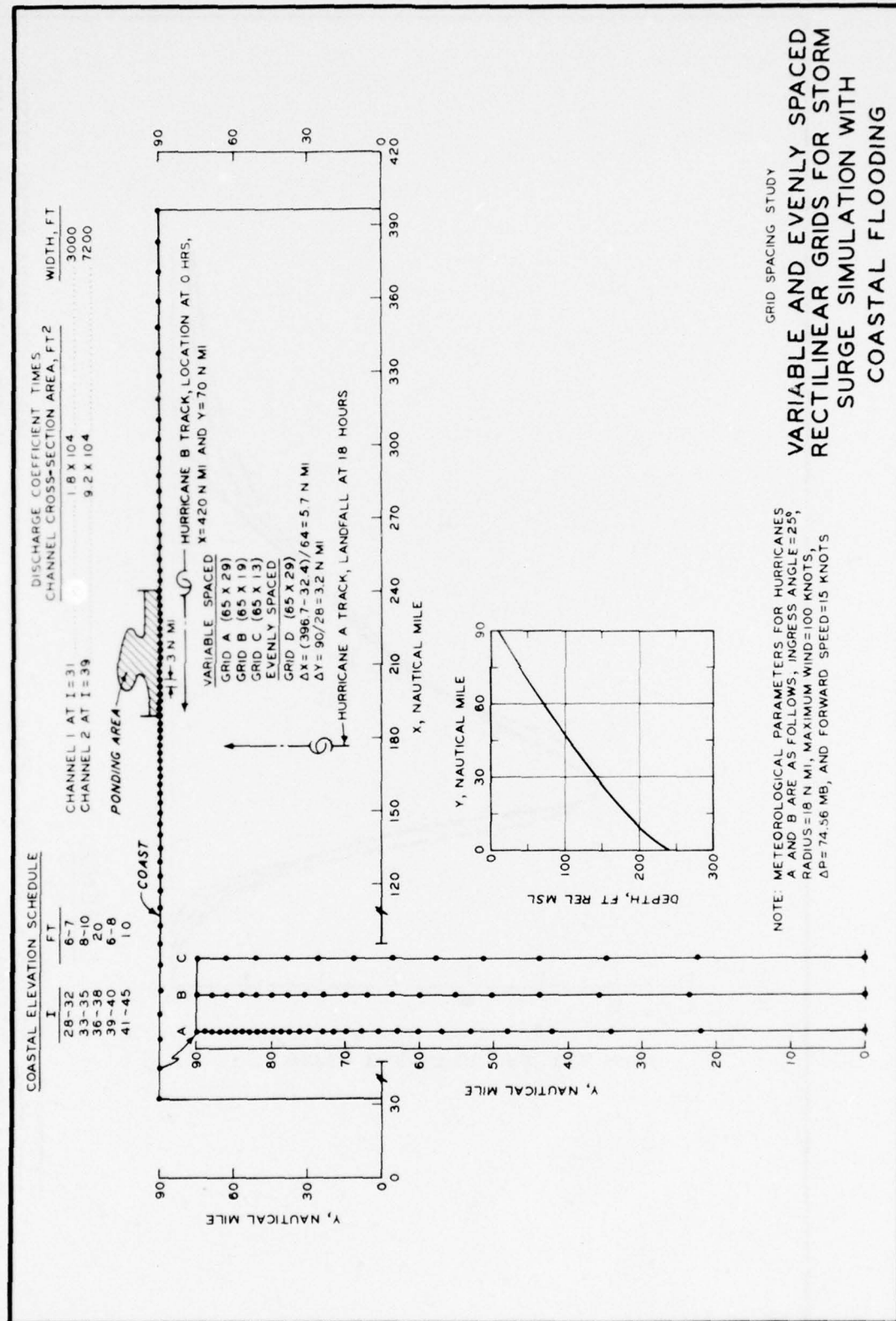
LEGEND

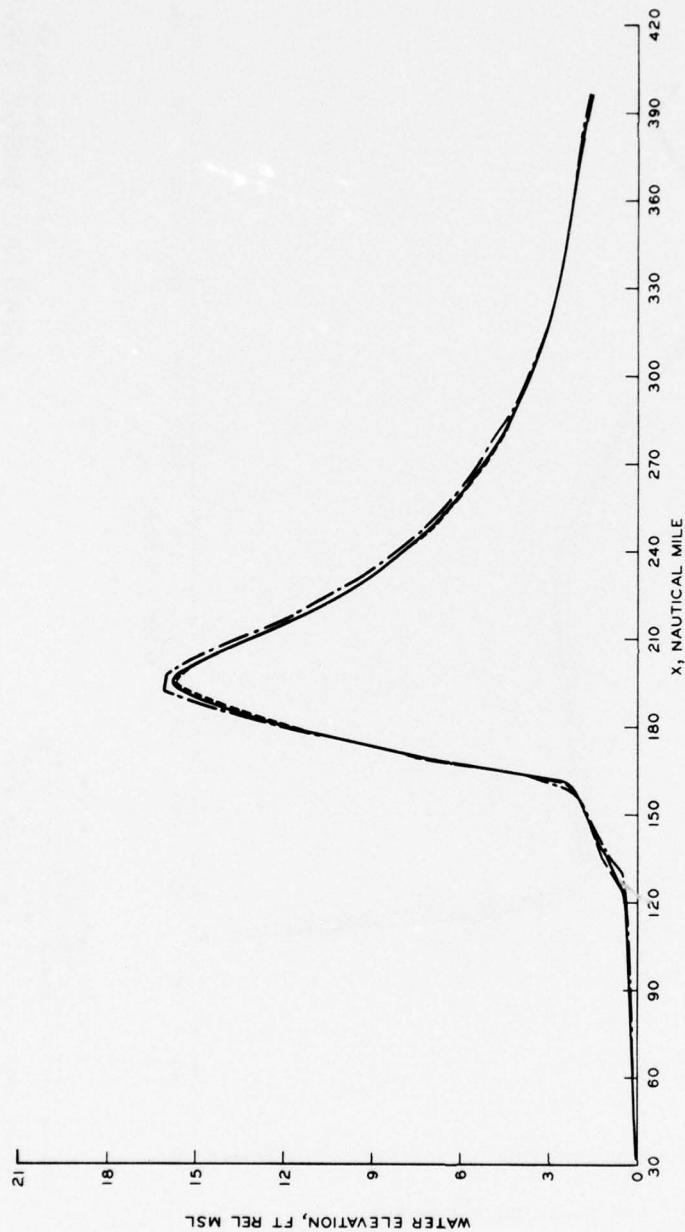


STATION 6 } PHYSICAL MODEL
STATION 5 }
STATION 2 }

"H-BAY" PONDING } NUMERICAL MODEL
AREA ELEVATION }

MURRELLS INLET MODEL STUDY
12-FT SURGE SIMULATION
HYDROGRAPH, MURRELLS INLET-BAY





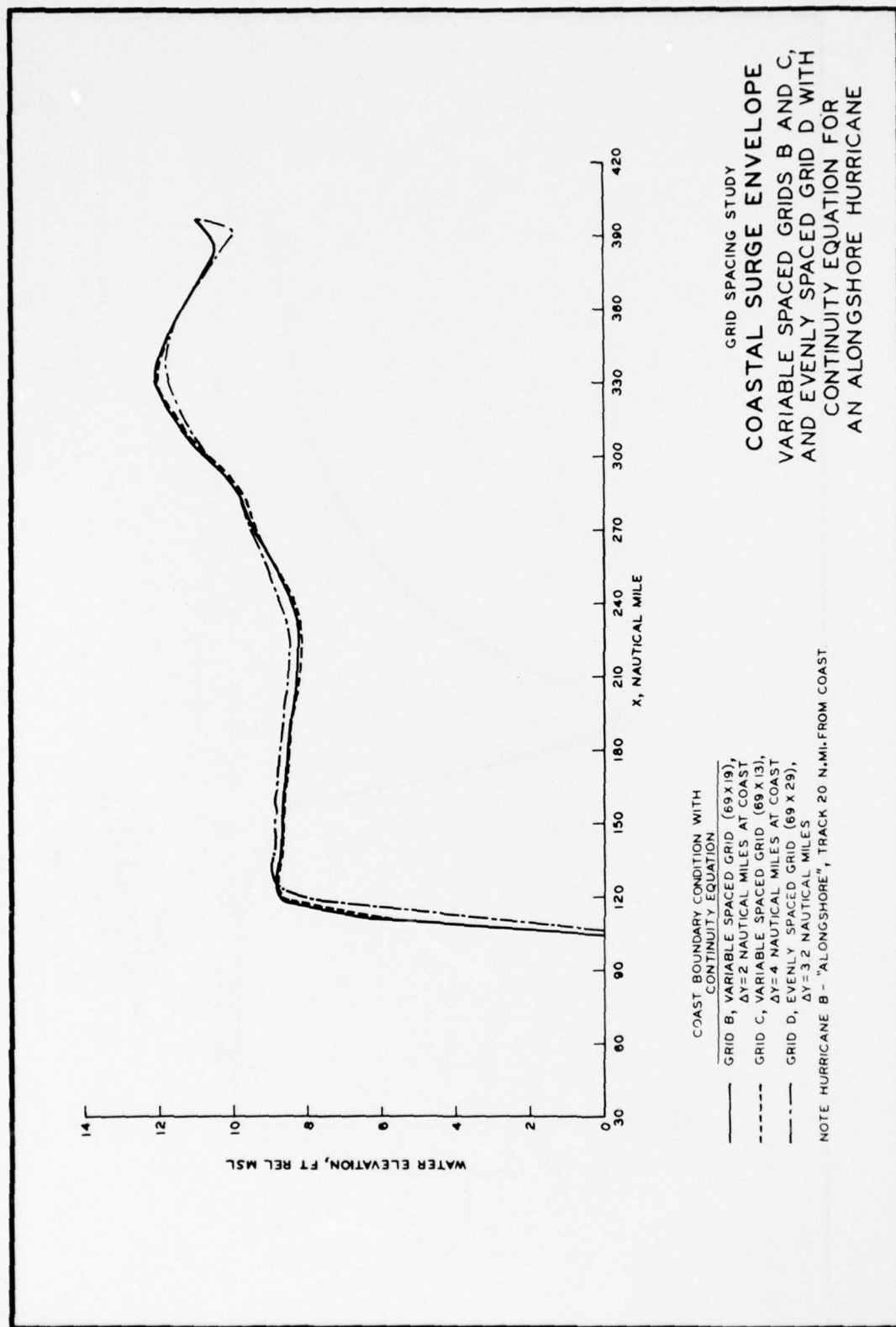
LEGEND

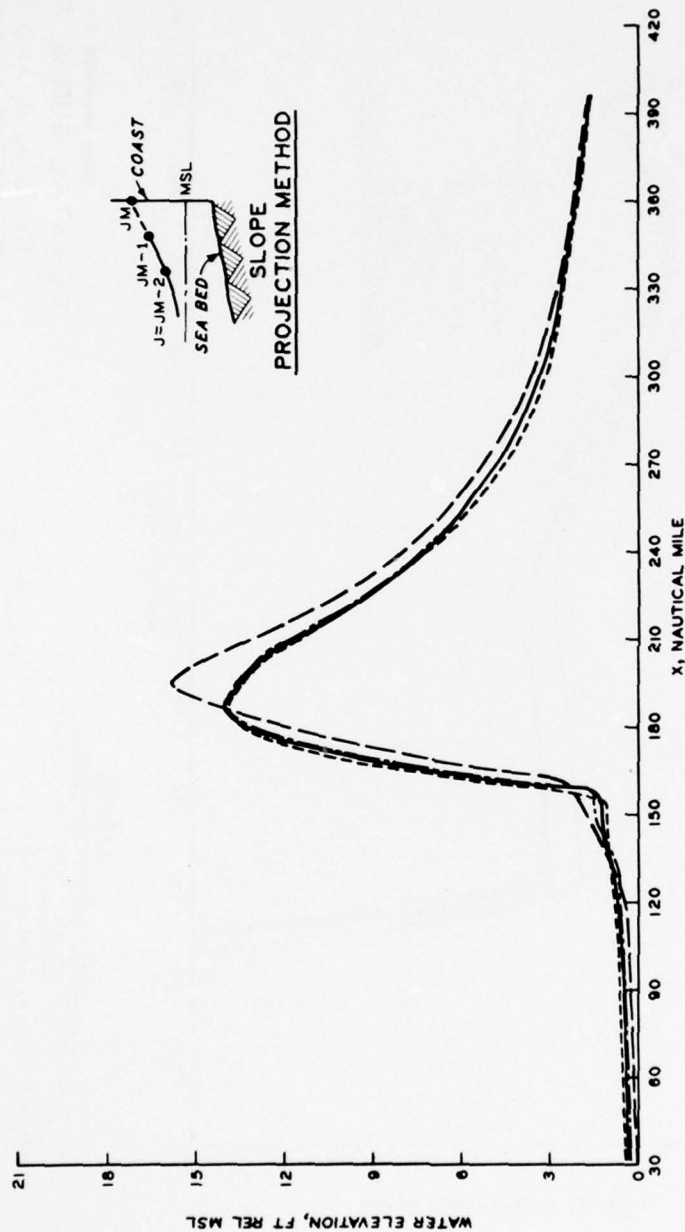
COAST BOUNDARY CONDITION WITH
CONTINUITY EQUATION

- GRID B, VARIABLE SPACED GRID (69 x 19)
 $\Delta Y = 2$ N.MI. AT COAST
- - - - GRID C, VARIABLE SPACED GRID (69 x 13)
 $\Delta Y = 4$ N.MI. AT COAST
- · - · - GRID D, EVENLY SPACED GRID (69 x 29)
 $\Delta Y = 3.2$ N.MI.

NOTE: HURRICANE A - "ONSHORE", LANDFALL AT $x = 177$ N.MI.

GRID SPACING STUDY
COASTAL SURGE ENVELOPE
VARIABLE SPACED GRIDS B AND C,
AND EVENLY SPACED GRID D WITH
CONTINUITY EQUATION FOR
AN ONSHORE HURRICANE





LEGEND

COAST BOUNDARY CONDITION

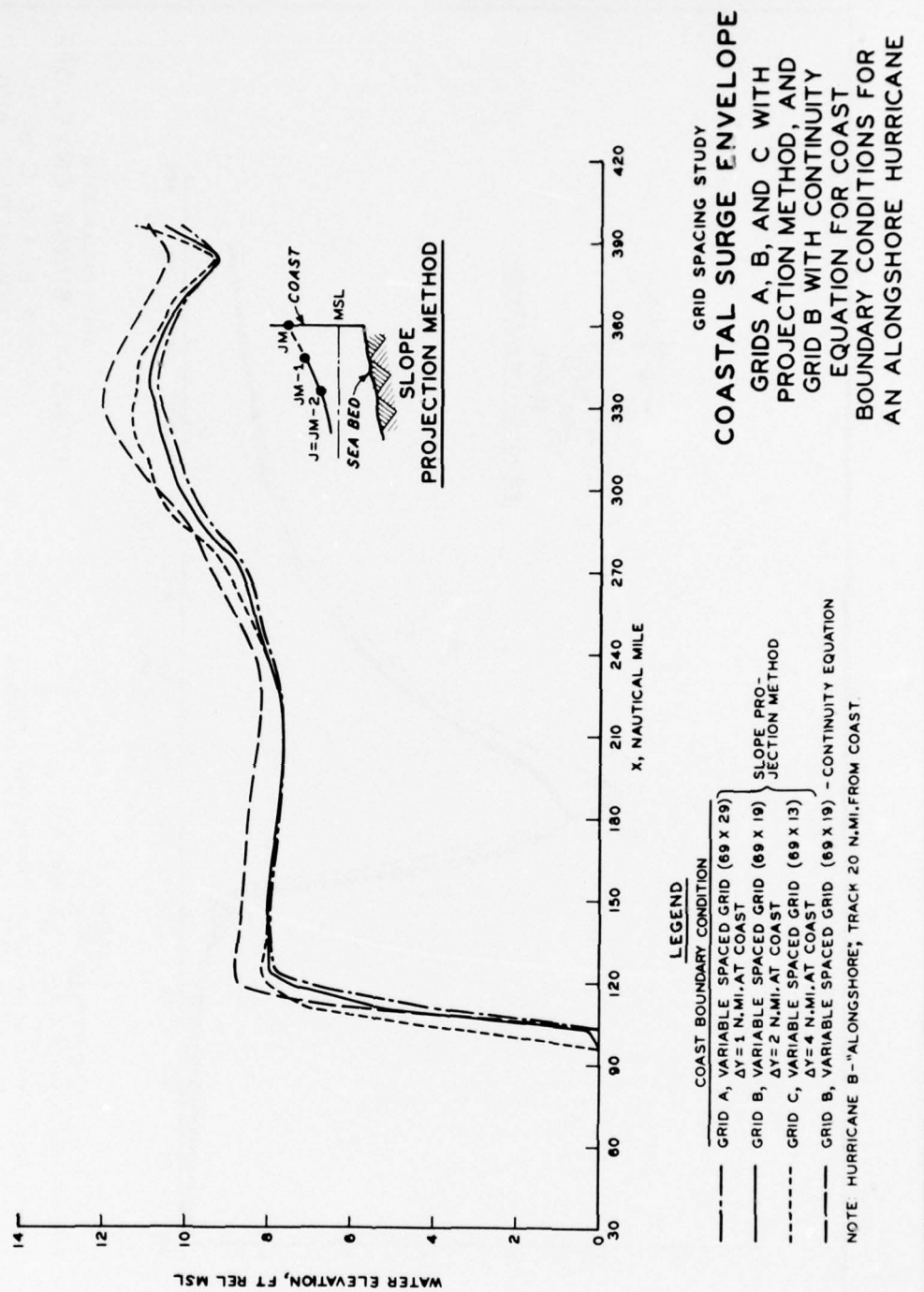
- GRID A, VARIABLE SPACED GRID (89 X 29)
- GRID B, VARIABLE SPACED GRID (89 X 19)
- GRID C, VARIABLE SPACED GRID (89 X 13)
- GRID B, VARIABLE SPACED GRID (89 X 19) - CONTINUITY EQUATION

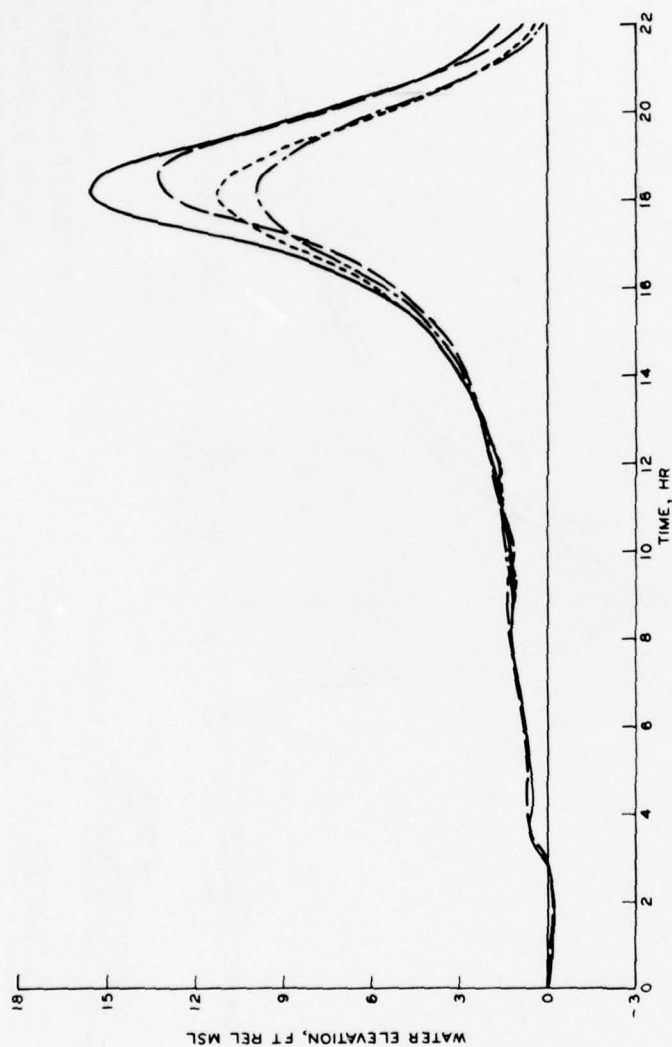
NOTE: HURRICANE A-"ONSHORE", LANDFALL AT X=177 N.M.I.

GRID SPACING STUDY

COASTAL SURGE ENVELOPE

GRIDS A, B, AND C WITH
PROJECTION METHOD, AND
GRID B WITH CONTINUITY
EQUATION FOR COAST
BOUNDARY CONDITIONS FOR
AN ONSHORE HURRICANE





LEGEND

COAST BOUNDARY CONDITION

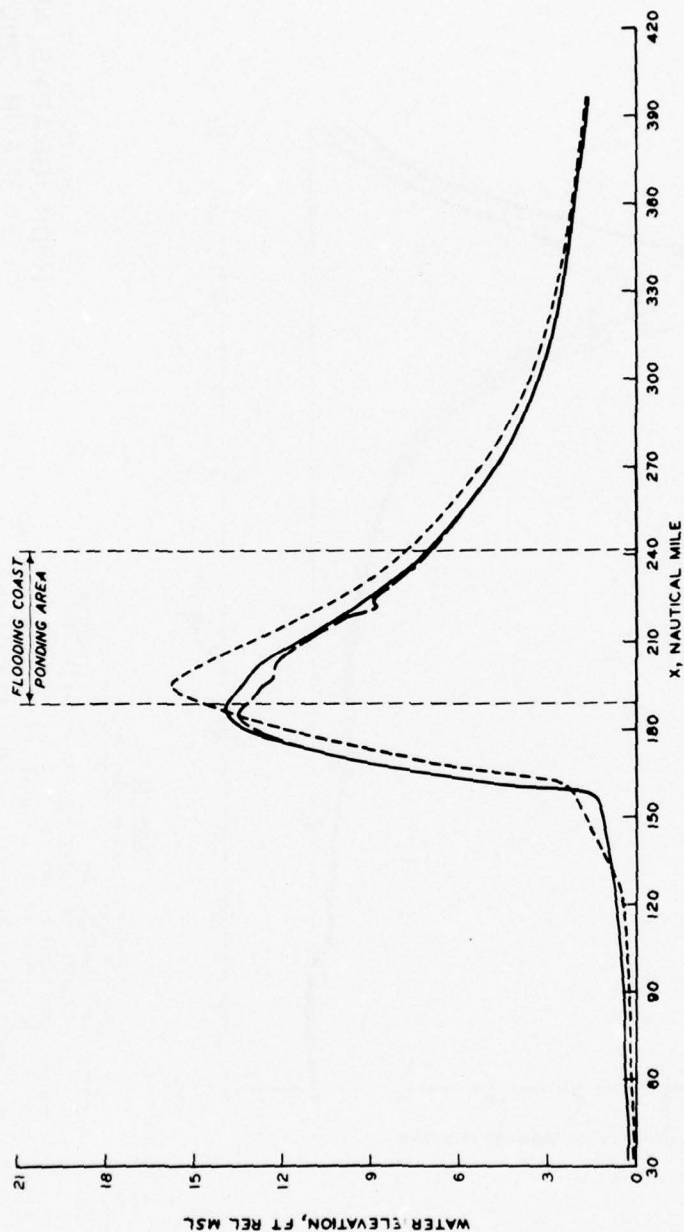
- GRID POINT (31, 15), 8 N.M.I. FROM COAST
- - - GRID POINT (31, 15), 8 N.M.I. FROM COAST
- · - · - GRID POINT (31, 15), 8 N.M.I. FROM COAST
- · - · - GRID POINT (31, 15), 8 N.M.I. FROM COAST

CONTINUITY EQUATION

SLOPE PROJECTION METHOD

NOTE: HURRICANE A - "ONSHORE", LANDFALL AT X=177 N.M.I.

GRID SPACING STUDY
 HYDROGRAPHS ALONG
 I=31 FOR GRID B
 CONTINUITY EQUATION AND
 PROJECTION METHOD FOR COAST
 BOUNDARY CONDITIONS FOR
 AN ONSHORE HURRICANE

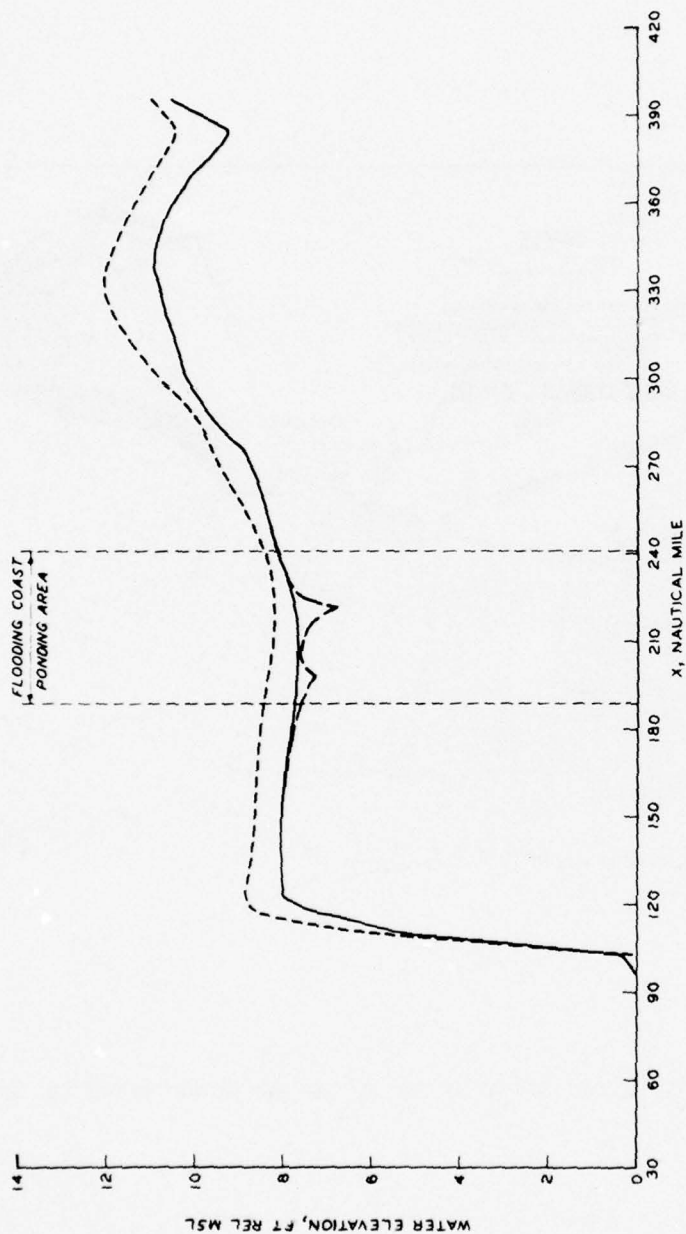


LEGEND

COAST BOUNDARY CONDITION
 SLOPE PROJECTION METHOD } NO FLOODING
 CONTINUITY EQUATION }
 FLOODING

NOTE: GRID B IS A VARIABLE SPACED GRID (69 x 19) WITH
 $\Delta Y = 2$ NAUTICAL MILES AT COAST
 HURRICANE A - "ONSHORE", LANDFALL AT $X = 177$ N.MI.

GRID SPACING STUDY
COASTAL SURGE ENVELOPE
 GRID B WITH CONTINUITY
 EQUATION, PROJECTION METHOD,
 AND FLOODING FOR COAST
 BOUNDARY CONDITIONS FOR
 AN ONSHORE HURRICANE

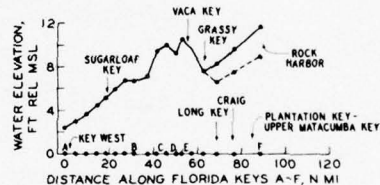
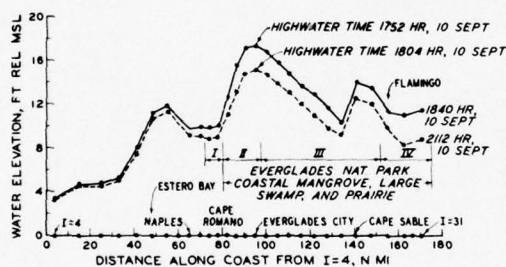
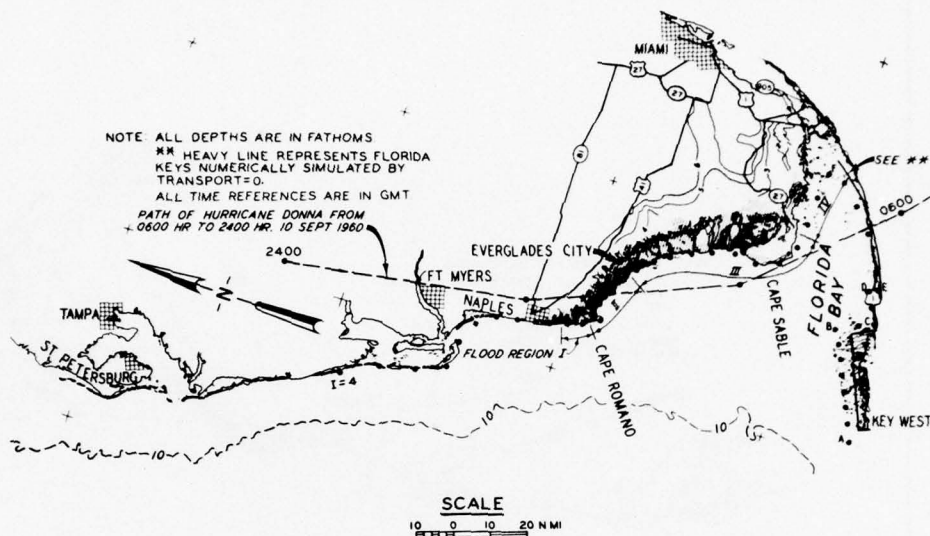


LEGEND

COAST BOUNDARY CONDITION
 SLOPE PROJECTION METHOD } NO FLOODING
 CONTINUITY EQUATION }
 FLOODING

NOTE: GRID B IS A VARIABLE SPACED GRID (89 X 19) WITH
 $\Delta Y = 2$ NAUTICAL MILES AT COAST
 HURRICANE B - "ALONGSHORE"; TRACK 20 N.MI. FROM COAST

GRID SPACING STUDY
COASTAL SURGE ENVELOPE
 GRID B WITH CONTINUITY
 EQUATION, PROJECTION METHOD,
 AND FLOODING FOR COAST
 BOUNDARY CONDITIONS FOR
 AN ALONGSHORE HURRICANE



LEGEND

— WALL COAST BOUNDARY CONDITION
 --- FLOODING COAST BOUNDARY CONDITION

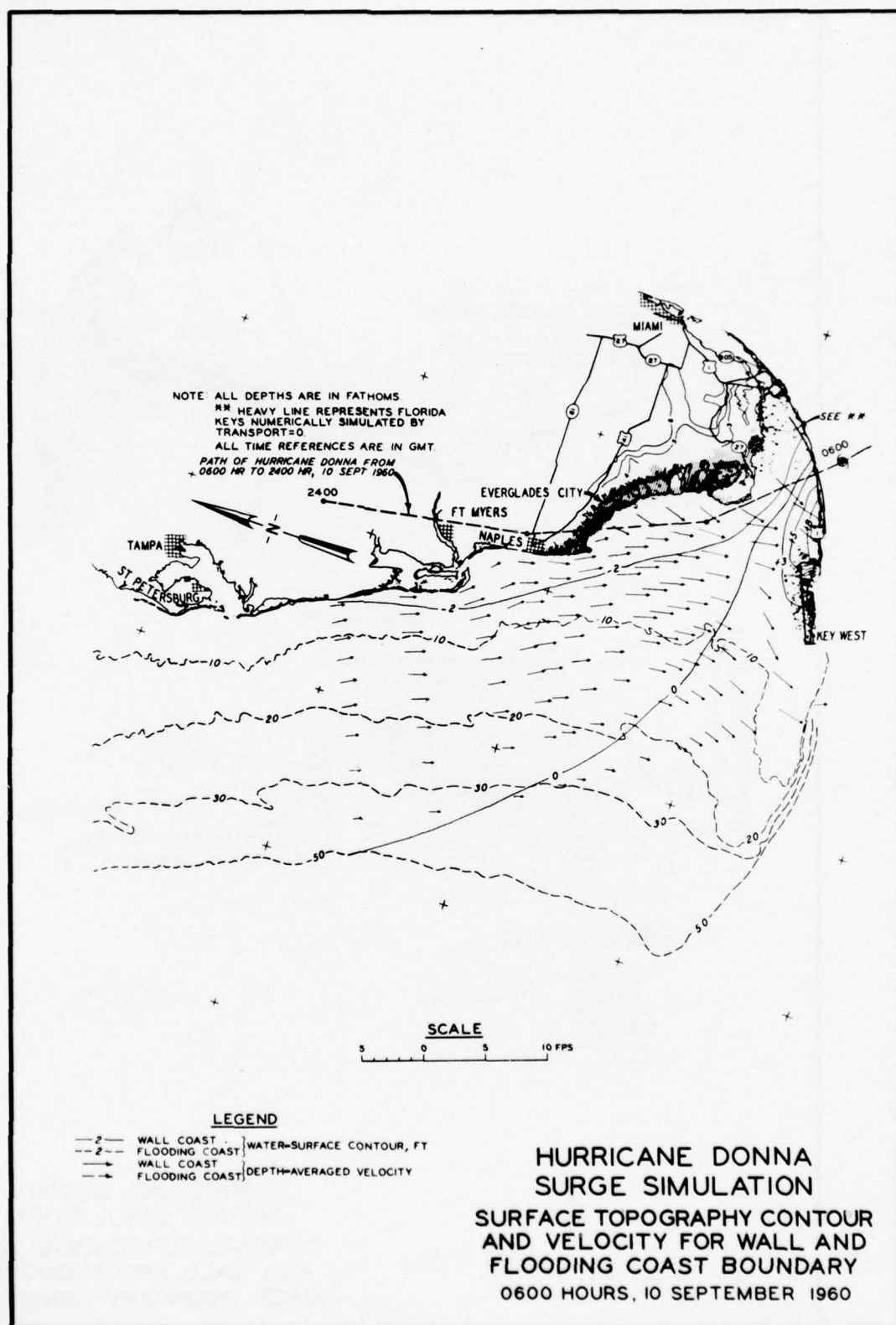
NOTE: COMPUTED SURGE DOES NOT INCLUDE ASTRONOMICAL TIDE

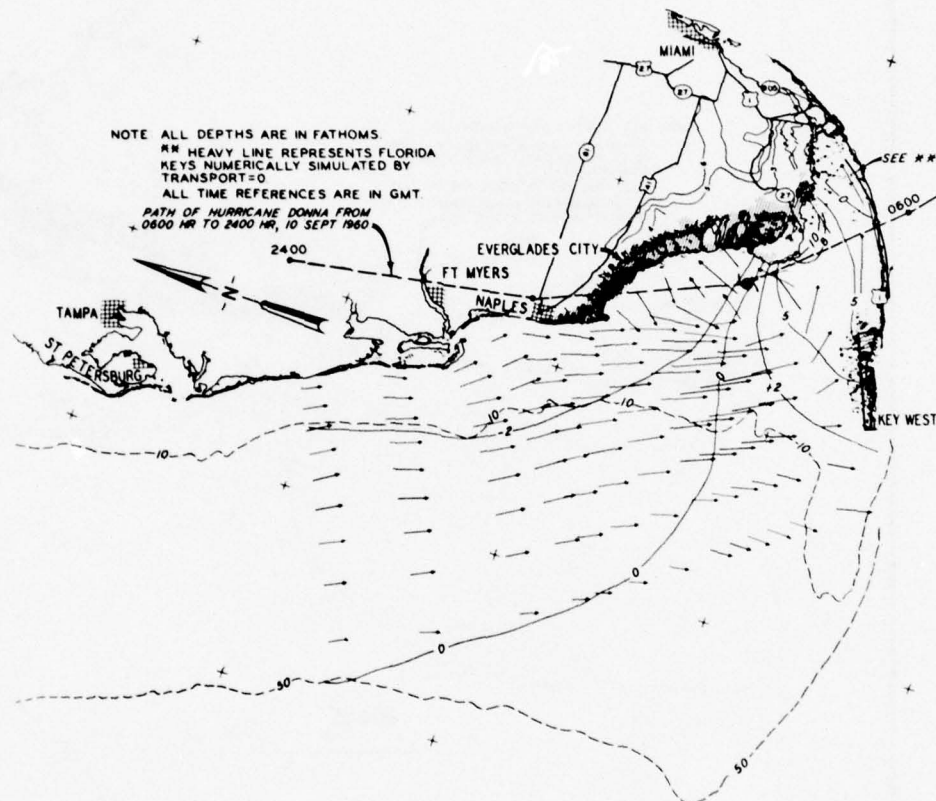
ASTRONOMICAL TIDE, 10 SEPT 1960

LOCATION	TIDAL RANGE, FT.
ST. PETERSBURG*	1.3
CAPE ROMANO	2.6
CAPE SABLE	2.9
KEY WEST*	1.3

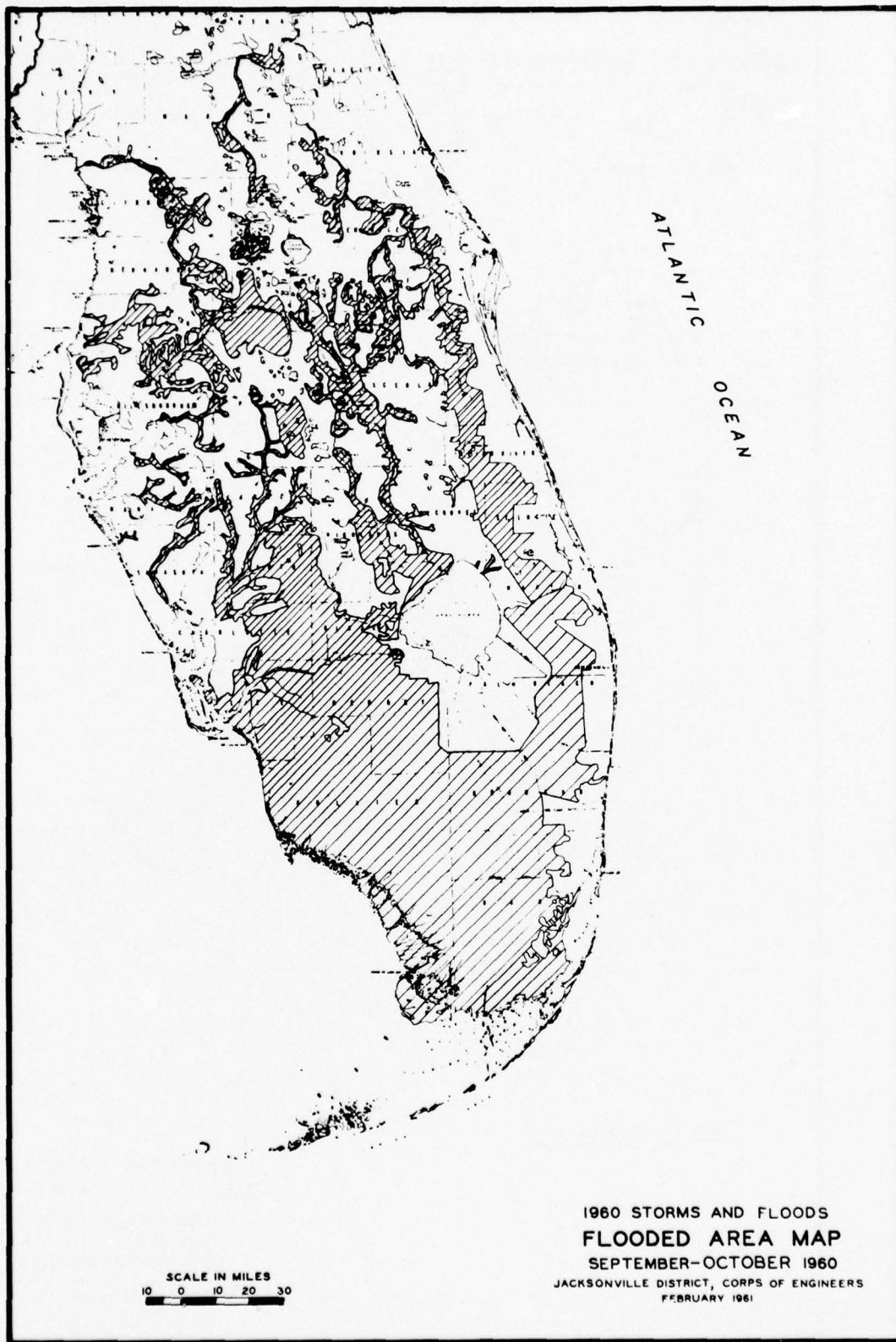
NOTE: * REPRESENTS TIDE PREDICTION SITE

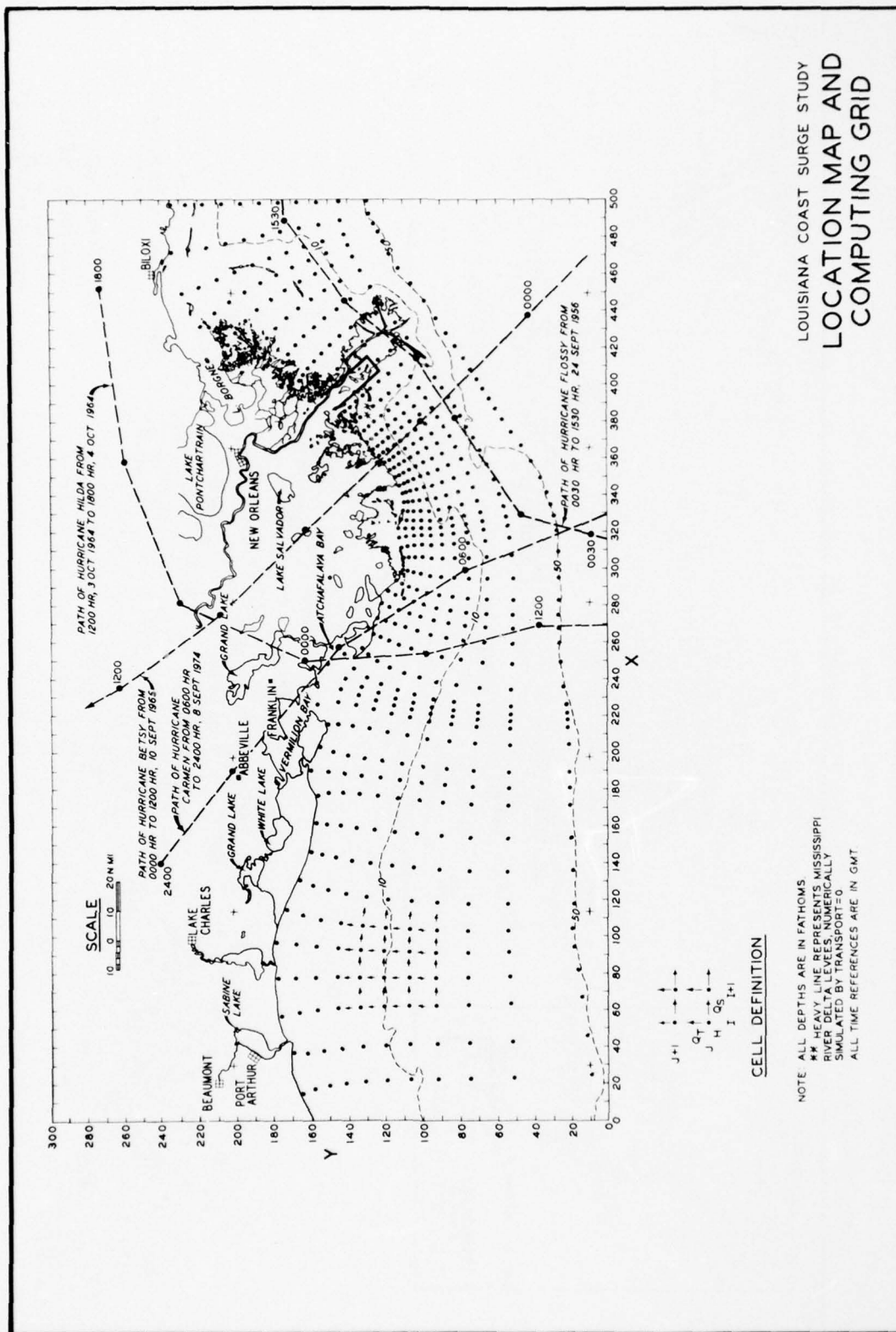
HURRICANE DONNA SURGE SIMULATION COASTAL SURGE ENVELOPE FOR WALL AND FLOODING COAST BOUNDARY CONDITIONS





HURRICANE DONNA
 SURGE SIMULATION
 SURFACE TOPOGRAPHY CONTOUR
 AND VELOCITY FOR WALL AND
 FLOODING COAST BOUNDARY
 1200 HOURS, 10 SEPTEMBER 1960

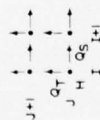


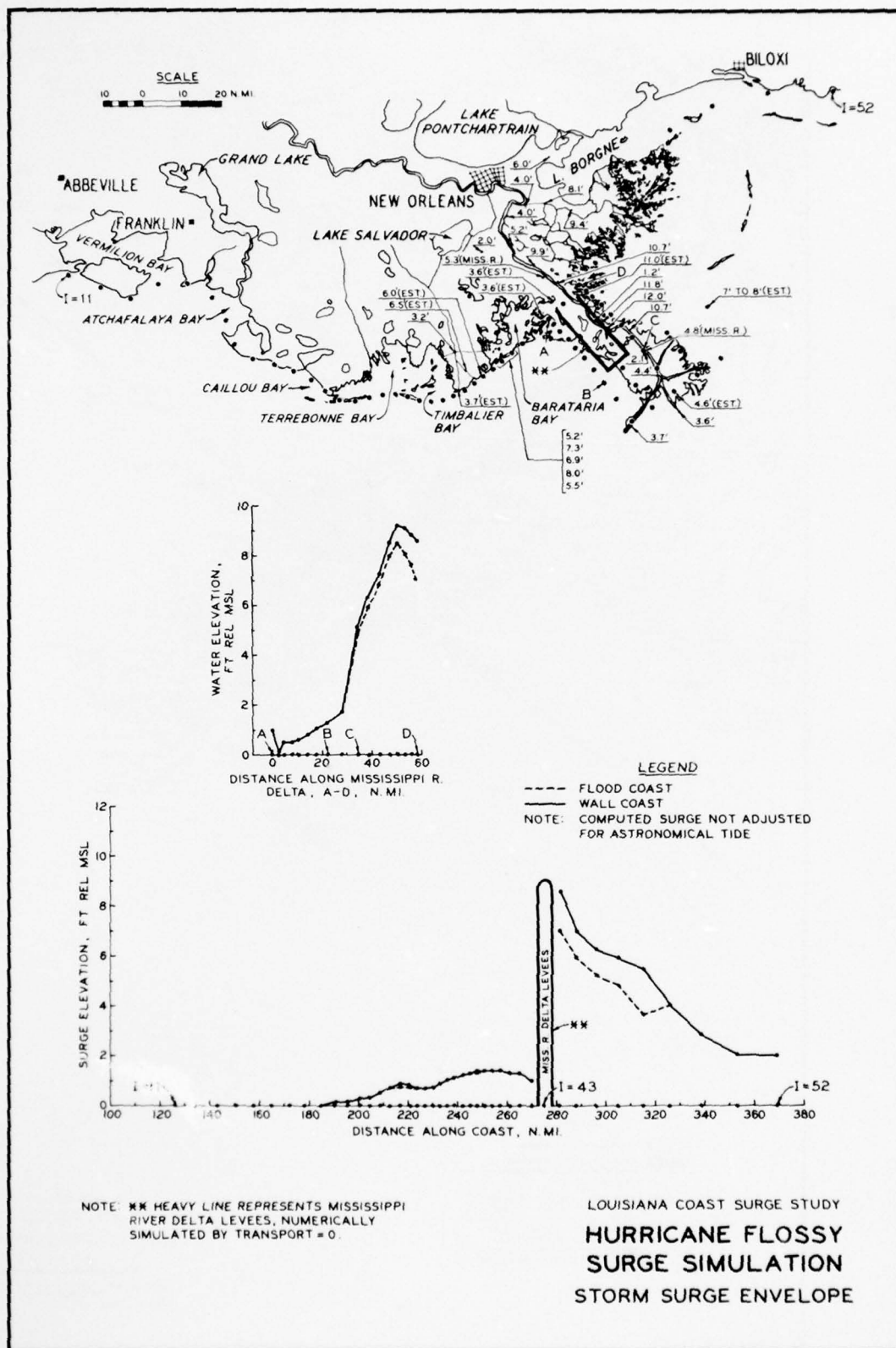


LOUISIANA COAST SURGE STUDY LOCATION MAP AND COMPUTING GRID

NOTE ALL DEPTHS ARE IN FATHOMS
 ** HEAVY LINE REPRESENTS MISSISSIPPI
 RIVER DELTA (LEVELS NUMERICALLY
 SIMULATED BY TRANSPORT=0)
 ALL TIME REFERENCES ARE IN GMT

CELL DEFINITION





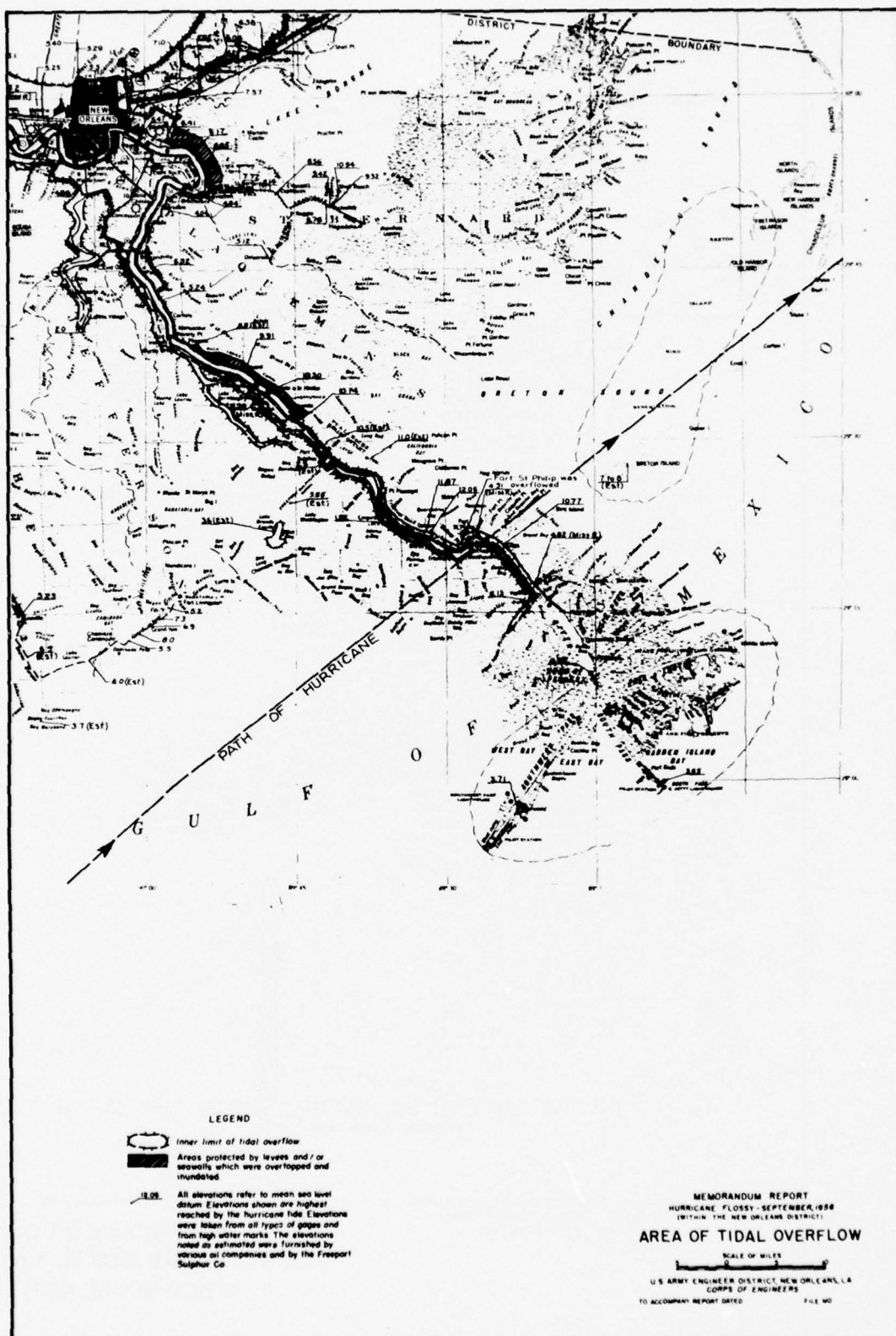
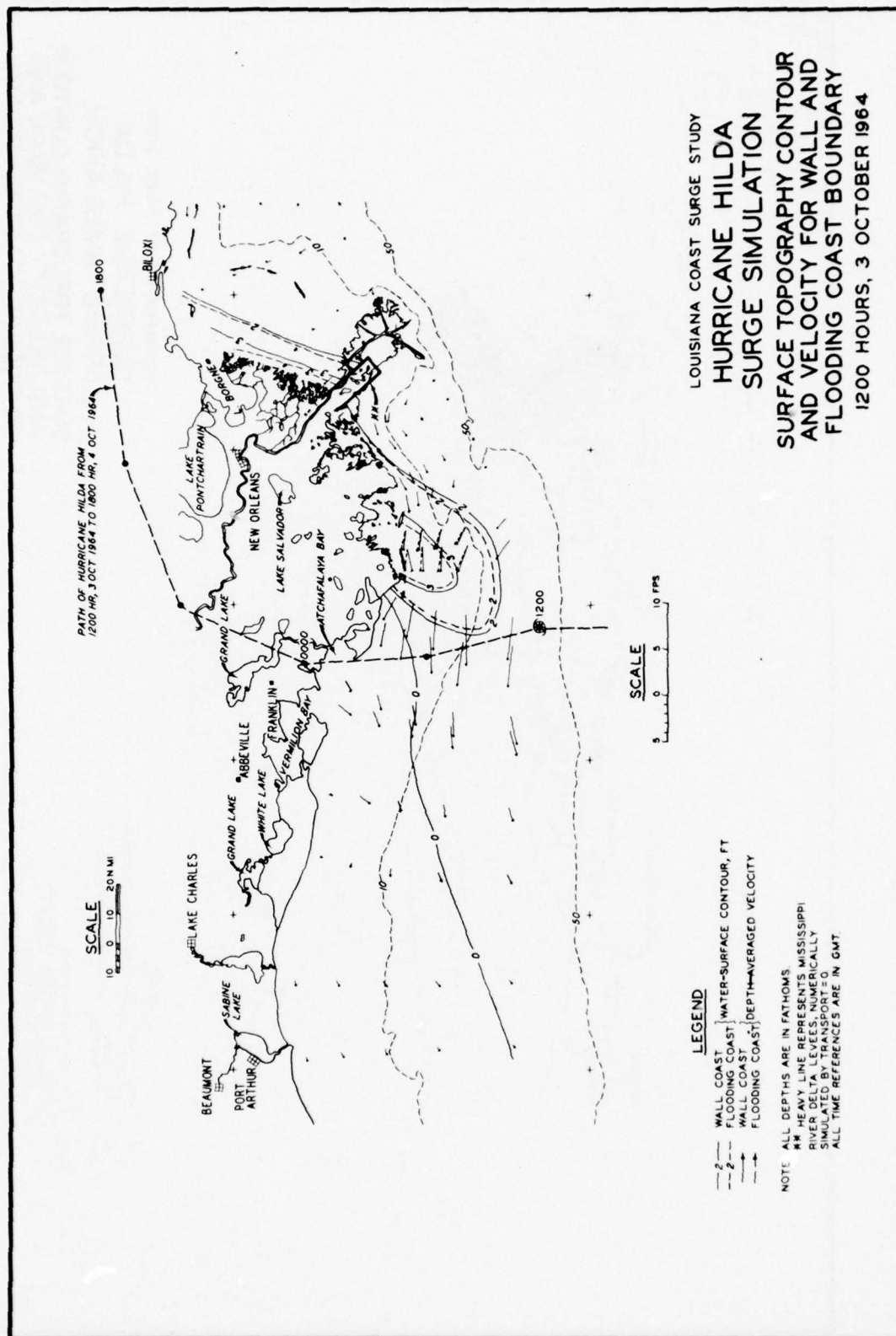
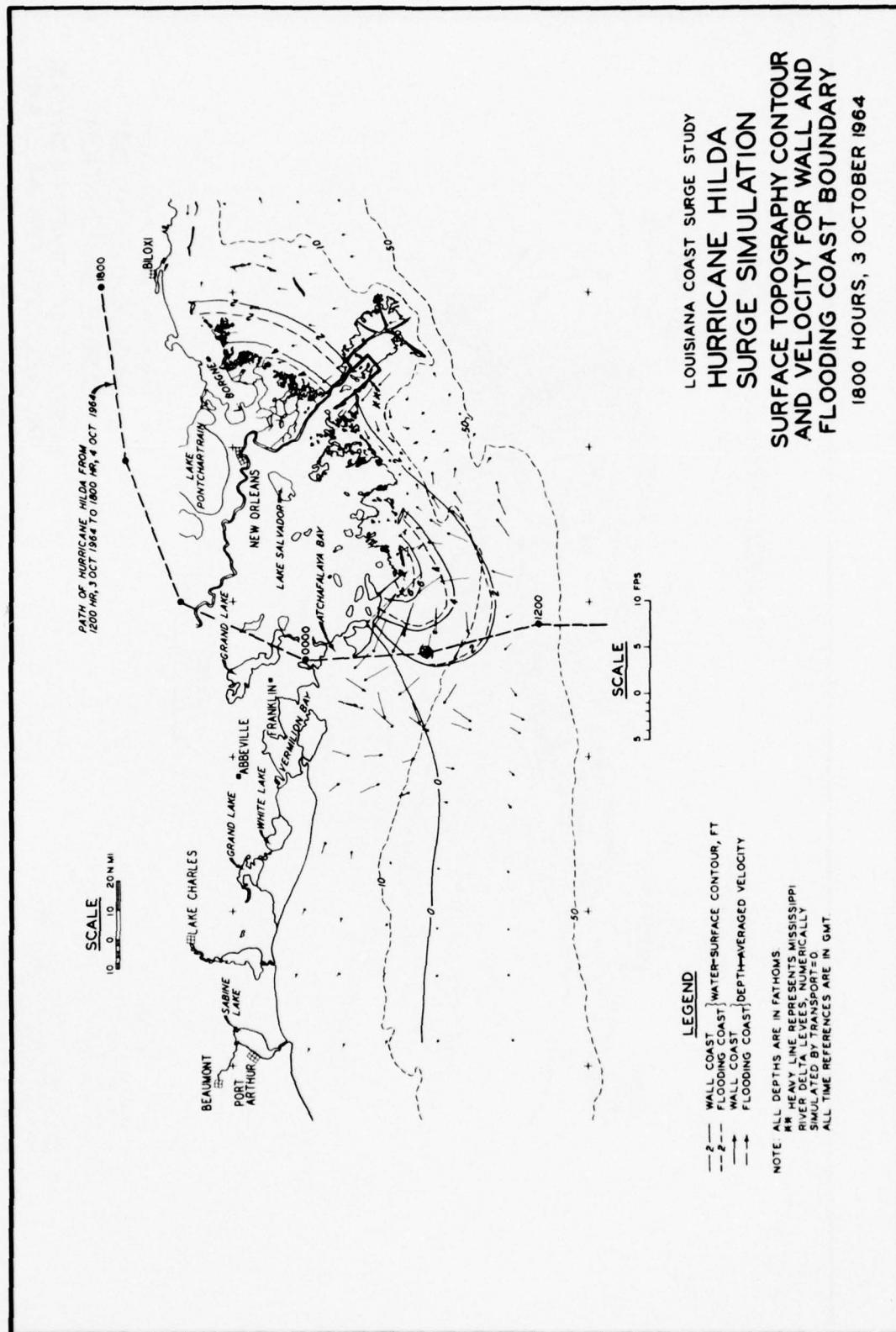
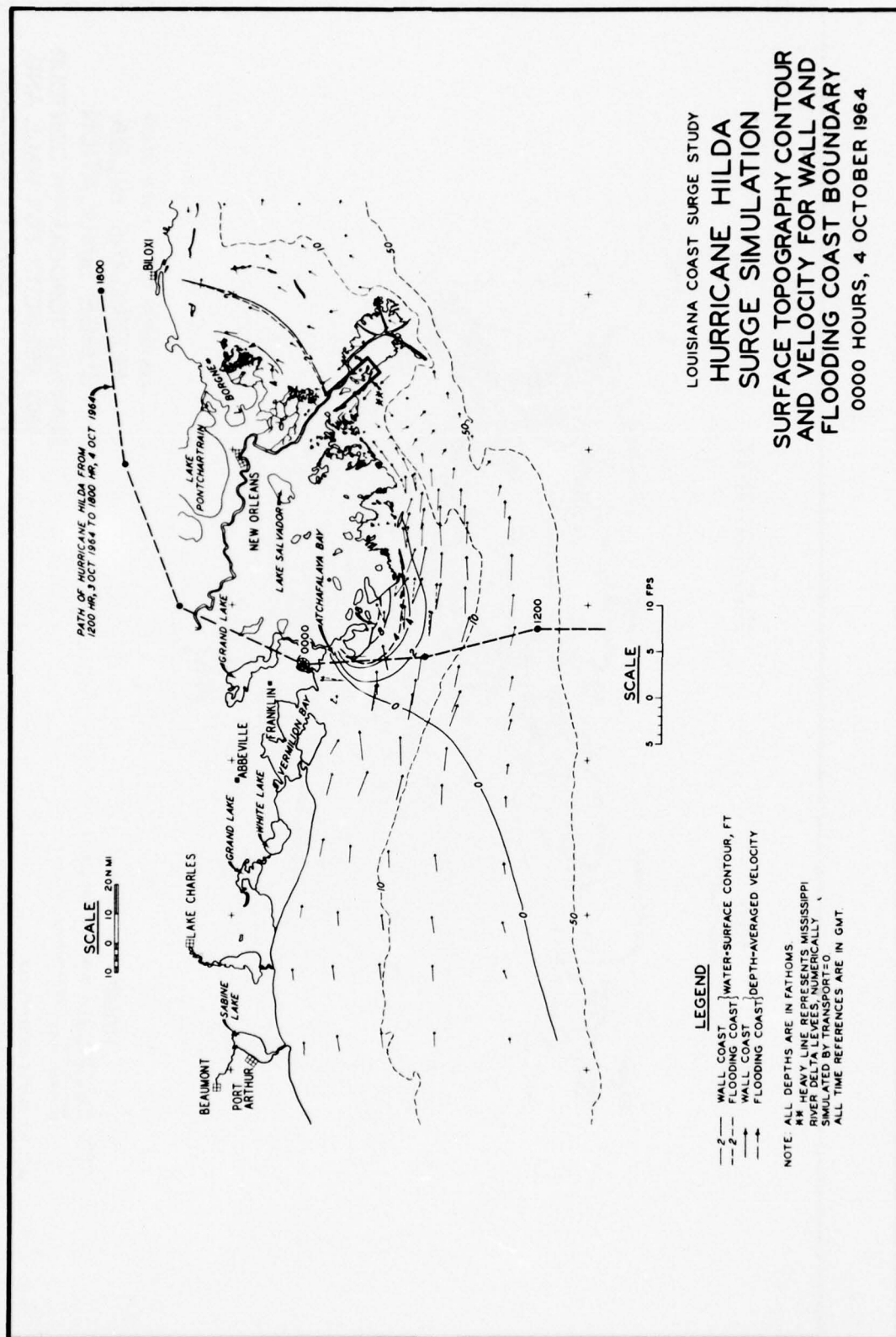


PLATE 48







LOUISIANA COAST SURGE STUDY
HURRICANE HILDA
SURGE SIMULATION
SURFACE TOPOGRAPHY CONTOUR
AND VELOCITY FOR WALL AND
FLOODING COAST BOUNDARY
0000 HOURS, 4 OCTOBER 1964

LOUISIANA COAST SURGE STUDY

HURRICANE HILDA

SURGE SIMULATION

SURFACE TOPOGRAPHY CONTOUR AND VELOCITY FOR WALL AND FLOODING COAST BOUNDARY

1800 HOURS, 4 OCTOBER 1964



SCALE

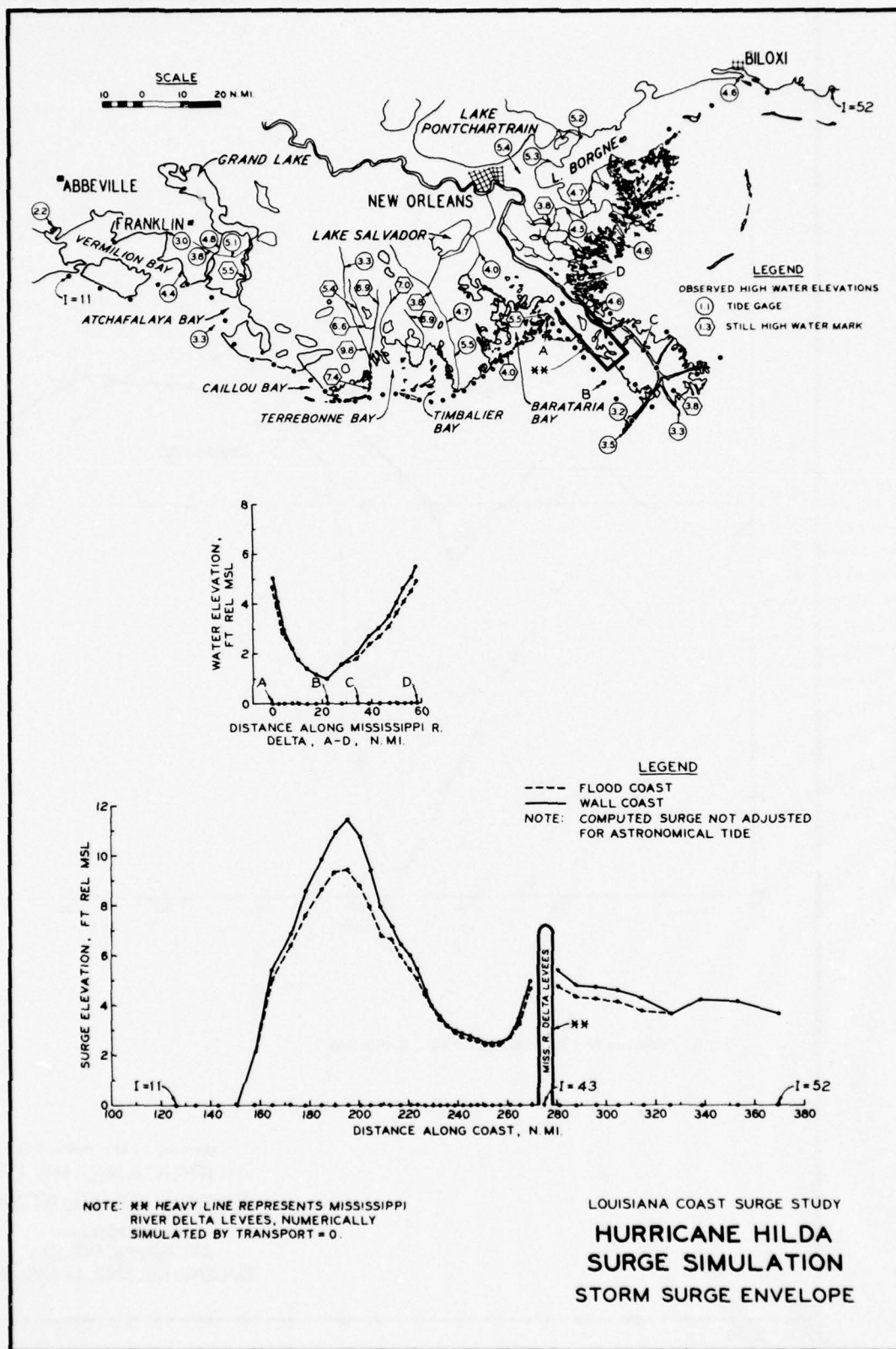
SCALE

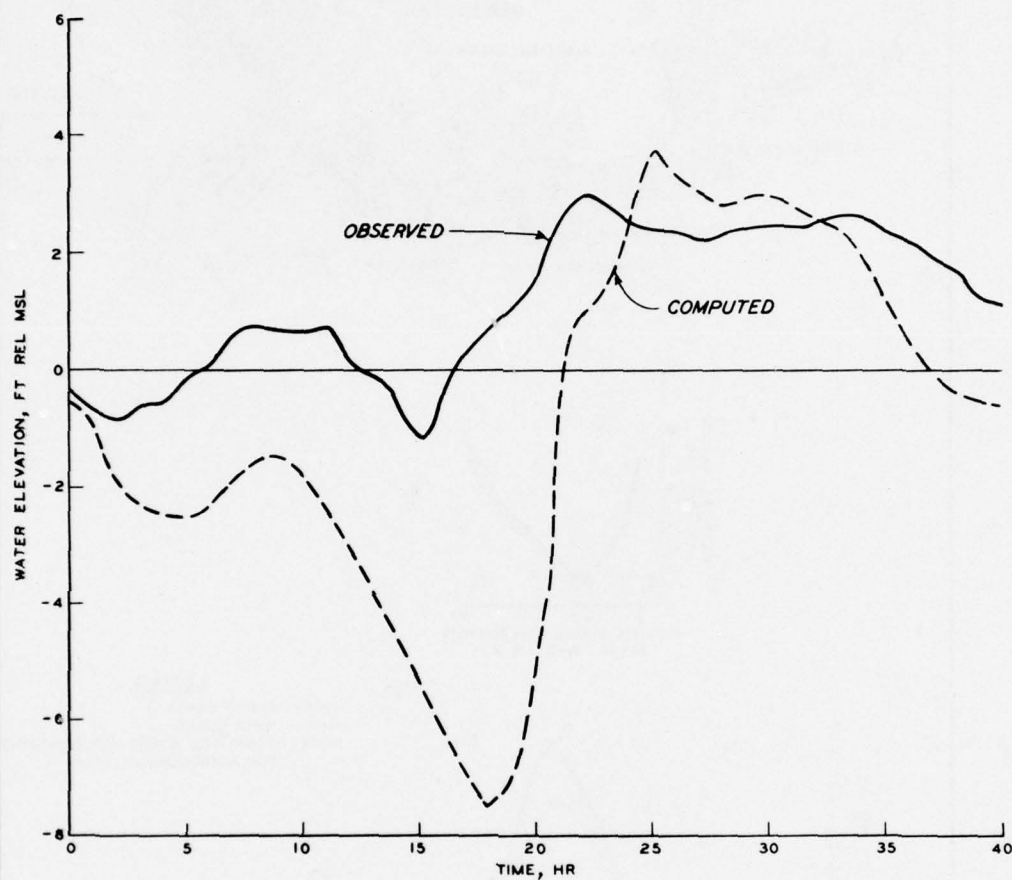
5 0 5 10 FPS

LEGEND

- 2-- WALL COAST } WATER-SURFACE CONTOUR, FT
 ---2--- FLOODING COAST }
 --> WALL COAST } DEPTH-AVERAGED VELOCITY
 ---> FLOODING COAST }

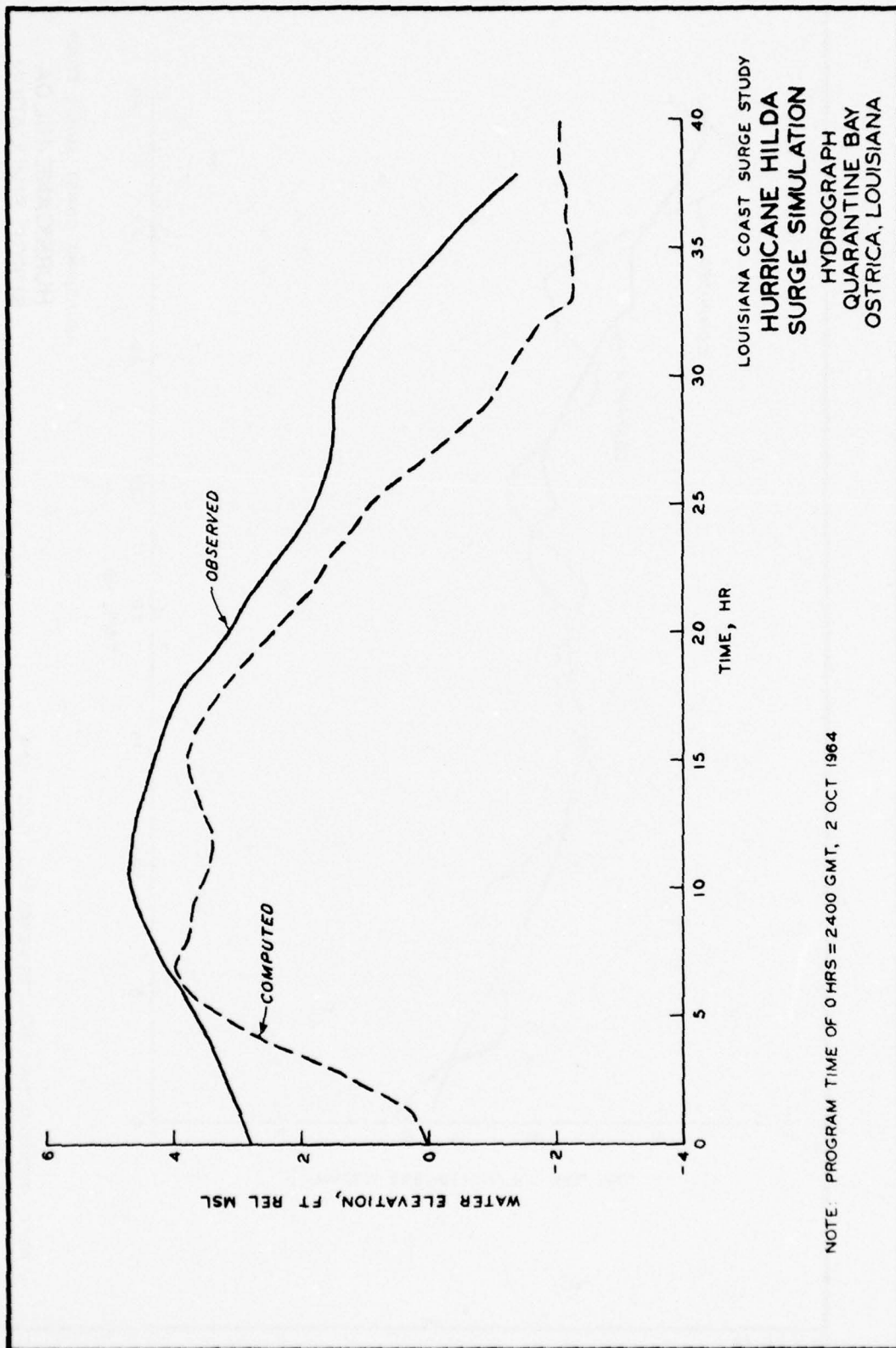
NOTE: ALL DEPTHS ARE IN FATHOMS.
 ** HEAVY LINE REPRESENTS MISSISSIPPI
 RIVER DELTA LEVES, NUMERICALLY
 SIMULATED BY TRANSPORT = 0
 ALL TIME REFERENCES ARE IN GMT

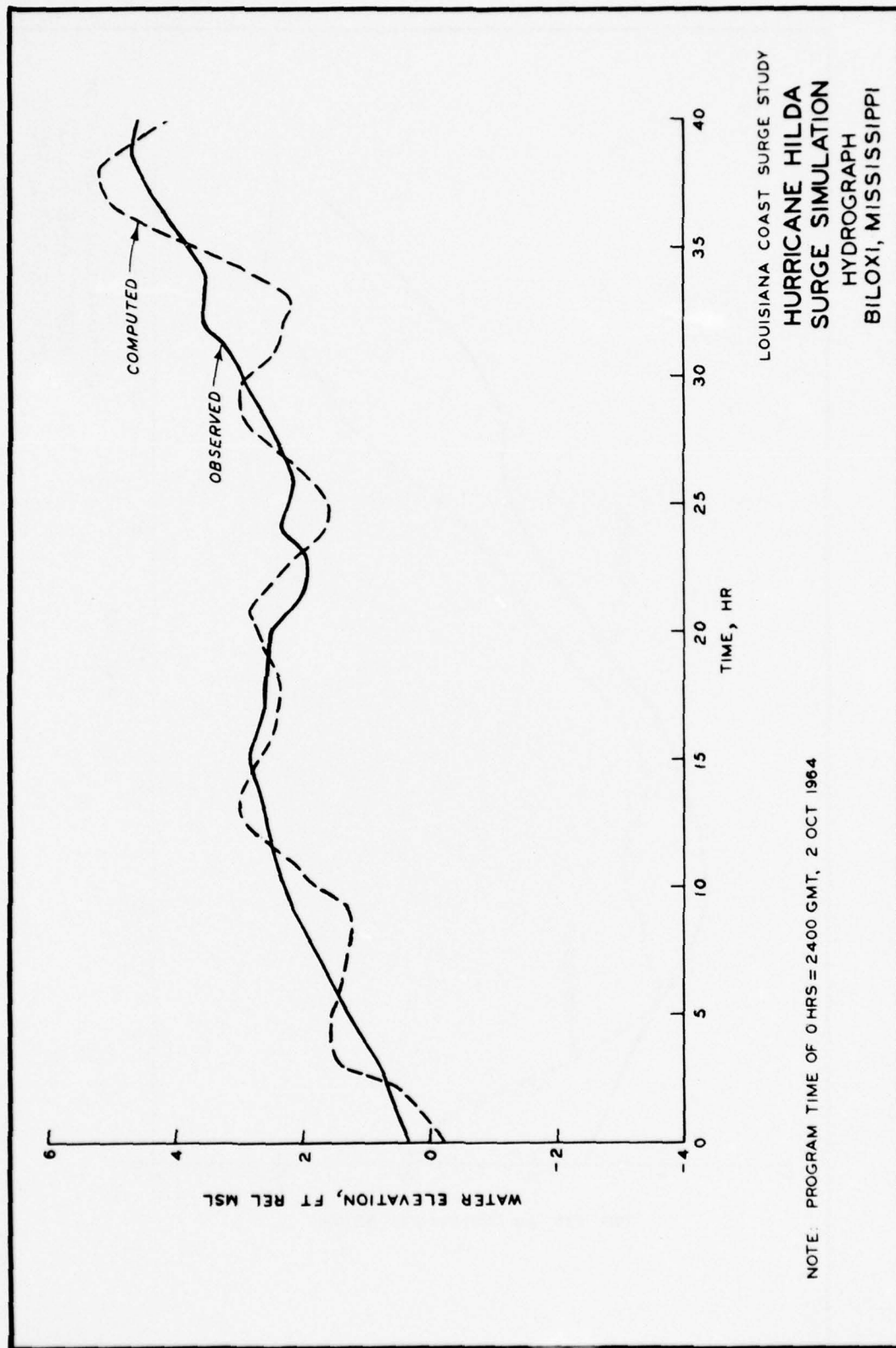


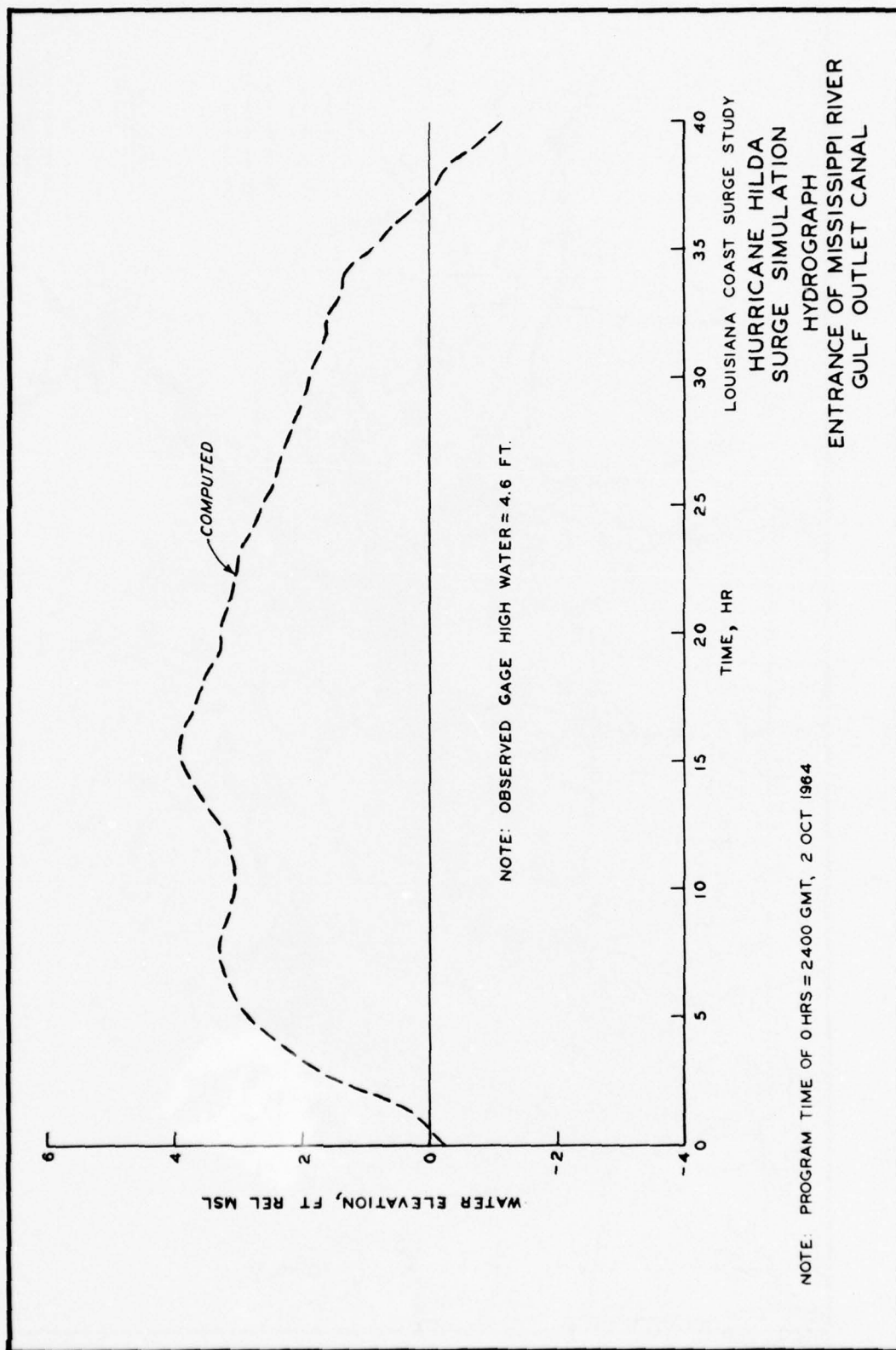


NOTE: PROGRAM TIME OF 0 HRS \approx 2400 GMT, 2 OCT 1984

LOUISIANA COAST SURGE STUDY
HURRICANE HILDA
SURGE SIMULATION
HYDROGRAPH
ATCHAFALAYA BAY
EUGENE ISLAND, LOUISIANA







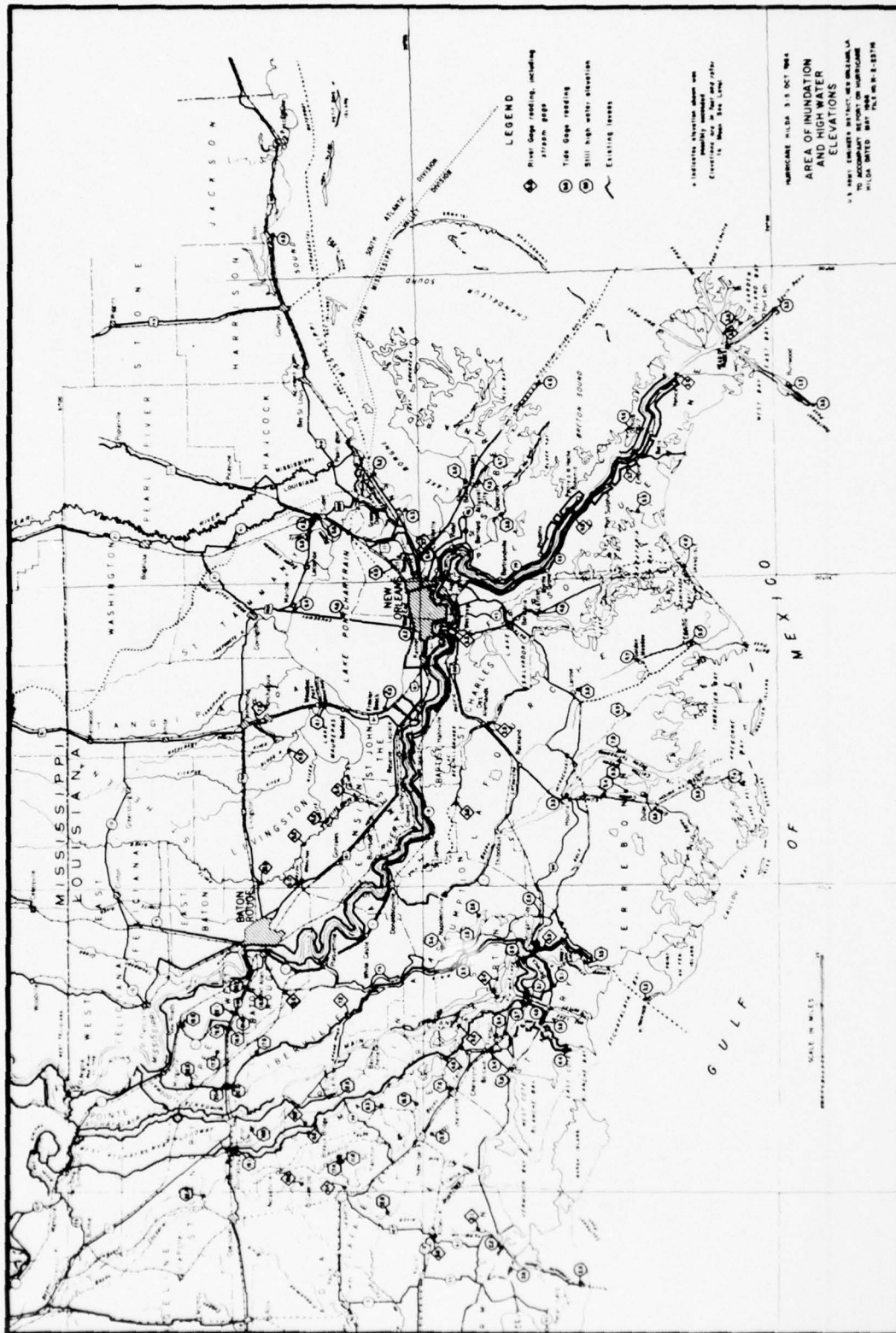
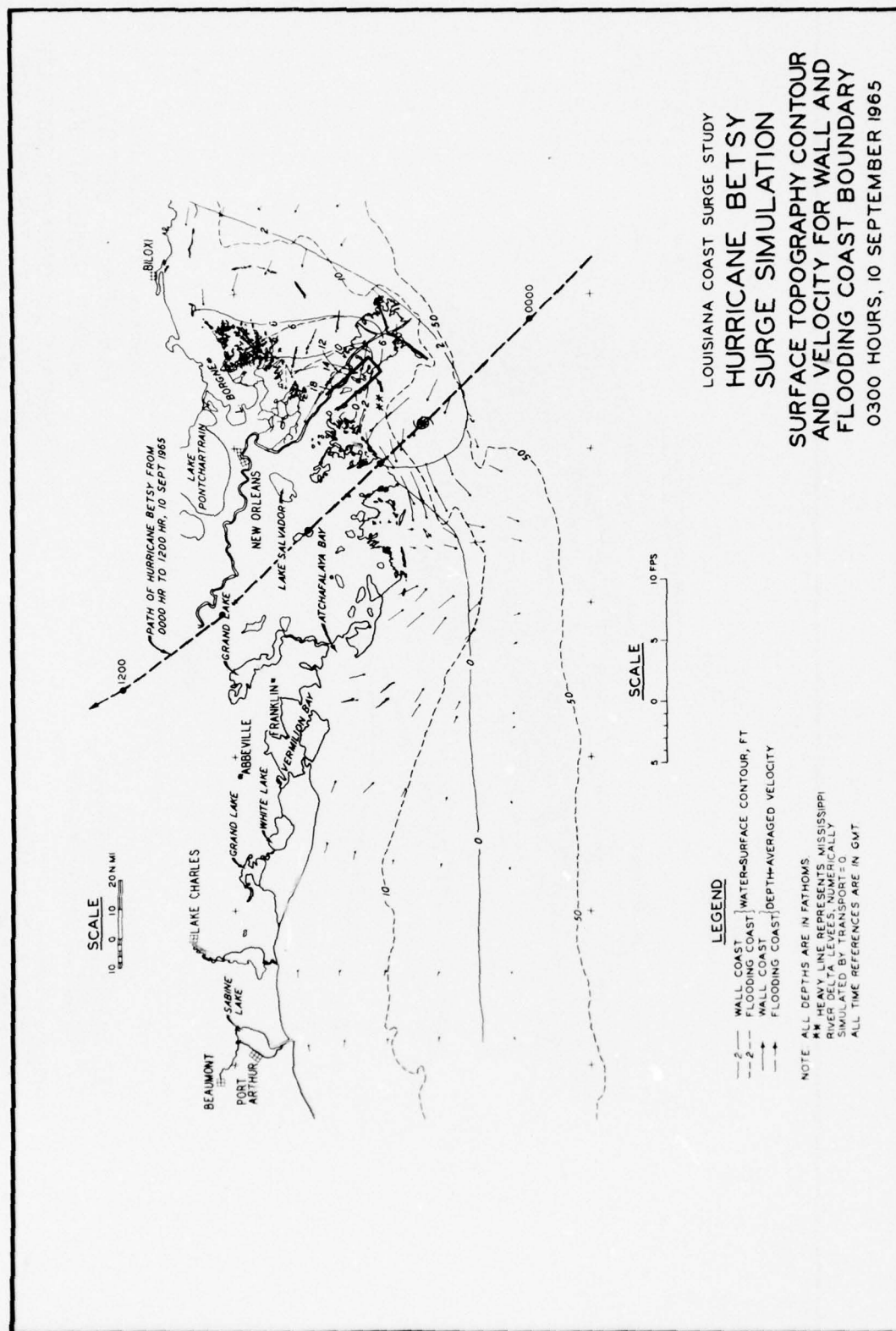
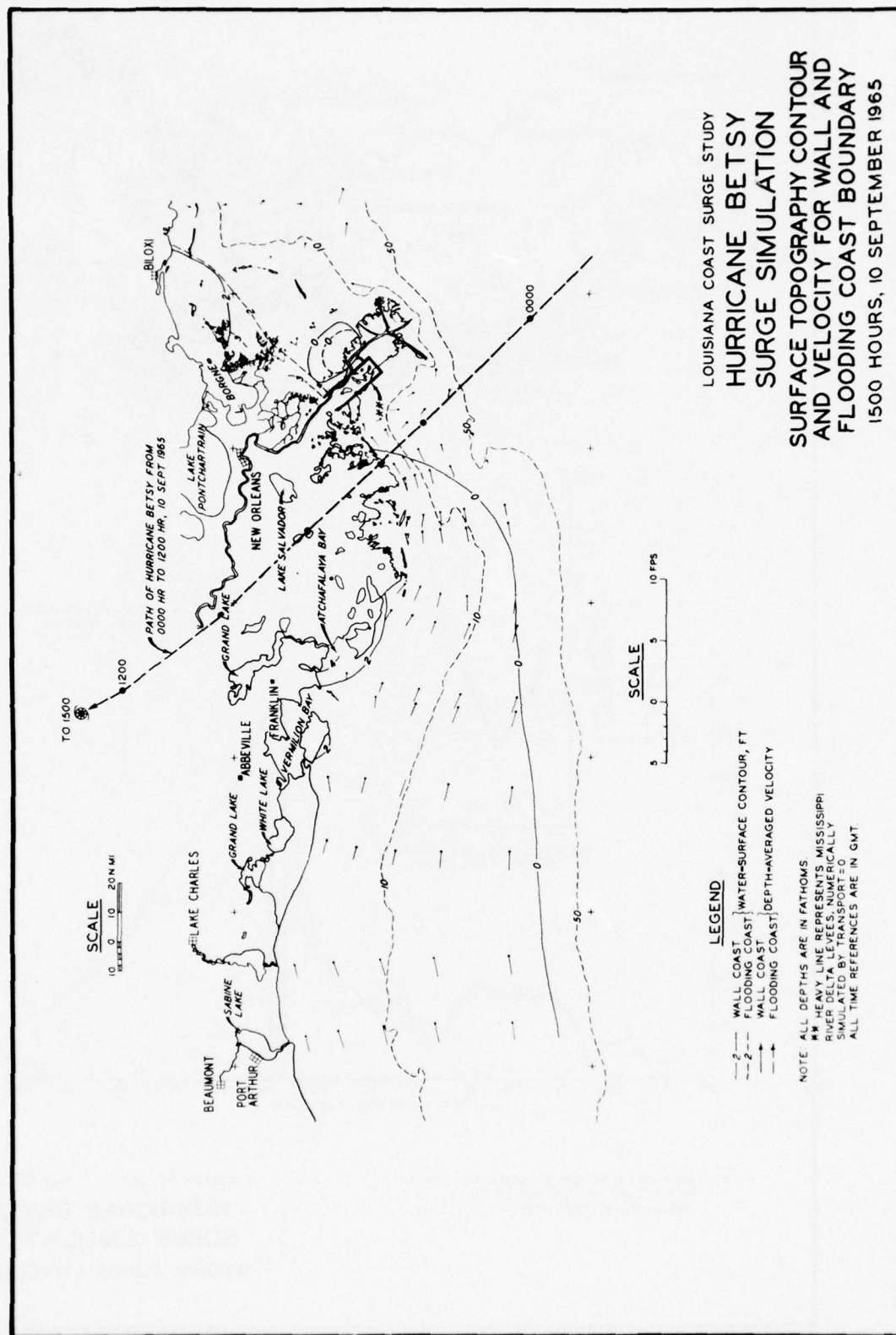
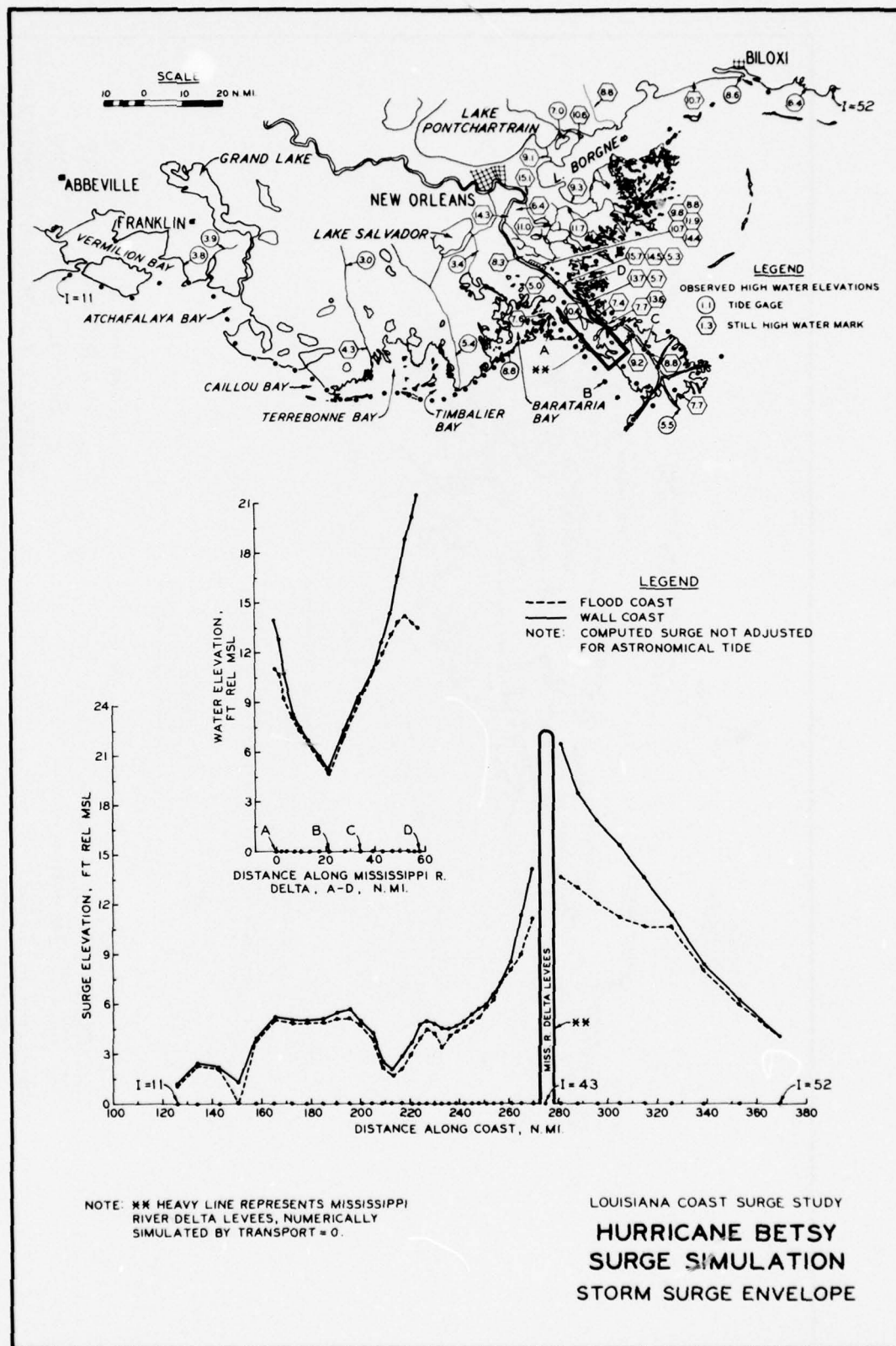
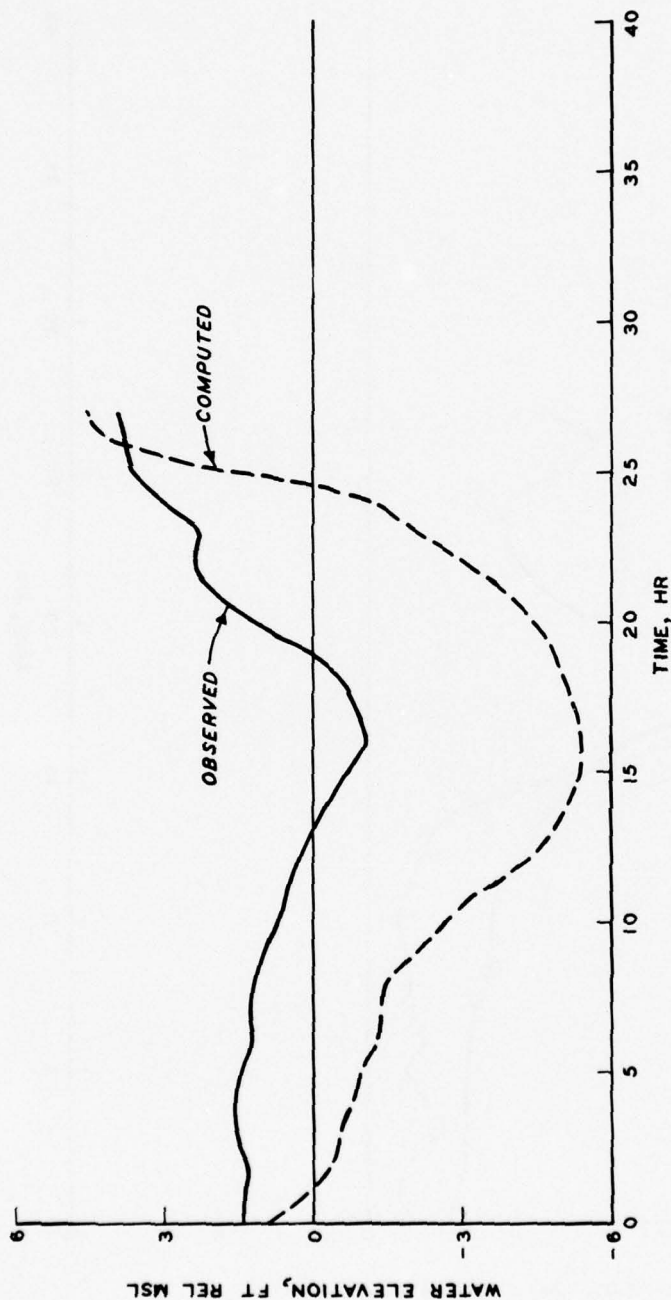


PLATE 60









LOUISIANA COAST SURGE STUDY
HURRICANE BETSY
SURGE SIMULATION
HYDROGRAPH
EAST COTE BLANCHE BAY
LUKE'S LANDING, LOUISIANA

NOTE: PROGRAM TIME OF 0 HRS \approx 1200 GMT, 9 SEPT 1965

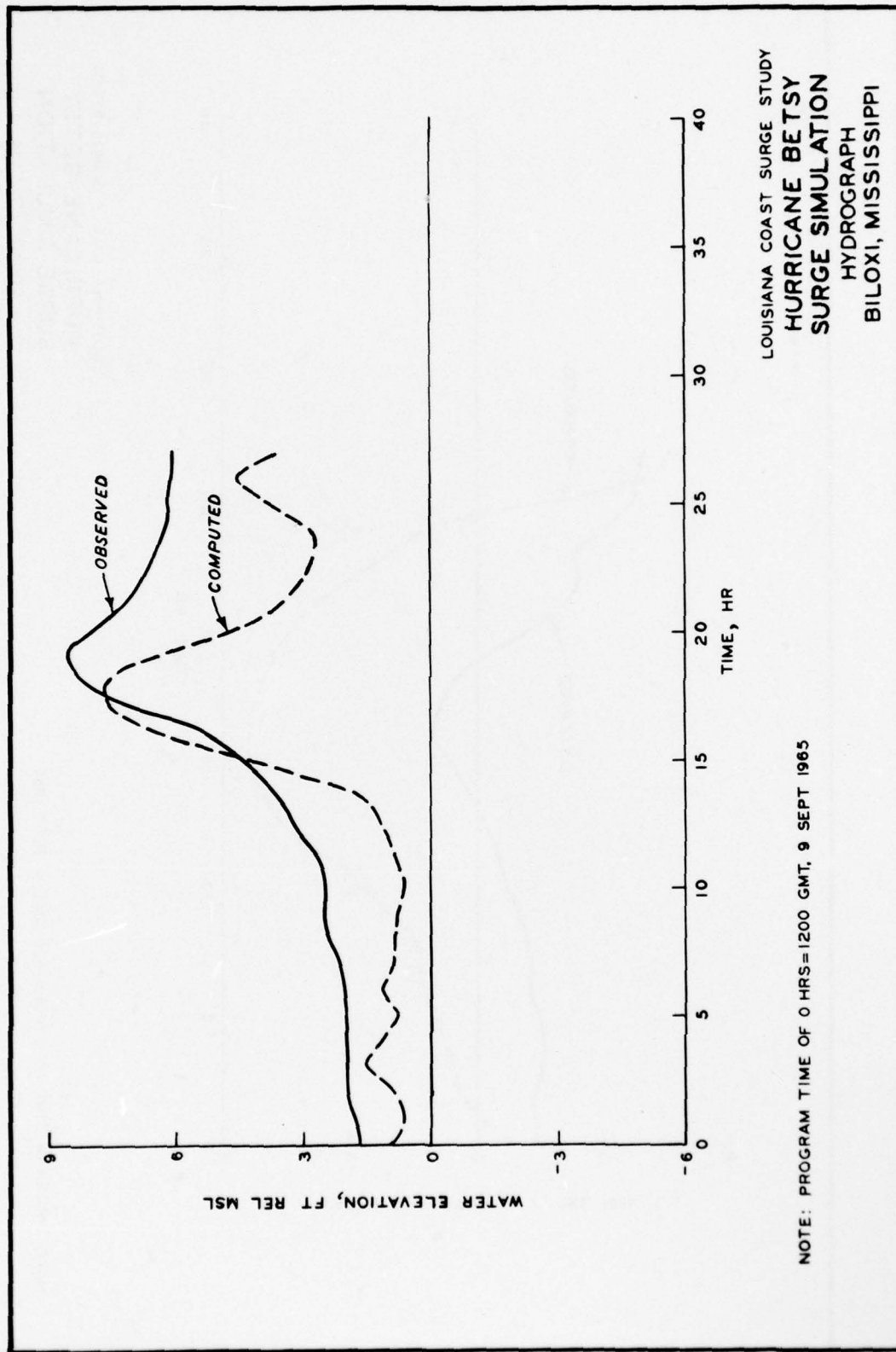
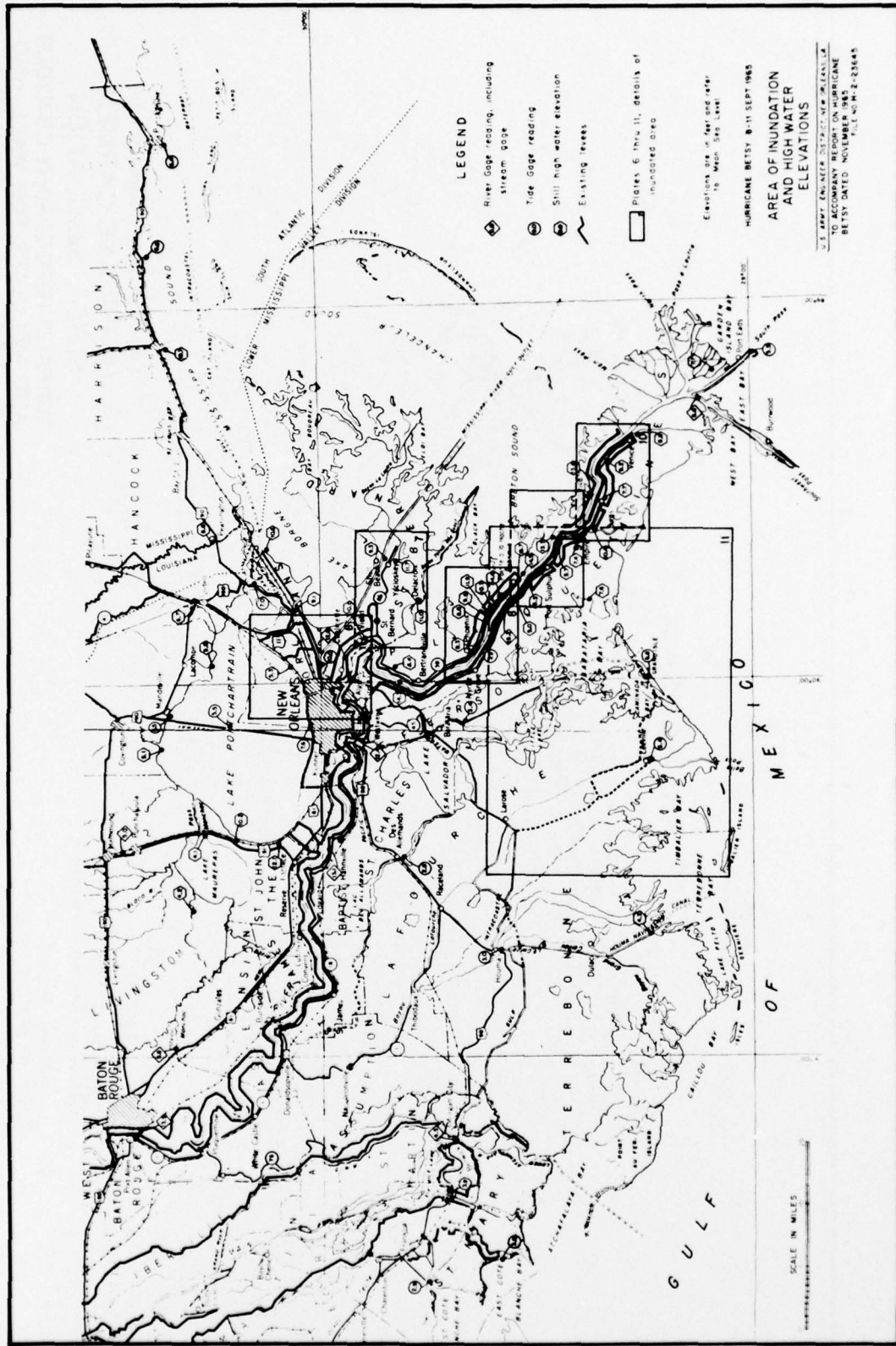
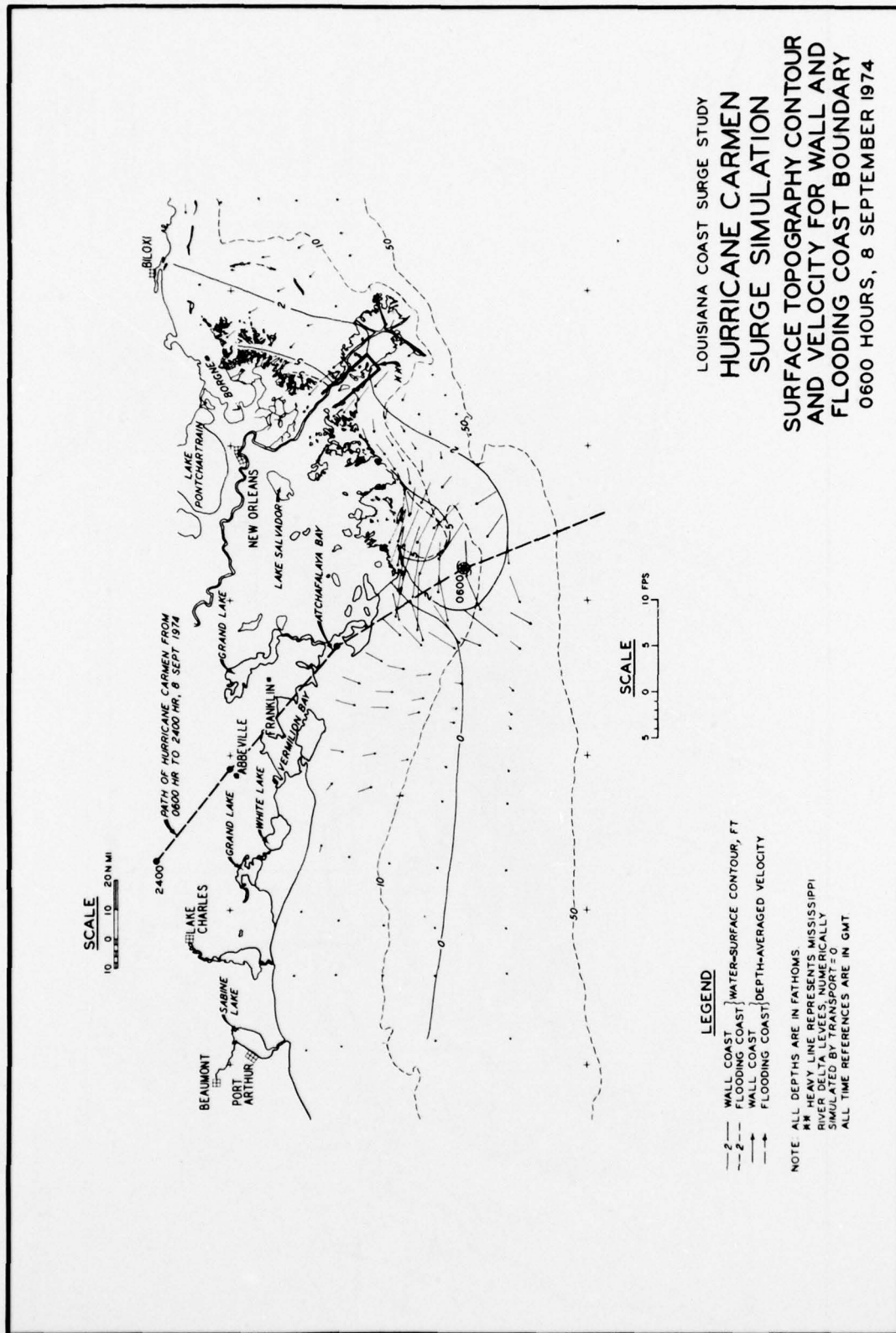
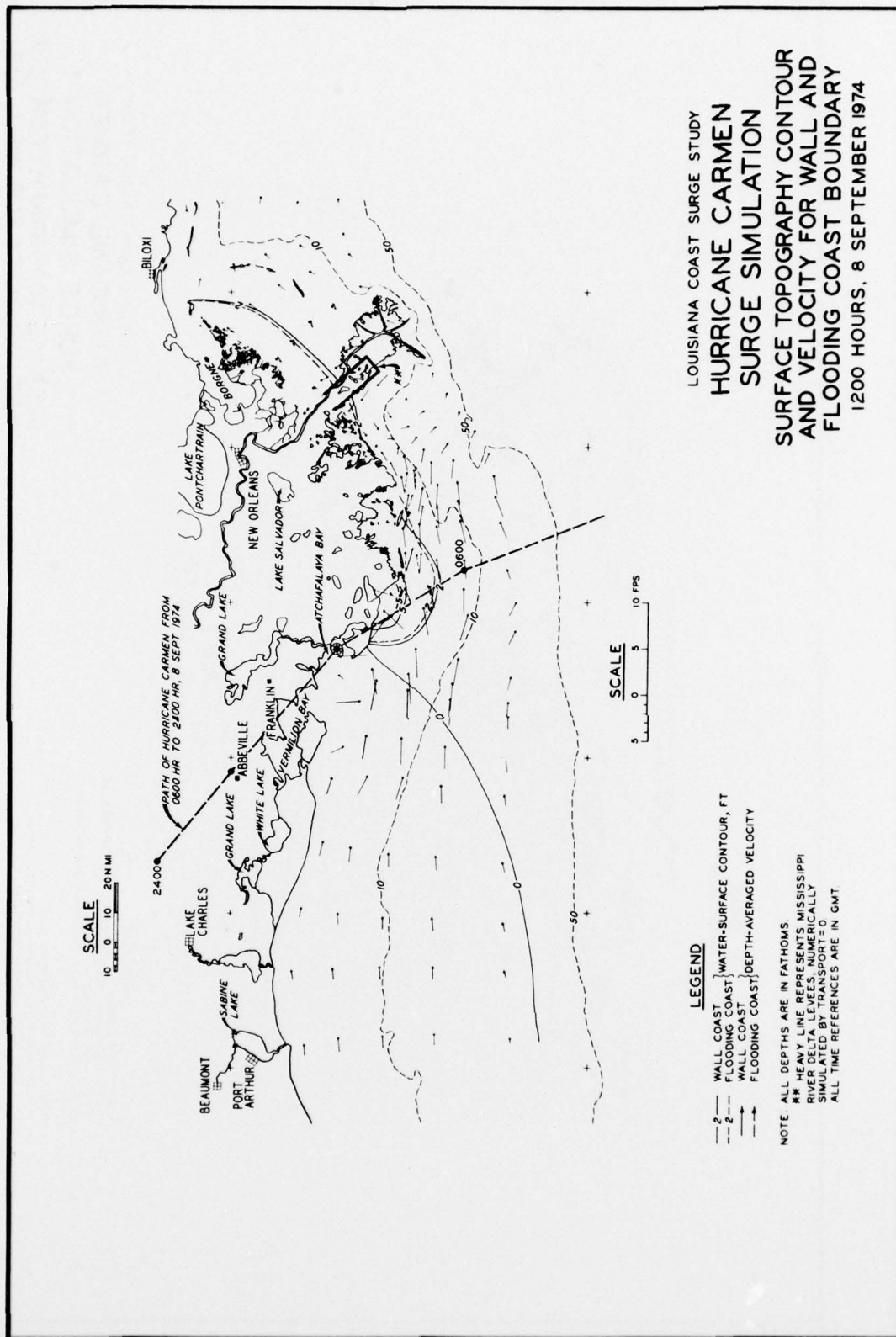


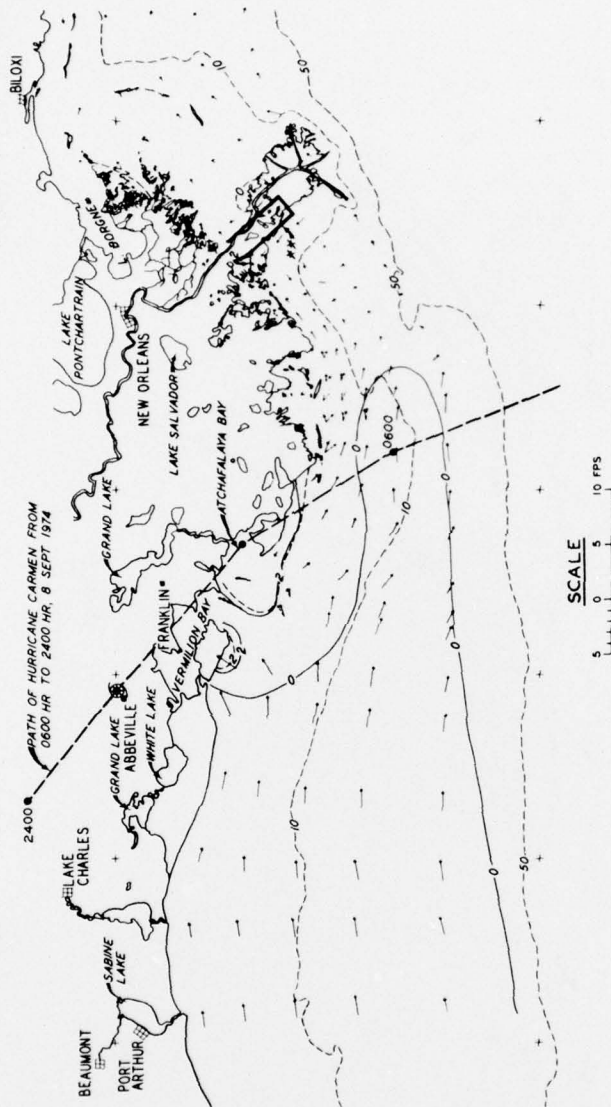
PLATE 68







SCALE
10 0 10 20 NM



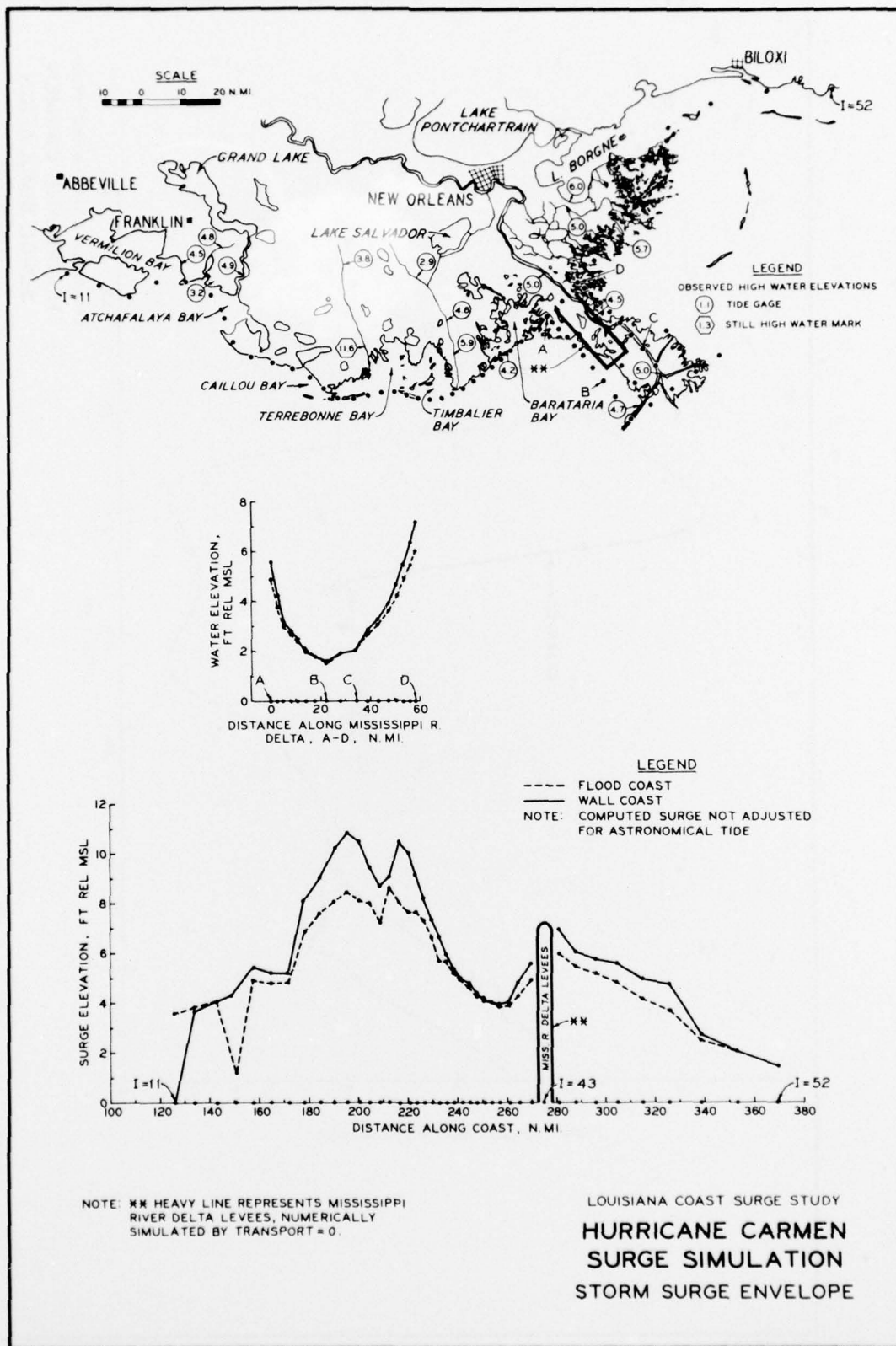
LEGEND

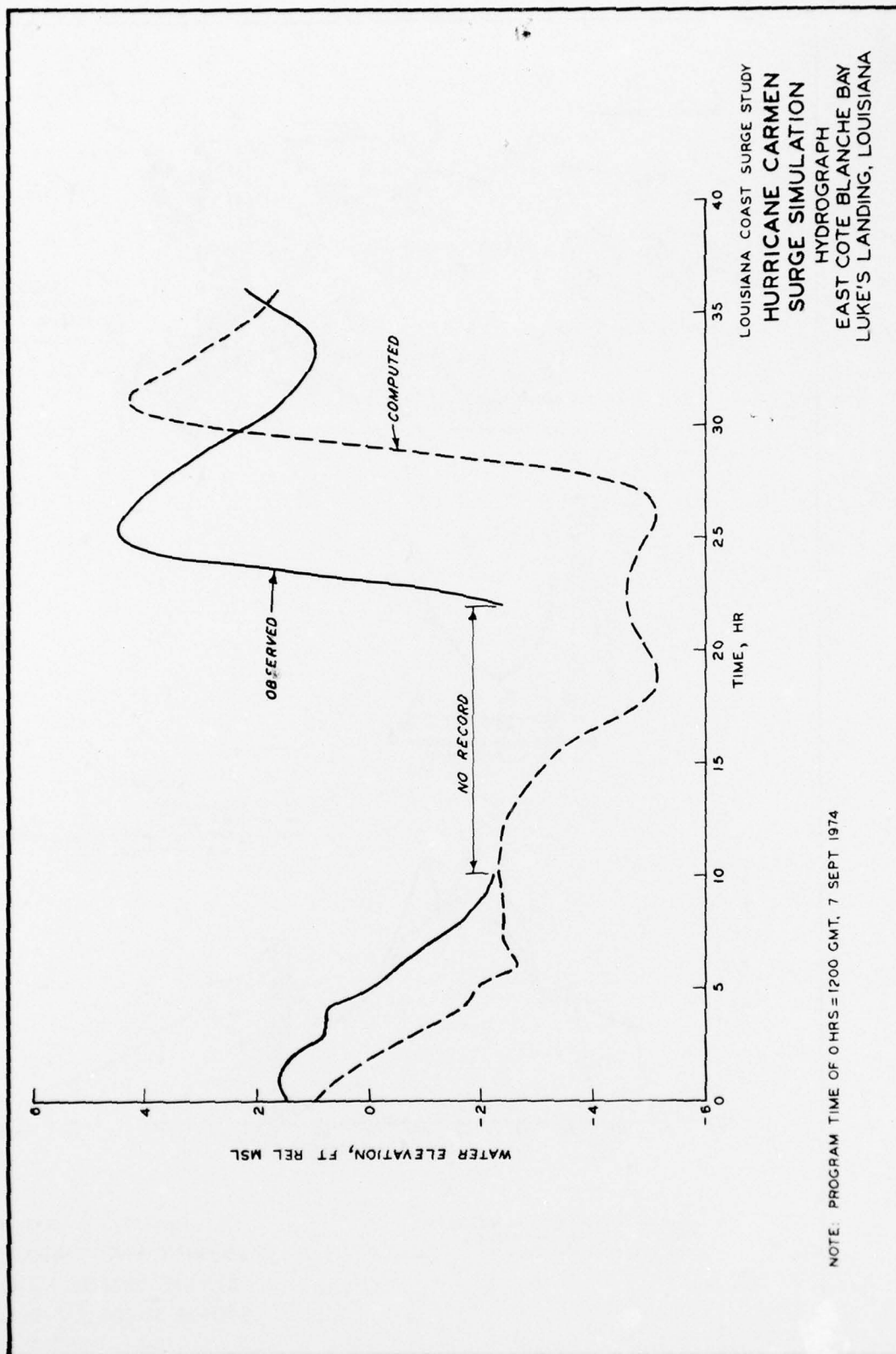
- 2 --- WALL COAST
- 2 --- FLOODING COAST
- 2 --- WATER-SURFACE CONTOUR, FT
- 2 --- WALL COAST
- 2 --- FLOODING COAST
- 2 --- DEPTH-AVERAGED VELOCITY

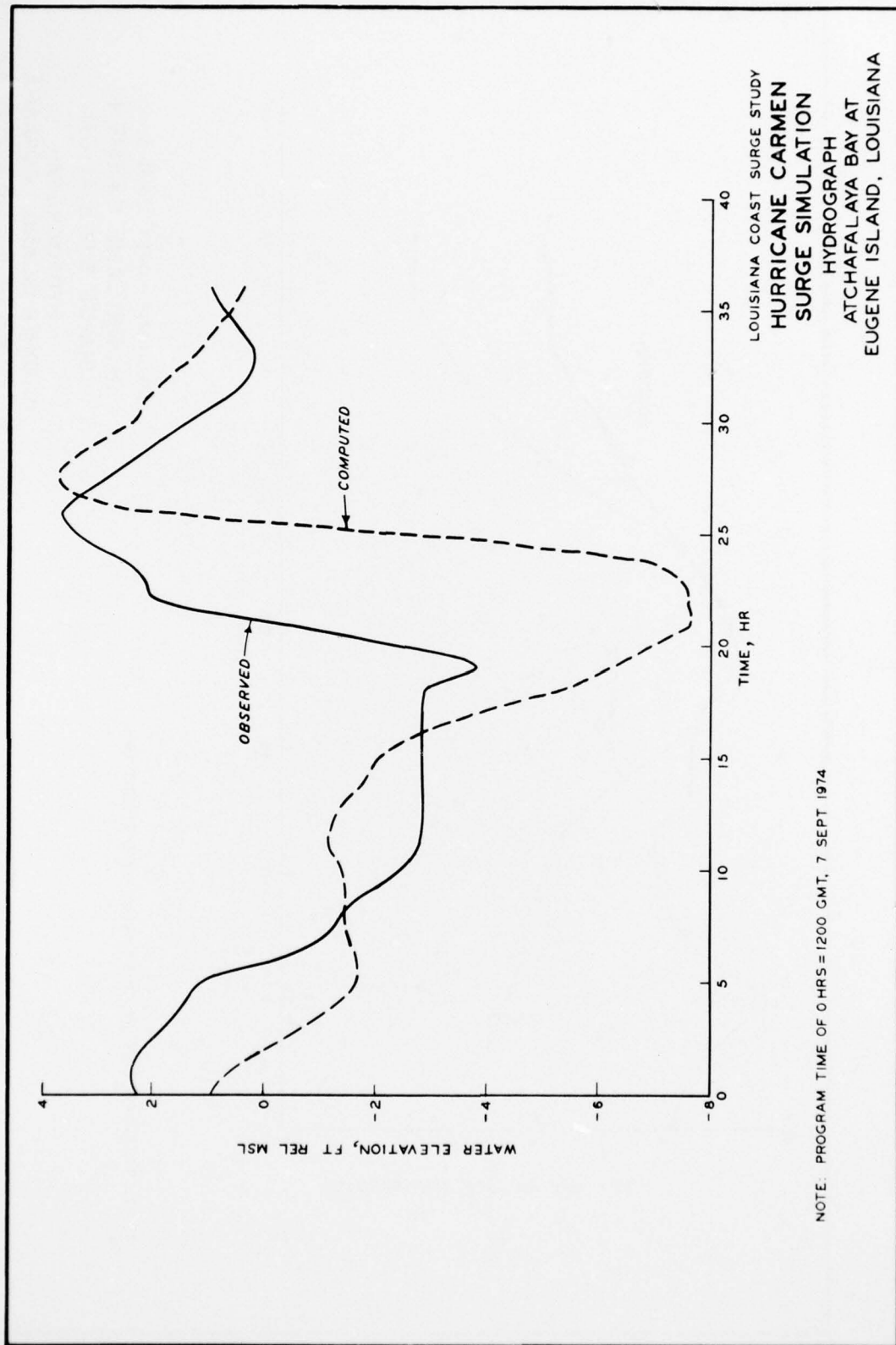
NOTE ALL DEPTHS ARE IN FATHOMS

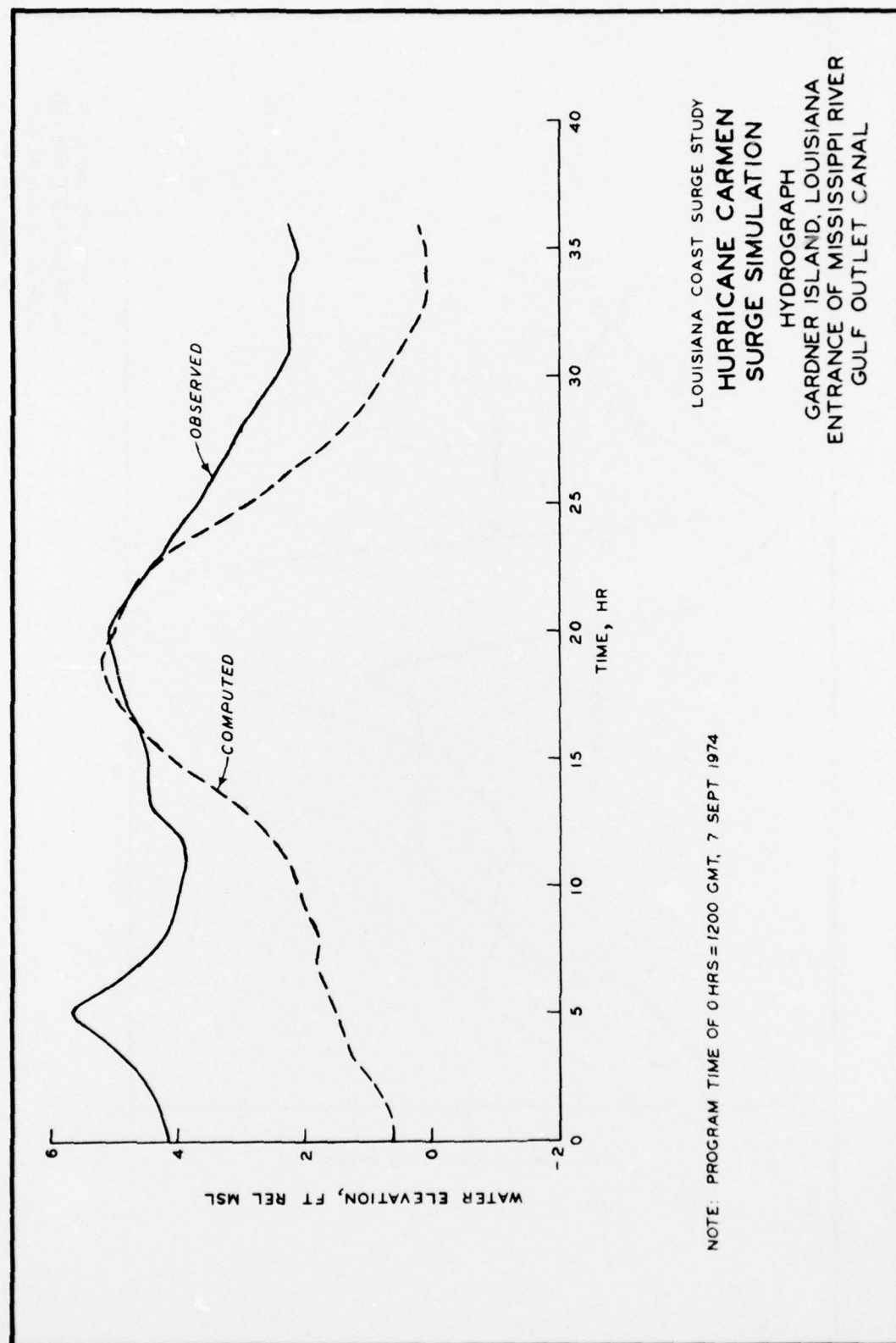
HEAVY LINE REPRESENTS MISSISSIPPI
RIVER DELTA LEVES, NUMERICALLY
SIMULATED BY TRANSPORT = 0
ALL TIME REFERENCES ARE IN GMT

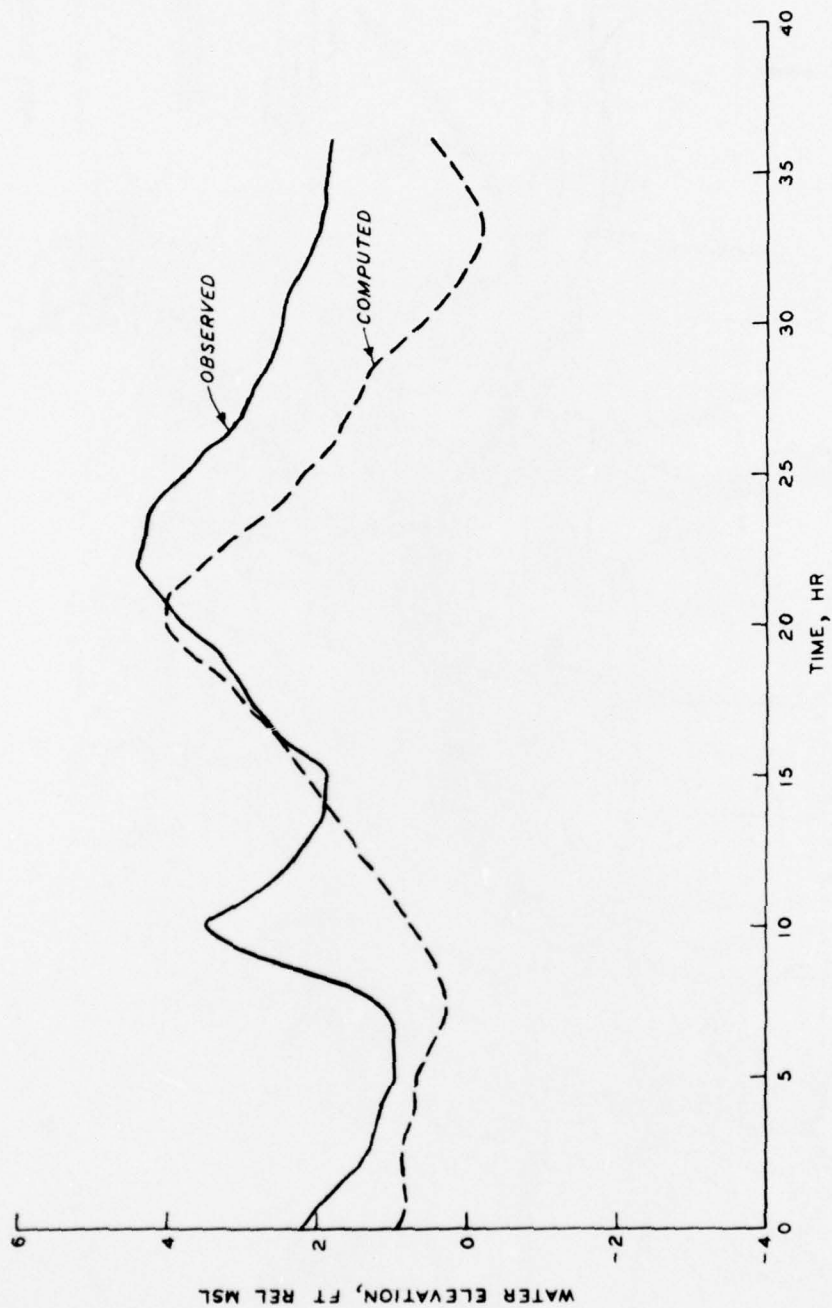
LOUISIANA COAST SURGE STUDY
HURRICANE CARMEN
SURGE SIMULATION
SURFACE TOPOGRAPHY CONTOUR
AND VELOCITY FOR WALL AND
FLOODING COAST BOUNDARY
1800 HOURS, 8 SEPTEMBER 1974











LOUISIANA COAST SURGE STUDY
HURRICANE CARMEN
SURGE SIMULATION
HYDROGRAPH
BILOXI, MISSISSIPPI

NOTE: PROGRAM TIME OF 0 HRS = 1200 GMT, 7 SEPT 1974

APPENDIX A: NOTATION

A_b	Storage area of the attached bay known as a function, H_b
A_c	Channel cross-sectional area at mean sea level
A_I	Surface area at mean sea level of the grid cell representative of H^+
A_s	Surface area of the attached bay at mean sea level
B_n	Transformation coefficients
C_d	Nondimensional variable wind drag coefficient
C_n	Transformation coefficient
C_D	Nondimensional channel discharge coefficient
C_E	Nondimensional coefficient for an overtopping barrier which is exposed on one side
C_S	Nondimensional coefficient for a submerged barrier
D	Depth of water ($H - D_o$)
D_o	Local water depth relative to mean sea level
f	Coriolis parameter
F	Scale factor associated with the orthogonal curvilinear coordinate system
g	Acceleration due to gravity
H	Water level relative to mean sea level
H_b	Water level relative to mean sea level in the ponding area
H_B	Hydrostatic elevation of the sea surface corresponding to the departure of the atmospheric pressure from ambient
H^+	Predicted water level at the coast barrier without correction for flooding
IM, JM	Number of grid points per computational lattice along the S and T axes
K_o	Nondimensional variable seabed drag coefficient that depends on the seabed condition and water depth
L_c^k	Length of coastline at unit elevations, Z_b^k , $k = 0, 1, 2, \dots$
M_f	Map factor relating prototype length to x,y units
P	Atmospheric pressure
P_o	Central atmospheric pressure of hurricane
P_∞	Far-field atmospheric pressure

Q_S, Q_T	Volume transport per unit width in the S and T directions or, equivalently, in the local direction of ξ and η in prototype space
r_H	Distance from hurricane center to H grid points
R_H	Distance from the storm center to the region of maximum winds
S	Ordinate axis of the stretched shelf coordinate system
S_n, S_p	Distance normal to the seaward boundary and along the coast
T	Abscissa axis of the stretch shelf coordinate system
T_n	Long-wave travel time
T_x, T_y	The x and y components of the forward speed of this hurricane center
W_c	Bay entrance channel width
W_x, W_y	The x and y wind-speed components for a moving hurricane
W_R	The maximum wind speed for the stationary hurricane
W_{10}	Wind speed at an elevation 10 meters above the water surface
x	Rectilinear coordinate in prototype space
X_e	The x coordinate of the hurricane center in prototype space
X_g	The x coordinate of the H grid points in prototype space
y	Rectilinear coordinate in prototype space
Y_e	The y coordinate of the hurricane center in prototype space
Y_g	The y coordinate of the H grid points in prototype space
Z_b^k	Unit elevations of coastal barrier as denoted by $k = 0, 1, 2, \dots$
β	The extent of η (+) in the image space of (ξ, η)
ΔS	Constant spaced computing grid increment between dependent variables in the S direction
Δt	Algorithm time increment between computing lattices
ΔT	Constant spaced computing grid increment between dependent variable in the T direction
η	The offshore curvilinear coordinate in prototype space and the abscissa in the image space of (ξ, η)
θ	The local angle between the ξ and x axis in prototype space
λ	The positive horizontal extent of the region to be mapped in prototype space and constrained to equal the extent of ξ in the image space.
u, v	Functions transforming ξ and η to the stretched shelf coordinate system (S,T)

ξ	The alongshore curvilinear coordinate in prototype space and the ordinate in the image space of (ξ, η)
ϕ	Hurricane wind ingress angle
ρ_a, ρ_w	Density of air and water
σ_S, σ_T	Seabed resistance stress divided by ρ_w in the S and T directions
τ_S, τ_T	Wind stress divided by ρ_w in the S and T directions

In accordance with letter from DAEN-RDC, DAEN-ASI dated 22 July 1977, Subject: Facsimile Catalog Cards for Laboratory Technical Publications, a facsimile catalog card in Library of Congress MARC format is reproduced below.

Wanstrath, John J

Nearshore numerical storm surge and tidal simulation / by John J. Wanstrath. Vicksburg, Miss. : U. S. Waterways Experiment Station ; Springfield, Va. : available from National Technical Information Service, 1977.

51, [20], 3 p. ; 78 leaves of plates : ill. ; 27 cm. (Technical report - U. S. Army Engineer Waterways Experiment Station ; H-77-17)

Prepared for Assistant Secretary of the Army (R&D), Washington, D. C., under Project 4A161101A91D.

References: p. 49-51.

1. Conformal mapping. 2. Hydrodynamics. 3. Long waves. 4. Mathematical models. 5. Water waves. I. United States. Assistant Secretary of the Army (Research and Development). II. Series: United States. Waterways Experiment Station, Vicksburg, Miss. Technical report ; H-77-17. TA7.W34 no.H-77-17